

Closed flux tubes in $D = 2 + 1$ $SU(N)$ gauge theories: dynamics and effective string description.

Andreas Athenodorou^{a,b} and Michael Teper^c

^aDepartment of Physics, University of Cyprus, POB 20537, 1678 Nicosia, Cyprus

^bComputation-based Science and Technology Research Center, The Cyprus Institute, 20 Kavafi Str., Nicosia 2121, Cyprus

^cRudolf Peierls Centre for Theoretical Physics, University of Oxford, 1 Keble Road, Oxford OX1 3NP, UK

Abstract

We extend our earlier calculations of the spectrum of closed flux tubes in $SU(N)$ gauge theories in $2 + 1$ dimensions, with a focus on questions raised by recent theoretical progress on the effective string action of long flux tubes and the world-sheet action for flux tubes of moderate lengths. Our new calculations in $SU(4)$ and $SU(8)$ provide evidence that the leading $O(1/l^\gamma)$ non-universal correction to the flux tube ground state energy does indeed have a power $\gamma \geq 7$. We perform a study in $SU(2)$, where we can traverse the length at which the Nambu-Goto ground state becomes tachyonic, to obtain an all- N view of the spectrum. Our comparison of the $k = 2$ flux tube excitation energies in $SU(4)$ and $SU(6)$ suggests that the massive world sheet excitation associated with the $k = 2$ binding has a scale that knows about the group and hence the theory in the bulk, and we comment on the potential implications of world sheet massive modes for the bulk spectrum. We provide a quantitative analysis of the surprising (near-)orthogonality of flux tubes carrying flux in different $SU(N)$ representations, which implies that their screening by gluons is highly suppressed even at small N .

E-mail: athenodorou.andreas@ucy.ac.cy, mike.teper@physics.ox.ac.uk

Contents

1	Introduction	1
2	Some background	2
3	Calculating flux tube energies	5
3.1	lattice setup	5
3.2	flux tube energies	5
3.3	errors	6
4	Leading non-universal correction	7
5	Massive modes and k-strings	10
6	Orthogonality of representations	11
6.1	$k = 2A$ and $k = 2S$	13
6.2	adjoint and singlet	15
7	Spectra	16
7.1	$SU(2)$, $SU(4)$, $SU(6)$ and $SU(8)$ with $p = 0$	17
7.2	adjoint	17
7.3	$p \neq 0$ spectra	19
7.4	continuum and $N \rightarrow \infty$	20
8	Conclusions	21
A	Tables	25

1 Introduction

In this paper we extend our earlier calculations on the spectrum of closed confining flux tubes that wind around a spatial torus [1, 2, 3] in $SU(N)$ gauge theories in $2 + 1$ dimensions. Our main motivation is to address questions raised by the remarkable recent analytic progress both in understanding the universal physics of long flux tubes [4, 5] (see also [6]) and in understanding the simplicity of the spectrum of shorter flux tubes [7, 8]. In addition we will emphasise a further feature that is surprising and potentially of significant theoretical interest.

Our earlier calculations of the l -dependence of the flux tube spectrum [1, 2] were primarily in $SU(6)$. In this paper we extend those calculations, as well as providing new calculations in $SU(2)$, $SU(4)$ and $SU(8)$. This enables us to say more about the N -dependence of the spectra and, in the case of $SU(2)$, to see what happens when l is decreased past the value at which the Nambu-Goto ground state becomes tachyonic.

We begin by sketching, in the next Section, the theoretical background. We then outline, in Section 3, the most relevant details of the lattice calculations; a fuller description may be

found in [1, 2]. In Section 4 we test the predictions of [4, 5] for the leading non-universal power correction to ‘long’ flux tubes. In Section 5 we examine more closely the resonant massive mode tentatively discussed in our earlier work on k -strings [2] and then unambiguously identified [8] using the powerful formalism based on the Thermodynamic Bethe Ansatz. In Section 6 we probe more quantitatively the remarkable absence of screening of all but the shortest flux tubes when these carry flux in higher representations, with explicit examples for $k = 2$ flux in $SU(4)$ and adjoint flux in both $SU(2)$ and $SU(4)$. In Section 7 we compare the l -dependence of the spectra of fundamental flux tubes in $SU(2)$, $SU(4)$, $SU(6)$ and $SU(8)$. We also analyse adjoint flux tubes in $SU(2)$ and $SU(4)$, and critically examine the remarkable agreement with Nambu-Goto of flux tubes with non-zero momentum along the flux tube. A summary and discussion of our results is given in Section 8.

Most of the qualitative discussion in this paper applies to flux tubes in $D = 3 + 1$ as much as to $D = 2 + 1$. However the specific results do differ and everything we say in this paper should be taken to be for $D = 2 + 1$ unless explicitly stated otherwise.

2 Some background

We begin with a brief overview of the ‘Nambu-Goto spectrum’ since it has been found to provide a good approximation to the observed spectrum of fundamental flux tubes [1, 2, 3]. (See also [9] and references therein.) This spectrum is obtained by the canonical light cone quantisation of a free bosonic string in $D = 26$ [10]. Using the formula in other dimensions is known to be inconsistent: while world-sheet Lorentz invariance is respected, bulk Lorentz invariance is not (except, interestingly enough, in $D = 3$ [11]) but is restored for long enough strings. The fact that it does in practice provide a very good approximation to the numerically determined spectrum [1, 2, 3], for reasons that were originally mysterious but are now much better understood [4, 5, 6, 7], makes it our first choice of comparison.

The spectrum is as follows. Upon quantisation the transverse fluctuations of the string become massless ‘phonons’ that live on the background closed string. In $D = 2 + 1$ there is only one transverse direction so the phonon is a single scalar field. Since the string is periodic with length l , the phonons would have momenta $|p| = 2\pi k/l$, with k an integer, if they were free. (Which we shall assume, albeit wrongly, for the moment.) The energy levels are then simply related to the number of phonons as follows. Label the positive momentum phonons as left-movers (L) and the negative ones as right-movers (R). Let $n_{L(R)}(k)$ be the number of left(right) moving phonons of momentum $|p| = 2\pi k/l$. Let the total energy of the left(right) moving phonons be $2\pi N_{L(R)}/l$, then

$$N_L = \sum_k n_L(k)k, \quad N_R = \sum_k n_R(k)k. \quad (1)$$

Let $p = 2\pi q/l$ be the total longitudinal momentum of the string, then since it is the phonons that provide the momentum we have

$$N_L - N_R = q. \quad (2)$$

Then in terms of these quantities the expression for the energy levels of the Nambu-Goto string in $D = 2 + 1$ is [10]

$$E_{N_L N_R, NG}^2(q, l) = (\sigma l)^2 + 8\pi\sigma \left(\frac{N_L + N_R}{2} - \frac{1}{24} \right) + \left(\frac{2\pi q}{l} \right)^2, \quad (3)$$

where the $1/24$ term can be thought of as arising from the oscillator zero-point energies, and σ is the string tension. These energy levels have, in general, a degeneracy which depends on the number of ways the particular values of N_L and N_R can be formed from the n_L and n_R in eqn(1).

At this point we note that the energy in eqn(3) is not the simple sum of phonon energies plus the energy of the background flux tube. That is to say, our interpretation of the states in terms of free phonons, with corresponding momenta, is a fiction. Nonetheless it provides a convenient mnemonic for describing the states, and so we shall usually maintain that language in our discussion below.

Let us take the closed string to wind around the spatial x -torus. Let the local transverse displacement of the string be $h(x)$. Then under the transverse parity $P : (x, y) \rightarrow (x, -y)$, we have $h(x) \rightarrow -h(x)$ and so $a_k \rightarrow -a_k$, where a_k is the creation operator for a phonon of momentum $2\pi k/l$. It arises from taking the Fourier decomposition of $h(x)$ and quantising it. The states are obtained by applying these creation operators to the ‘vacuum’ of the world sheet theory. So all this implies that the (transverse) parity of a state is simply given by the total number of phonons:

$$P = (-1)^{\text{number of phonons}}. \quad (4)$$

We can also consider a longitudinal parity transformation, $(x, y) \rightarrow (-x, y)$. Since this will also reverse the direction of the flux, hence giving an operator with (usually) zero overlap onto the original operator, we always couple it with charge conjugation to undo the flux reversal. This gives us the combined operator P_r . Now under P_r the individual phonon momenta are reversed, as is the overall momentum. Thus this quantum number is only useful in the $p = 0$ sector and here the lightest non-null pair of states with $P_r = \pm$ is $\{a_2 a_{-1} a_{-1} \pm a_1 a_1 a_{-2}\}|0\rangle$ and is quite heavy. In practice this means that this quantum number is of minor utility in our calculations and we shall mostly ignore it in the labelling of our states (but will return to it later). We do not consider transverse momentum since that brings nothing new. So the useful quantum numbers for a string of length l are the longitudinal momentum p , the (transverse) parity P and occasionally the longitudinal parity P_r .

As shown in [1] the spectrum in eqn(3) provides an excellent description of the flux tube spectrum even down to small values of $l\sqrt{\sigma}$. That flux tubes should follow this very simple string spectrum was unexpected, but is now better understood. First of all it was shown in [5, 4] (see also the earlier work in [12, 13]) that if one considers a general effective string action and considers strings long enough that one can express the energy as a power series in $1/l^2\sigma$, then the first 3 correction terms to the leading linear piece are universal. Here the universality class includes all theories where the only massless modes on the world sheet are the Goldstones associated with the spontaneous breaking of translation symmetry. In addition the coefficients of these $1/l$, $1/l^3$ and $1/l^5$ terms in the expansion of $E_n(l)$ around

σl are precisely the same as one obtains, to that order, by expanding the expression for $E_{N_L, N_R}(q, l)$ in eqn(3) in powers of $1/l$. This explains why, in general, longer flux tubes are well described by the Nambu-Goto spectrum. Why this should continue to be the case for much shorter flux tubes has been elucidated in [7]. One can show that the $D = 1 + 1$ world sheet theory is, to a first approximation, integrable. The physics of this integrable theory is determined entirely by the phase shift in the elastic scattering of two phonons. This phase shift must be chosen to reproduce the finite volume Nambu-Goto spectrum in $D = 26$ and at lower D one then obtains the Nambu-Goto spectrum in eqn(3) if one calculates in the asymptotic Bethe Ansatz approximation. One can write the effective world sheet action that reproduces this phase shift, and one can then incorporate new higher order terms or terms corresponding to new massive fields as needed. One can then reverse the process to calculate the corresponding scattering phase shifts. By working backwards and searching for the classic signal of a phase shift passing through the value of π , this provides a powerful framework for determining whether the numerically determined flux tube spectrum contains the contribution of massive resonant states [8].

As remarked above, we now know from the universality arguments [5, 4] that the leading correction at large l to the Nambu-Goto expression for the energy $E_n(l)$ is at $O(1/l^7)$. If, as we expect, the dynamics of confining flux tubes is determined by an effective string action, then we should be able to see such a correction in our numerically determined spectrum. To see it one needs to be at large enough l that one has a convergent expansion of $E_n(l)$ in powers of $1/l^2$. While it is not obvious what the lower limit for such l might be, a plausible estimate is given by the value of l at which the expansion of the Nambu-Goto expression in eqn(3) begins to diverge. For $p = 0$ this corresponds to the restriction

$$l\sqrt{\sigma} \geq \left| 4\pi \left(N_L + N_R - \frac{1}{12} \right) \right|^{\frac{1}{2}}. \quad (5)$$

For the lowest few $p = 0$ energy levels this corresponds to $l\sqrt{\sigma} \gtrsim 1.05, 4.91, 7.02, \dots$ respectively and apart from the ground state the corresponding energies for such l are quite large. Since the numerical determination of the energies becomes less precise the larger the energy (see below) this limits our numerical determination of the leading non-universal power correction to the ground state – at least for now. In our earlier study of the $SU(6)$ flux tube spectrum [1] we attempted to do this, but were only able to show that the power of the leading correction is ≥ 5 . One purpose of this paper is to do better than that.

One of the striking features of the fundamental flux tube spectrum calculated in [1] is the absence of any sign of massive modes in the spectrum, even at smaller l where the energy gaps begin to be quite large. This is surprising since one usually thinks of the string tension as being dynamically generated by the bulk fields which have a mass gap. This motivated the numerical study of higher representation flux tubes such as k -strings [2]. Since the $k = 2$ flux tube may be regarded as a bound state of two $k = 1$ (fundamental) flux tubes, there must be a massive mode associated with the binding which should manifest itself in the flux tube spectrum. And indeed the energy of the first excited $k = 2$ state appears to be consistent with a massive excitation on the $k = 2$ flux tube but a naive ‘by eye’ judgement, as in [2],

is too subjective to be at all convincing. The recent analysis of the same data using the Thermodynamic Bethe Ansatz formalism to relate the observed energy spectra to phase shifts [8] shows a phase shift passing through π and hence, almost unambiguously, a corresponding massive mode. So a second focus of this paper is to add to what we can infer about that massive mode.

3 Calculating flux tube energies

Our lattice calculations are standard and so we provide only a minimal sketch here. A more complete discussion can be found in our earlier papers [1, 2].

3.1 lattice setup

Our lattice field variables are $N \times N$ $SU(N)$ matrices, U_l , residing on the links l of the periodic $L_s^2 L_t$ lattice, whose spacing we label a . The Euclidean path integral is

$$Z = \int \mathcal{D}U \exp\{-\beta S[U]\}, \quad (6)$$

where $\mathcal{D}U$ is the Haar measure and we use the standard plaquette action,

$$\beta S = \beta \sum_p \left\{ 1 - \frac{1}{N} \text{ReTr} U_p \right\} \quad ; \quad \beta = \frac{2N}{ag^2}. \quad (7)$$

Here U_p is the ordered product of link matrices around the plaquette p . We write $\beta = 2N/ag^2$, where g^2 has dimensions of mass and becomes the continuum coupling when $a \rightarrow 0$.

3.2 flux tube energies

To calculate the flux tube spectrum, we calculate correlation functions of a suitable set of lattice operators $\{\phi_i\}$. Expanding the correlators in terms of the energy eigenstates, $H|n\rangle = E_n|n\rangle$, and expressing $t = an_t$ in lattice units, we have

$$C_{ij}(t) = \langle \phi_i^\dagger(t) \phi_j(0) \rangle = \langle \phi_i^\dagger e^{-Han_t} \phi_j \rangle = \sum_k c_{ik} c_{jk}^* e^{-aE_k n_t}, \quad (8)$$

where $c_{ik} = \langle vac | \phi_i^\dagger | k \rangle$. We now perform a variational calculation on e^{-aH} . Suppose $\phi = \psi_0$ maximises $\langle \phi^\dagger(a) \phi(0) \rangle / \langle \phi^\dagger(0) \phi(0) \rangle$ over the vector space spanned by the $\{\phi_i\}$, then ψ_0 is our best estimate of the wave-functional of the ground state. Repeating this calculation over the basis of operators orthogonal to ψ_0 gives us ψ_1 , our best estimate for the first excited state. And so on for the higher excited states. We then calculate the correlators of the ψ_i which, if our original basis is well chosen, have a good overlap onto the corresponding state $|i\rangle$ and will be dominated even at small t by that state, $\langle \psi_i^\dagger(t) \psi_i(0) \rangle \propto \exp(-E_i t)$, so that we can

accurately estimate the desired energy E_i . We can clearly do this for each set of quantum numbers separately.

The states that we are interested in are loops of flux closed around the x -torus. Thus our operators will also wind around the x -torus. The simplest such operator is the Polyakov loop

$$l_p(n_t) = \sum_{n_y} \text{Tr} \left\{ \prod_{n_x=1}^{L_x} U_x(n_x, n_y, n_t) \right\}, \quad (9)$$

where we take the product of the link matrices in the x -direction around the x -torus, $(x, y, t) = (an_x, an_y, an_t)$, and we sum over n_y to produce an operator with zero transverse momentum, $p_\perp = 0$. (Recall that $p_\perp \neq 0$ is not interesting.) This operator is x -translation invariant and so has zero longitudinal momentum, $p = 0$. It also has positive parities, $P = P_r = +$. To access other quantum numbers we need to add ‘kinks’ to this simple operator. To have a good overlap onto the light physical states we need to use operators that are ‘smeared’ on physical length scales, achieved here using a simple spatial ‘blocking’ algorithm [1, 14]. One set of such operators that we use is explicitly shown in Table 2 of [1]. We have also constructed and used a second set of operators that differs in detail but is morally the same. These sets of ‘kinky’ and ‘blocked’ operators provide the basis $\{\phi_i\}$ for our variational calculation of the flux tube spectrum.

Our $SU(N)$ matrices are in the $N \times N$ fundamental representation so the trace in eqn(9) is in the fundamental, and so $l_p(n_t)$ should project onto flux tubes carrying fundamental flux. To project onto a flux tube carrying flux in another representation we take the corresponding trace, using standard expressions for the latter [2, 15].

3.3 errors

To calculate E_i from $\langle \psi_i^\dagger(t) \psi_i(0) \rangle$, we need to go to large enough t that the correlator is dominated by $\exp(-E_i t)$. To determine when that happens we define an effective energy

$$aE_{eff}(n_t) = -\ln \left\{ \frac{\langle \psi_i^\dagger(n_t) \psi_i(0) \rangle}{\langle \psi_i^\dagger(n_t - 1) \psi_i(0) \rangle} \right\}. \quad (10)$$

Once a single exponential dominates the value of $\langle \psi_i^\dagger(t) \psi_i(0) \rangle$, then $aE_{eff}(t = an_t)$ will become independent of n_t and aE_{eff} will equal the desired energy aE_i . So identifying such an ‘effective energy plateau’ is the essential step in calculating E_i .

In pure glue Monte Carlo calculations the statistical errors on the correlators are roughly independent of $t = an_t$ while the average value from which we extract the energy decreases roughly exponentially in t . Thus we need the ‘effective energy plateau’ to set in at small n_t , if our calculation is to be usefully accurate, and this requires that the operator ψ_i has a very good overlap onto the true wave-functional. It is also clear that the larger the value of aE_i , the more rapidly the statistical error on $aE_{eff}(n_t)$ will grow with n_t . The corresponding systematic error is that we then take the plateau to start at a value of n_t that is too small and so we over-estimate the value of aE_i . (The diagonal correlator is a sum of exponentials with

positive coefficients, so $aE_{eff}(n_t)$ should decrease monotonically with n_t .) This important systematic error will therefore grow as we consider higher excited states at fixed l , or if we go to larger l for a fixed eigenstate such as the ground state.

For excited states the corresponding correlator may contain a small admixture of lighter states that will eventually dominate as n_t grows. In this case what we are looking for is an effective energy plateau that exists over a limited range of n_t . At some point this procedure will become ambiguous, and even more so if the state is unstable with a non-zero decay width. It is therefore clear that the most reliable energy determinations will be those of the ground states in the various quantum number sectors.

It is clear that at the foundation of our calculation must be a reliable identification of the effective energy plateaux. We have shown examples in [1] for fundamental flux tubes, and in [2] for flux in higher representations, so in this paper we will limit ourselves to displaying only a few examples where one has good reason to worry whether a flux tube actually exists, such as the adjoint flux tube.

4 Leading non-universal correction

As remarked above, if we expand the energy levels, $E_n(l)$, of $D = 2 + 1$ closed flux-tubes in powers of $1/l^2\sigma$, then the first non-universal term is expected to appear at $O(1/l^{\gamma \geq 7})$ relative to the leading linear term, σl [4, 5] (see also [6]). Since the universal terms are the same as the terms one obtains by expanding the Nambu-Goto spectrum in eqn(3), we can write the predicted large- l spectrum as

$$E_n(l, p) = E_{n,NG}(l, p) + \frac{c}{(l\sqrt{\sigma})^{\gamma \geq 7}} + \dots \quad (11)$$

where the power γ is an odd integer, and c contains a factor of $\sqrt{\sigma}$ and so has dimensions of energy. Since the expansion of $E_{n,NG}(l)$ in powers of $1/l$ only converges (if we ignore the momenta) for $l^2\sigma > l_0^2\sigma \sim 4\pi(N_L + N_R - 1/12)$, it is only for lengths $l \gg l_0$ that the prediction in eqn(11) is expected to be valid. These are large values of l if $N_L + N_R \neq 0$ and our current numerical calculations do not have the statistical accuracy needed to identify such a correction at such large l . It is only for the ground state, $N_L = N_R = 0$, that we can hope to identify such a correction. Indeed, in this case the expansion of $E_{NG}(l)$ is valid for $l_0^2\sigma > \pi/3$ which includes the full range within which the theory is confining for $N \geq 3$. In [1] we analysed the ground state energy for $SU(6)$ at a lattice spacing $a\sqrt{\sigma} \simeq 0.086$, where any lattice spacing corrections will be very small, and concluded that a power correction as in eqn(11) must have $\gamma \geq 5$ but our statistical accuracy did not enable us to unambiguously confirm the theoretical prediction that $\gamma \geq 7$. One of our main goals in this paper is to improve upon that earlier result. This has involved making additional calculations in $SU(6)$ at the same value of β , and new calculations in $SU(8)$ and in $SU(4)$ at approximately the same value of $a\sqrt{\sigma}$.

We begin with our calculation of the spectrum in $SU(8)$ at $\beta = 306.25$. The string tension is essentially determined by the ground state energy, $E_0(l)$, at larger l while the non-universal correction term will only be visible (given our errors) at very small l . Once we have determined

$a^2\sigma$ we can calculate $E_{0,NG}(l)$ and plot the difference $E_0(l) - E_{0,NG}(l)$ thus exposing, in Fig.1, deviations from Nambu-Goto at small l . If we assume that the correction is an odd inverse power of l , as in eqn(11), then we find that the best fit with a power is $\gamma = 9$, as displayed in the figure. In addition while $\gamma = 7$ also gives an acceptable fit, we can exclude any value $\gamma \leq 5$, thus confirming the theoretical prediction.

Since this is our largest value of N , and so our ‘best’ calculation in terms of minimising various systematic uncertainties, we will go into the statistical analysis in more detail. As is apparent from Fig.1 only the lowest 4 or 5 values of l are relevant for the $1/l^\gamma$ fit. To avoid the χ^2 contribution of these points being swamped by the higher l points, we perform a best fit at each γ to all the data, but then only consider the χ^2 contribution of these lowest 4 (or 5) points. Since $a^2\sigma$ is effectively determined by the larger l points, we are effectively determining 2 parameters, c and γ , using this ‘reduced’ χ^2 and so we have 2 (or 3) degrees of freedom. From this we extract the statistical p-values shown in Figs.2,3. The solid points come from using the energies listed in Table 2, where we have used time-correlated fits to the correlation functions for $l \leq 20$ and non-correlated fits for $l > 20$. We also show the result of using correlated fits at all l (open circles) or non-correlated fits at all l (open boxes). The conclusion, $\gamma \geq 7$, is the same with all these choices, irrespective of whether we use the lowest 4 or 5 values of l in the analysis.

Our second calculation involves extending the $SU(6)$ calculation at $\beta = 171$ that was reported in [1]. The ground state energies are listed in Table 3. As in $SU(8)$ the values for $l \leq 20$ have been obtained from time-correlated fits to the correlation functions, while the $l > 20$ fits are time-uncorrelated. Again as in $SU(8)$, we fit all values of $l \geq 14$ but consider only the χ^2 of the lowest 4 or 5 points in obtaining the p-values displayed in Fig 5. We see that while this analysis is consistent with $\gamma \geq 7$ it certainly does not exclude $\gamma = 5$ and so is unable to provide an unambiguous test of the theoretical predictions. This motivated the $SU(8)$ calculation we have summarised above. The essential difference between our $SU(6)$ and $SU(8)$ calculations is that in $SU(8)$ $l = 14a$ turns out to be slightly closer to the deconfining transition than in $SU(6)$, so the deviation is larger and provides a more severe constraint on the power fit. At the same time N is larger so the strong first order ‘deconfining’ transition is more abrupt, its presence has less effect when one is close to it, and the world-sheet dynamics is less likely to be compromised when very close to the phase transition.

We turn now to the ground state energies in $SU(4)$ at $\beta = 74$. These are listed in Table 4. We extract the deviation from Nambu-Goto just as in $SU(8)$ and plot the result in Fig.6, where we show a fit with an $O(1/l^7)$ correction. The p-values corresponding to fits with various values of γ are shown in Fig.7, and we see that the evidence for $\gamma \geq 7$ is strong. In this $SU(4)$ calculation (unlike the $SU(8)$ one) we have also calculated the higher representation $k = 2$ ground state which we plot in Fig.8. Although the errors are larger, the deviations from Nambu-Goto are much larger, and the power fit is very strongly constrained, as we see in Fig.9. Both the fits to the lowest four values of l , and the fits to all l , completely constrain the value of the inverse power to $\gamma = 7$. Since this is such a strong result and since we know that in $SU(4)$ the ‘deconfining’ transition is only weakly first order [16] so that the nearby $l/a = 13$ energy might be influenced by it, it is worth asking what happens if drop this $l/a = 13$ value from the fit. Doing so we obtain a set of p-values also shown in Fig.9. While the fit to the

power γ is now less constrained, so that $\gamma = 7$ and 9 are both allowed, a value of $\gamma < 7$ is still completely excluded.

We conclude from these calculations that the leading correction to Nambu-Goto can be fitted by a power as in eqn(11) and that the power is constrained to be

$$\gamma \geq 7, \tag{12}$$

as expected from the analysis of the leading non-universal contribution in [4, 5].

All the above has assumed that the deviation from Nambu-Goto at very small $l\sqrt{\sigma}$ is given by an (effective) power correction $O(1/l^\gamma)$. Since the deviation is only significant (given the errors) for the 4 or 5 smallest values of l , it is obvious that we have to make an assumption about the functional form of the correction to obtain any useful constraint. Having said that we will briefly explore one plausible alternative to a power-like correction, which is an exponential, $O(e^{-ml})$. One could expect such a correction to σ to arise from the emission and absorption of the lightest particle in the bulk gauge theory, in which case m should be the mass gap. And in that case the coupling should decrease with N , so that the coefficient of the exponential correction $\rightarrow 0$ as $N \rightarrow \infty$. More speculatively, an exponential might also arise as the correction to the expansion of $E(l)$ in powers of $1/l^2\sigma$ if that expansion were asymptotic.

It turns out that fitting a correction of the form $\propto e^{-ml}$ works remarkably well, as we see in Figs.11,10. In fact, it is easy to see, as we now show, that this follows automatically if a powerlike fit works well and that power is large. If the power is large then the correction decreases rapidly as $l\sqrt{\sigma}$ increases. With finite errors, and given a lower bound provided by the ‘deconfining’ transition, the range of l where the deviation from Nambu-Goto is visible will be small, as we see in Figs.1,4,6. Suppose that the relevant range is $l \in [l_1 - \delta_1, l_1 + \delta_1]$ with $\delta_1 \ll l_1$ as will be the case if the range is narrow. Then we can write the power correction at $l = l_1 + \delta l \in [l_1 - \delta_1, l_1 + \delta_1]$ as

$$\begin{aligned} \frac{1}{l^\gamma} &= \frac{1}{(l_1 + \delta l)^\gamma} = e^{-\gamma \ln(l_1 + \delta l)} \\ &= c e^{-\gamma \ln(1 + \frac{\delta l}{l_1})} \\ &= c' e^{-\frac{\gamma}{l_1} \delta l} \left(1 + \frac{\gamma}{2} \left(\frac{\delta l}{l_1} \right)^2 + \dots \right) \\ &\simeq c'' e^{-\frac{\gamma}{l_1} l} \end{aligned} \tag{13}$$

for our typical $\delta l/l_1$ and γ , and within finite errors. Thus a good fit with a $\propto 1/l^\gamma$ correction necessarily implies a good fit with a $\propto e^{-ml}$ correction, where $m \simeq \gamma/l_1$. Indeed the masses in our exponential fits do satisfy this expectation.

Of course the above argument works both ways; if an exponential correction is the correct dynamics then this can imply that a powerlike correction will also fit well. However we note that while the best value of the power is $\gamma = 7, 9$, which is in line with the theoretical expectations, the values of m obtained using an e^{-ml} correction do not coincide with the bulk mass gap, and the coefficient, although it decreases by about 35% between $SU(4)$ and $SU(8)$, does not decrease anything like $1/N^2$. It therefore appears quite implausible that the correction is really exponential rather than powerlike.

5 Massive modes and k -strings

A striking feature of the spectrum of fundamental representation confining flux tubes in $D = 2 + 1$ $SU(N)$ gauge theories is the lack of any sign of massive modes [1]. This is in contrast to $D = 3 + 1$ [17]. This is puzzling if one believes that the confining flux tube has some non-zero but finite ‘intrinsic’ width, since this would imply the existence of corresponding massive modes. Motivated by this puzzle we calculated in [2] the spectrum of flux tubes carrying flux in higher representations than the fundamental. Any such flux tube, if stable, can be thought of as a bound state of some number of (anti)fundamental flux tubes, and the massive modes inducing that binding should be encoded in the flux tube spectrum in some way. Particularly relevant are k -strings which one can think of as bound states of k fundamental flux tubes. Two flux tubes carrying flux $k, k' \leq N/2$ can be shown not to mix if $k \neq k'$ using a standard centre symmetry argument. From earlier lattice calculations [15, 18] we know that the lightest k string has a string tension $\sigma_k < k\sigma_f$ for $k > 1$ so it will be stable against decay to k fundamental flux tubes. In particular the ground state $k = 2$ and $k = 3$ flux tubes are absolutely stable. Since these are stable bound states, the finite binding energy per unit length must be associated with some massive mode and it is interesting to see if one can identify it within the spectrum. In [2] we found that the energy of the first excited k -string state had a behaviour with l consistent with that of a massive mode, but that this interpretation was far from unambiguous given the heuristic nature of our analysis. This uncertainty has subsequently been removed by the approach in [8] that uses a world-sheet effective field theory framework that allows one to work back from the spectrum to the scattering phase shifts of the phonons living on the world sheet. These calculations [8] have confirmed the existence of a massive resonance on the world sheet of $k = 2$ and $k = 3$ flux tubes, and that its mass, M_k , is indeed very close to that of the nearly constant gap between the ground and first excited flux tube states.

The above massive mode calculations used the $SU(6)$ k -string spectra in [2]. It is of interest to ask if this mode only knows about the world-sheet theory, and so knows only about σ_k , or if it knows about the bulk gauge theory. In the former case $M_k/\sqrt{\sigma_k}$ should be some fixed number independent of which $SU(N)$ group generates the bulk physics. Since σ_k/σ_f varies with N this predicts that $M_k/\sqrt{\sigma_f}$ should vary with N . In the latter case it should be $M_k/\sqrt{\sigma_f}$ or M_k/m_G , where m_G is the bulk theory mass gap, that are weakly dependent on N (up to $O(1/N^2)$ corrections). To address this question we will compare what one finds in $SU(6)$ and $SU(4)$, on the lattices and at the β -values discussed in Section 4.

To begin with, we plot in Fig.12 the lightest few states with positive parities and $p = 0$, in the spectrum of $k = 2A$ flux tubes in $SU(6)$. We see that for $2.5 \lesssim l\sqrt{\sigma} \lesssim 5.5$ the gap between the ground and first excited states is roughly constant and so we interpret the first excited state as a massive mode on the ground state flux tube. The next excited state is quite close to the first excited Nambu-Goto level and approaches it as we increase l , so we would interpret that as being (predominantly) the Nambu-Goto state with one left and one right moving massless phonon on the flux tube. There appears to be a level crossing at $l\sqrt{\sigma} \sim 5.5$ (with level repulsion in the neighbourhood) so by the time we are at $l\sqrt{\sigma} \sim 6$ we would interpret the first excited state as being the Nambu-Goto state with one left and

one right moving massless phonon, while the second excited state is now the massive mode on the flux tube. Some of the complication of the spectrum may well arise from a state that contains two massive modes. We also show, in Fig.13, a corresponding plot for $SU(4)$. The level crossing appears to occur a little earlier, at $l\sqrt{\sigma} \sim 5$, but otherwise it is similar to the $SU(6)$ spectrum. Finally we display in Fig.14 the spectrum of the lightest $k = 3A$ flux tube states in $SU(6)$. Here the features identified in the $k = 2A$ spectrum are even more clearly on display: a near-constant gap to the first excited state, a separate stringy state approaching the first excited Nambu-Goto level, together with level crossing at larger l and associated level repulsion. As we see from Table 1 the binding of the $SU(6)$ $k = 3$ ground state, as measured by the ratio $\sigma_{k=3}/3\sigma_f \simeq 0.61$, is stronger than that of the $SU(4)$ $k = 2$ ground state, where $\sigma_{k=2}/2\sigma_f \simeq 0.68$, or of the $SU(6)$ $k = 2$ ground state, where $\sigma_{k=2}/2\sigma_f \simeq 0.81$, and this may be a reason for the particular clarity of the massive mode signal we see in Fig.14.

The energy gap between ground and first excited k -string states can be extracted from the energies in Table 6. We plot the $k = 2A$ energy gap in units of the world-sheet string tension, $\sigma_{k=2A}$, versus the length l in Fig.15. In addition to the calculations listed in Table 6 we have also included some values obtained in $SU(8)$, $SU(12)$ and $SU(16)$ as part of our glueball spectrum calculation in [19]. The $SU(8)$ and $SU(12)$ calculations are at values of $a\sqrt{\sigma_f}$ similar to those of our $SU(4)$ and $SU(6)$ calculations, while the $SU(16)$ lattice spacing is somewhat larger (but we do not expect this to matter). We contrast this with the plot in Fig.16 where the same energy is expressed in units of the bulk theory (infinite volume) mass gap. We observe that the variation with N in the latter plot is much smaller than that in the former. This suggests, quite strongly, that the mass of the massive mode is determined by the physics of the bulk $SU(N)$ theory, which is indeed what one might expect if it reflects the binding of two fundamental strings into a $k = 2$ string.

In Fig.17 we compare the energy gaps of $k = 2$ and $k = 3$ flux tubes in our $SU(6)$ calculation. We see that they indicate an identical massive mode when expressed in units of the bulk mass gap, which again would not be quite the case if we used the corresponding $\sqrt{\sigma_k}$ to scale the energy gaps. (But not a strong effect because the $k = 2$ and $k = 3$ string tensions happen to be quite close here.)

6 Orthogonality of representations

If we have a source in a (non-singlet) representation \mathcal{R} of the $SU(N)$ group, it will be linearly confined so that the flux between it and a corresponding distant anti-source will be carried by a flux tube in the same representation \mathcal{R} , and with a string tension $\sigma_{\mathcal{R}}$. Or at least this is what would happen if there were no screening. In reality, however, the vacuum contains a condensate of adjoint gluons which will presumably screen such a source down to the representation \mathcal{R}' which has the smallest associated string tension. Since adjoint screening leaves a source in the same k -string sector [2], each such sector (usually referred to as a sector of fixed \mathcal{N} -ality, with $\mathcal{N} = k$) contains its own absolutely stable minimum energy flux tube, which is what we are usually referring to when we speak of a ' k -string'. Since one believes the gluon condensate to be strongly coupled, one would naively expect the screening to have a large probability as

soon as it is energetically favoured, so that the \mathcal{N} -ality of the flux would be its only useful label. For a flux tube which is not tied to sources but which is closed around a spatial torus of length l , such a screening will be energetically favoured for all $l > l_c = 1/T_c$ (possibly qualified at small l by corrections to the linear piece of the energy). So what we would expect to obtain from the t -dependence of a correlator of operators representing closed strings in any representation \mathcal{R} of a k -sector is simply the energy of the associated k -string. And if we consider two operators in different representations \mathcal{R} and \mathcal{R}' but in the same k -sector, then we would expect their overlap to be substantial.

In practice one finds that these naive expectations are largely contradicted by actual calculations. In effect the screening appears to be a very weak process. For example, if one looks at closed flux tubes in the $k = 2A$ and $k = 2S$ representations, which are the symmetric and antisymmetric pieces of $f \otimes f$, one finds a reasonably well defined $k = 2S$ flux tube energy which is much larger than the corresponding $k = 2A$ energy. Compare, for example, Fig.1 and Fig.11 in [2]. Similarly in the $k = 3$ sector: compare Fig.15 and Fig.19 in [2]. Moreover one finds that typical overlaps between closed flux tube operators in different representations (within the same k -sector) are very small, perhaps even consistent with zero up to finite volume effects. This was already noted in, for example, [3] (see Tables 2,3 therein) and [2] (see Section 4.1 therein). These observations were made using individual operators chosen from within a small basis. (This basis was designed to have a good projection onto ground states but not onto excited states.) Here we will improve the analysis by using our large basis of flux tube operators, and calculating the overlaps using the orthonormal operators produced by our variational calculation, which are our best estimates for the actual energy eigenstates. Moreover we will be able to compare in some detail what happens in $SU(4)$ and $SU(6)$ for $k = 2$, and we will include $SU(2)$ when we consider $k = 0$ (i.e. the adjoint flux tube).

We begin with our various winding operators $l_{p,j}$ which are constructed using link matrices in the fundamental representation. Typically we have 17 operators at each blocking level, and we have all blocking levels n_b such that $2^{n_b-1} \leq l/a$. (For small l/a we sometimes include a larger ‘transverse’ blocking level.) Taking the trace we obtain $\text{Tr}_f l_{p,j}$ as our basis for flux tubes in the fundamental. To obtain a basis in the $k = 2$ symmetric, antisymmetric (2A,2S) and $k = 0$ adjoint representations we simply take

$$\begin{aligned} \text{Tr}_{2A} l_j &= \frac{1}{2} (\text{Tr}_f \{l_j^2\} - \{\text{Tr}_f l_j\}^2), \\ \text{Tr}_{2S} l_j &= \frac{1}{2} (\text{Tr}_f \{l_j^2\} + \{\text{Tr}_f l_j\}^2), \\ \text{Tr}_{adj} l_j &= \{\text{Tr}_f l_j\}^2 - 1, \end{aligned} \tag{14}$$

where we drop the subscript p on l_p from now on to declutter the notation. We then take spatial sums of these to project onto $p = 0$ and positive parities. We can equally well consider $p \neq 0$ and negative parity. We label these normalised operators $\phi_{\mathcal{R},j}(t)$, suppressing other quantum number labels. In our earlier work [2, 3] we considered a few individual overlaps $\phi_{2A,j}(0)\phi_{2S,j}(0)$ and showed they were small and rapidly decreasing as l increases. However since $\phi_{\mathcal{R},j}(t)$ and $\phi_{\mathcal{R},l}(t)$ are not orthonormal (in fact the overlap for $j \neq l$ is often large) we did not make a statement about the total overlap between the bases. So here we shall

produce an orthonormal set of operators from the $\phi_{\mathcal{R},j}(t)$. A particularly useful choice, which is the one that we shall use below, is provided by our variational procedure which produces orthonormal linear combinations $\psi_{\mathcal{R},j}(t)$ which are our best variational estimates for the wavefunctionals of the energy eigenstates. We shall illustrate our results for what happens in general with two particular cases: the overlap between flux tubes in the $k = 2$ symmetric ($2S$) and antisymmetric ($2A$) representations, and the overlap between the adjoint flux tube and the (singlet) vacuum.

6.1 $k = 2A$ and $k = 2S$

Consider the square of the overlap of our best (variational) operator for the $2A$ ground state flux tube onto our whole $2S$ basis

$$\mathcal{O}_{2Ags,2S} = \sum_k \left| \langle \psi_{2A,j=0}^\dagger(0) \psi_{2S,k}(0) \rangle \right|^2, \quad (15)$$

or of our $2S$ ground state on to our $2A$ basis

$$\mathcal{O}_{2Sgs,2S} = \sum_k \left| \langle \psi_{2S,j=0}^\dagger(0) \psi_{2A,k}(0) \rangle \right|^2, \quad (16)$$

or of our whole $2A$ basis on our whole $2S$ basis

$$\mathcal{O}_{2A,2S} = \sum_k \sum_j \left| \langle \psi_{2A,j}^\dagger(0) \psi_{2S,k}(0) \rangle \right|^2. \quad (17)$$

Note that because the operators all have unit normalisation, these overlaps have different maximum values, i.e. while $\mathcal{O}_{2Ags,2S} \leq 1$ and $\mathcal{O}_{2Sgs,2A} \leq 1$, we have $\mathcal{O}_{2A,2S} \leq \text{number of operators}$. Note also that these expressions only provide an approximation to the true overlaps since our basis of operators is not complete. However we believe that this approximation is a good one since we find that highly excited states contribute little to either overlap and our basis of operators is large enough to have a good overlap onto the lighter states. There are of course many other instructive overlaps that one can consider, but for brevity we shall here focus on those defined in eqns(15,16,17).

We begin by showing in Fig.18 the total overlap, $\mathcal{O}_{2A,2S}$, between our $2A$ and $2S$ bases as a function of the flux tube length l , obtained in $SU(4)$ at $\beta = 74$. We do so for 3 bases of operators which are distinguished by the maximum ‘blocking level’ of the operators in the basis. Since a blocked link at level 6 has length 32 lattice spacings, we only include it for $l/a \geq 32$. (The reader will notice that we have included blocking level 5 for $l/a \leq 16$ in Fig.18. This is not a normal blocked link, but rather a blocking level 4 link that has been smeared further in the transverse directions.) The maximum value of $\mathcal{O}_{2A,2S}$ is $17 \times$ (number blocking levels), and this is the normalisation to bear in mind when reading this plot.

We observe that at very small l , close to $l_c \equiv 1/T_c$, the total $2A/2S$ overlap is substantial. (Recall that this is the overlap squared.) However we also see that as the length of the flux

tube increases the overlap decreases very rapidly, more or less exponentially with l . At the largest values of l the signal is effectively lost in the noise and our results are consistent with $\mathcal{O}_{2A,2S} \xrightarrow{l \rightarrow \infty} 0$, i.e. the complete absence of any screening. An important remark is that for all our values of l the basis up to blocking level 5 is not significantly improved by including blocking level 6, for at least the lightest 10 states (in the positive parity sector). By contrast, going from maximum blocking 4 to level 5 provides a marked improvement. Thus we may consider the basis with maximum blocking level 5 as providing a good representation of the total overlap in a large volume.

The results with a maximum blocking level of 6 illustrate a general feature of our overlaps in various representations. When the blocking level is large enough that the operator effectively wraps around the spatial volume in all directions, then the corresponding overlaps become substantial, even though they follow the usual pattern of rapidly decreasing as the volume is further increased. This substantial overlap appears to be a finite volume effect that may well be peculiar to our operator construction, and is something that we need to understand better.

We turn now to our best operator for the $2A$ ground state, again in $SU(4)$ at $\beta = 74$. The overlap of this operator onto the actual ground state is $\sim 99\%$ if we use the basis up to blocking level 5, and so provides us with an excellent approximation to the true overlap. We see from Fig.19 that the overlap of this state onto our $2S$ basis is large for the very shortest flux tubes. (Recall that the maximum value of the overlap is unity in this case.) So here there appears to be no suppression of screening. However the screening decreases rapidly - at least exponentially - as l increases and is consistent with vanishing as $l \rightarrow \infty$. In practice, calculating within the $k = 2A$ sector provides us with an excellent approximation to the absolute ground state in the $k = 2$ sector.

Finally we show in Fig.20 the same plot, but for the overlap of the $2S$ ground state onto the $2A$ basis. In this case the overlap of our best variational operator onto the ground state is only $\sim 90\%$. This ground state has a large energy and should be unstable into a pair of fundamental flux tubes with equal and opposite momentum. Since $\sigma_{2S} \simeq 2.6\sigma_f$ there is plenty of phase space for such a decay. (Moreover this process is not large- N suppressed, as we see from eqn(14).) It is therefore worth making a brief detour to see if there is in fact a $k = 2S$ ground state that is sufficiently stable to be well defined. So we plot in Fig.21 the effective energies obtained from our best variational correlators

$$aE_{eff}(n_t) = -\ln \frac{C(n_t)}{C(n_t - 1)}, \quad (18)$$

for various l in our $SU(4)$ calculation. A well defined state should produce a plateau in $aE_{eff}(n_t)$ starting from some value of $t = n_t a$, indicating that the correlator is then given by a single exponential. A state with a small decay width will produce an apparent plateau in the values of $aE_{eff}(n_t)$ but will, for large enough n_t , decrease towards an asymptotic value given by the lightest decay state. If the overlap of our best operator onto the corresponding eigenstate is not very large, the start of the plateau is pushed out to larger n_t , and will be submerged in statistical errors, especially for the larger energies that one obtains at large l . So we see in Fig.21 reasonable evidence for a plateau for the smaller values of l , but at larger

l the evidence for a plateau is much less convincing. Since $\sigma_{2S} \rightarrow 2\sigma_f$ and $\sigma_{2A} \rightarrow 2\sigma_f$ as $N \rightarrow \infty$ the phase space for decay diminishes for larger N , and so one might expect the $2S$ flux tube to become more stable. We show in Fig.22 the results of some calculations in $SU(8)$ at $\beta = 306.25$ which indeed show much clearer plateaux in aE_{eff} at larger l , aided by the visibly better overlaps. (For the corresponding plot in $SU(6)$ at $\beta = 171$ see Fig.11 in [2].) We conclude from this detour that it is meaningful to talk of a (presumably ‘resonant’) $2S$ ground state and to discuss its overlap on to the $2A$ basis. Returning to Fig.20, what we see is very similar to what we saw for the $2A$ ground state, except that at intermediate values of $l\sqrt{\sigma}$ the overlaps in this case are somewhat larger. But again what we see is consistent with rapidly vanishing overlaps as $l \rightarrow \infty$.

6.2 adjoint and singlet

As our second example we consider adjoint ($k = 0$) flux tubes and their overlap onto the colour singlet ($k = 0$) vacuum. We work in $SU(2)$ and $SU(4)$ at couplings $\beta = 16, 74$ respectively, where the values of the lattice spacing, $a\sqrt{\sigma_f}$, are roughly the same as in $SU(6)$ at $\beta = 171$. Such a flux tube can decay, for example to the vacuum or a glueball via gluon screening, or into a pair of fundamental and antifundamental flux tubes. Gluon screening is large- N suppressed, but the decay into a pair of fundamental flux tubes is not, as one can see from eqn(14). In addition the adjoint string tension (in units of σ_f) increases as N decreases, so that the phase space for these decays increases at lower N . All this suggests that even if adjoint flux tubes are well-defined at larger N , as shown for example in our study of $SU(6)$ in [2], they may not exist as meaningful states in $SU(2)$, and perhaps even in $SU(4)$.

As a first step in addressing this question, we show in Fig.23 the effective masses obtained from our variationally determined ground state correlator in $SU(2)$. (We use vacuum subtracted operators, although this is usually unnecessary.) For all except the largest values of l there is a reasonably clear plateau, at least for some intermediate range of n_t . However the overlaps of the ground states onto our best operators are not very good, as shown by the marked increase of $aE_{eff}(n_t)$ as $n_t \rightarrow 0$. Thus for the largest values of l it is hard to infer a plateau: the signal drops into the statistical noise before one has clear evidence either way. Nonetheless the fact that we do see plausible evidence for a quasi-stable state for almost all our values of l is striking given our earlier comments. In addition, the fact that the energy increases with l tells us that we are not dealing with a particle-like state, but rather with some kind of string-like state. Indeed the effective plateau mass for say $l = 38$, where we see a clear plateau, is $\sim 50\%$ higher than the lightest glueball. (See below for a more detailed analysis.)

We show the corresponding plot for $SU(4)$ in Fig.24. Here the overlaps are evidently very good, and the existence of a well-defined ‘flux tube’ state seems evident for all our values of l .

We now turn to a quantitative measure of the overlap between adjoint and singlet. The first quantity we calculate is the total overlap squared onto the vacuum of our basis of adjoint operators,

$$\mathcal{O}_{adj}^{tot} = \sum_k (\langle \psi_{adj,k} \rangle)^2, \quad (19)$$

where $\{\psi_{adj,k}\}$ are the orthonormal operators obtained from our variational procedure applied

to our original non-orthonormal basis of adjoint operators which, in turn, are obtained from the fundamental ones using eqn(14). In Fig.25 and Fig.26 we show the values of this total overlap for $SU(2)$ and $SU(4)$ respectively. As in the earlier discussion of $k = 2$ overlaps, we show separately what one obtains using a basis that contains operators up to blocking level 5 and up to 6 (at the larger values of l where it has been calculated). As in the $k = 2$ case we observe a rapid decrease of the overlap \mathcal{O}_{adj}^{tot} with increasing l , consistent with the overlap vanishing as $l \rightarrow \infty$. At small l the overlap onto the vacuum is large. (Recall that $\mathcal{O}_{adj}^{tot} \leq 1$.) And again the operators with the highest blocking levels that wrap around the whole spatial volume have a large overlap, although at any fixed blocking level, however large, the overlap decreases at least exponentially fast with l .

A related question is what is the overlap of the ground state adjoint flux tube onto the vacuum. One way to approach this question is as follows. Consider the orthonormal vacuum subtracted operators that arise from the variational procedure, $\psi_{adj,i} \equiv \tilde{\psi}_{adj,i} - \langle \tilde{\psi}_{adj,i} \rangle$. We take the ground state operator $\psi_{adj,i=0}$, which is our best estimate for the adjoint flux tube ground state, and plot the value of the vacuum expectation value that was subtracted from that operator normalised by the vacuum subtracted correlator (which we show explicitly although its value is unity):

$$\mathcal{O}_{adj}^{gs} = \frac{\langle \tilde{\psi}_{adj,k=0} \rangle^2}{\langle \psi_{adj,k=0}^2 \rangle}. \quad (20)$$

This quantity provides a measure of the would-be vacuum expectation value of the adjoint flux tube. We plot this quantity in Figs 28, 27 for our $SU(2)$ and $SU(4)$ calculations. We see that the vacuum expectation value is very small except at the very smallest values of l , and rapidly decreases as we increase l . A more direct measure is provided by applying the variational procedure to our adjoint operators without any vacuum subtraction, and calculating the vacuum expectation value squared of the ground state. This in fact produces very similar results to what we see in Figs 28, 27, except that at the very smallest values of l , $l/a \leq 18$, where the whole basis has a large overlap onto the vacuum, the variational calculation automatically picks the vacuum as the ground state. We also note that, once again, where the operator wraps around the whole spatial volume we see large overlaps. However this appears to be finite volume effect, since at any fixed blocking level, the overlap eventually decreases rapidly with l and indeed with N . So apart from this finite volume effect, we see that even a modestly long adjoint flux tube has a negligible probability to be screened to the vacuum.

In retrospect it would have been interesting to perform a similar analysis for the overlap of the adjoint flux tube onto, say, the lightest glueball. Technically this is trivial: it would simply involve combining in a single global basis both our glueball and flux tube operators. Unfortunately in the present work we did not calculate such an enlarged cross-correlation matrix and so are not able to address this question.

7 Spectra

So far we focused on the absolute ground state. Here we will discuss part of the larger spectrum. In particular it is interesting to see how much of the striking simplicity that we

observed in $SU(6)$ [1] appears at smaller values of N , such as $SU(4)$ and $SU(2)$. We also discuss more explicitly the continuum and large- N limits.

7.1 $SU(2)$, $SU(4)$, $SU(6)$ and $SU(8)$ with $p = 0$

An amusing feature of $SU(2)$ is that the deconfining length, $l_c\sqrt{\sigma} = \sqrt{\sigma/T_c}$, is smaller than the length at which the Nambu-Goto ground state becomes tachyonic, $l_0\sqrt{\sigma} = \pi/3$. Earlier calculations with a small basis of operators [1] have indicated that in this range of l the dependence of the energy on l is governed by the critical exponents of the (second-order) deconfining transition. In Fig.29 we show the difference between the calculated energy and the Nambu-Goto energy versus l . (Using the calculated value of σ as a convenient normalisation.) For the point with $l < l_0$ we replace $E_0^{NG} \rightarrow 0$ since its actual value is imaginary. We see that down to $l\sqrt{\sigma} \sim 1.5$ the calculated energy stays very close to the Nambu-Goto prediction, just as it does for larger N . However the deviation below that is in the opposite direction to what we observe at larger N . Unlike a strong first order transition, a second order finite volume transition will affect the l -dependence in the neighbourhood of the transition and this is presumably what we are seeing here.

In Fig.30 we show the low-lying flux tube spectrum in $SU(2)$ and compare it to the predicted Nambu-Goto energy levels. While the first excited state is close to Nambu-Goto for $l\sqrt{\sigma} > 3.5$, it is only for $l\sqrt{\sigma} \geq 5$ that the next energy level is more-or-less reproduced (in both degeneracy and energy) by our calculated spectrum. This approach to the asymptotic universal values is much slower than what one observes in $SU(6)$ [1].

It is interesting that the Nambu-Goto ground state energy works so well. It is essentially the linear piece plus pieces that can be interpreted as the zero point energies of the Nambu-Goto excited state oscillators. (Or, in a different language, [7], the effect of the vacuum gas of winding phonons on the world sheet.) It may seem puzzling that the latter appear to be closely reproduced at small values of l where the excited state energies themselves differ greatly from the Nambu-Goto predictions. This suggests that these differences are constrained to largely cancel each other. As one might expect, for example, from splittings due to mixing.

In Fig.31 we show the corresponding $SU(4)$ spectrum. The approach to Nambu-Goto with increasing l is more rapid than in $SU(2)$, but markedly less so than in the case of $SU(6)$ which is displayed in Fig.32. We also show the $SU(8)$ spectrum in Fig.33, which is very similar to $SU(6)$, confirming our expectation that the latter is effectively in the large- N limit.

We list the energies of the lightest four $P = +$ and the lightest two $P = -$ states in Tables 2, 3, 4 and 5.

7.2 adjoint

As emphasised in Section 6.2, the adjoint flux tube is expected to be unstable. Nonetheless, as we have seen from the effective energy plots in [2] for $SU(6)$ and in Fig.23 for $SU(2)$ and Fig.24 for $SU(4)$, the ground state adjoint flux tube appears to be well-defined in both $SU(4)$ and $SU(6)$ and, to some extent, in $SU(2)$.

We saw in [2] that in $SU(6)$ the adjoint flux tube energy does indeed grow approximately linearly with l at large l , just as one would expect for a state that is a string-like flux tube. In Fig.34 we show what happens for $SU(4)$. We plot separately the energy one obtains from the apparent effective energy plateau that one obtains with the (variationally) best ground state operator using bases that include blocking levels up to 4, 5, 6 respectively. We find that using blocking levels up to 5 provides a best operator with a very good overlap at all l . Including blocking level 6 makes for an almost insignificant improvement in the overlap. By contrast, while using blocking levels up to 4 is adequate at the very smallest values of l , it becomes inadequate at larger values, reflected in a poor plateau and a systematic upward error in the energy estimate. We observe that the ground state energy rapidly becomes much larger than the lightest ($V = \infty$) glueball mass, $am_{0^{++}} \sim 0.37$, as we increase l , showing that the overlap onto glueballs must be very small. This complements our earlier observation concerning vacuum overlaps. In addition we see that, except for the smallest values of l , the energy is significantly larger than that of two fundamental loops, just as we observed for $SU(6)$ in [2]. This strongly suggests that, once l is reasonably large, what we have in $SU(4)$ is indeed an adjoint flux tube that has a decay width that is small enough for it to be well-defined.

The analogous results for $SU(2)$ are shown in Fig.35. Once again we see an energy that increases with l well beyond the mass of the lightest glueball ($am_{0^{++}} \sim 0.41$ in this case), which together with our earlier results on the vacuum overlaps shows that decays which are large- N suppressed appear to be very small in $SU(2)$ – even though we are now at the smallest possible (non-Abelian) value of N . However, in contrast to $SU(4)$, the energy decreases as we enlarge our basis to include ever more smeared operators and is consistent with decreasing at any fixed l to the lightest scattering state composed of two (anti)fundamental flux tubes. (The dashed line in Fig.35.) That does not necessarily mean that there is no quasi-stable adjoint flux tube. It could simply be that our highly smeared operators effectively include good operators for a pair of fundamental flux loops. However the more likely explanation is that the decay width of any adjoint flux tube state into a pair of fundamental flux loops is large enough that it cannot be reasonably identified by our simple methods.

In $SU(2)$ our variational calculation does not produce trial excited states from which we are able to extract energies by identifying an effective energy plateau; as we have seen, there are already difficulties with the ground state. In $SU(4)$, by contrast, we are usually able to estimate the energies of the first two excited states and we plot these in Fig.36 together with the ground state and also the Nambu-Goto predictions for the lowest energy levels. (Recall that the latter are determined by the adjoint string tension, which in turn is determined by the ground state energies at larger l .) We see that the observed spectrum bears no relation at all to the simple Nambu-Goto spectrum (even at our largest l) in marked contrast to the remarkable success of the latter in describing the spectrum of fundamental flux tubes. Even if one looks at the deviations of the ground state from Nambu-Goto, and fits that with an inverse power, one finds a power roughly $\propto 1/l^3$ which is inconsistent with what one expects from the universal terms in an effective string action [4, 5]. We have seen in Figs.26,27 that the vacuum overlaps are very small, and there is no sign of a glueball contribution to the correlator, so the decays and mixings that would be suppressed at large- N appear to be negligible here. It may be that it is the mixings and decays involving a pair of (anti)fundamental flux tubes that lead

to the complexity of our observed adjoint spectrum. In the large- N limit the spectrum should become that of two non-interacting fundamental flux tubes, each with its own excitation spectrum based on a string with tension σ_f . This will be different from the spectrum of a single string with a tension $\lim_{N \rightarrow \infty} \sigma_{adj} = 2\sigma_f$, both for the excitation energy at $O(1/l^3)$ and for the zero-point energy at $O(1/l)$ and, in particular, because of the sum over the relative transverse momenta of the two (anti)fundamental flux tubes.

7.3 $p \neq 0$ spectra

A striking feature of the calculated flux tube spectra is how closely the ground states with non-zero longitudinal momentum, p , follow the Nambu-Goto spectrum in eqn(3). In the case of $SU(6)$ one sees this not only for the fundamental flux tube [1] but also for the flux in higher representations such as, amongst others, the $k = 2A, 2S$, $k = 3A, 3M, 3S$, and adjoint $k = 0$ [2]. In Fig.37 we show how the energies of the $SU(2)$ ground states vary with l for longitudinal momenta $p = 0, 2\pi/l, 4\pi/l, 6\pi/l$. We also show the Nambu-Goto predictions. We see that even for $SU(2)$ the agreement with Nambu-Goto is very good, with only very small deviations at the smallest values of l . One can ask whether these deviations fall within our systematic errors. In particular, our Nambu-Goto spectrum is for the continuum theory, but at the smallest values of l our values of ap are not small, and one should then worry about $O((ap)^2)$ lattice spacing corrections. While we are not able to quantify these corrections, we can obtain an estimate of their potential magnitude by replacing the continuum momentum by the one which arises in the free field propagator of the most simply discretised bosonic action

$$(ap)^2 \rightarrow 2 - 2 \cos(ap). \quad (21)$$

Doing so we obtain the dashed curves in Fig.37. We note that the lattice spacing corrections are very small, but comparable in size to the small deviations of the calculated energies from continuum Nambu-Goto. So while the deviations may well be real, we cannot claim to estimate these since they appear to be within our systematic uncertainties.

Given that the close agreement at smaller values of l is not just at large N but extends all the way down to $SU(2)$, and also that in the case of $SU(2)$ it extends below the value of l where the $p = 0$ Nambu-Goto ground state becomes tachyonic, one needs to ask what is the significance of this apparent agreement with Nambu-Goto. The first thing to note is that much of the gap between $p \neq 0$ and $p = 0$ at small l arises from the contribution of the momentum, $p = 2\pi n/l$ which becomes large as l decreases, even for $n = 1$, and will dominate the energy. We see this in Fig.38, where each dashed line is simply the energy of a massless particle of momentum p , i.e. $E = p = 2\pi n/l$. Of course in the confining phase we believe that we have a background flux tube. If we take the simplest possible model, which is that the phonons on the world sheet are completely non-interacting (see below), then the energy of the ground state of momentum p will be $E = p = 2\pi n/l$ plus that of the background flux tube, σl , i.e.

$$E_{free,gs}^2(l; p) = \left(\sigma l + \frac{2\pi n}{l} \right)^2 = (\sigma l)^2 + 4\pi\sigma n + \left(\frac{2\pi n}{l} \right)^2. \quad (22)$$

This is plotted as the solid lines in Fig.38 and by eye it agrees as well as Nambu-Goto did in Fig.37. This should be no surprise: the Nambu-Goto energy for this case where all the phonons are left movers (or all right movers) is

$$E_{NG,gs}^2(l;p) = (\sigma l)^2 + 4\pi\sigma \left(n - \frac{1}{12} \right) + \left(\frac{2\pi n}{l} \right)^2, \quad (23)$$

which differs from $E_{free,gs}^2(l;p)$ by an amount that is invisibly small in Figs.37,38. Indeed the subenergy of any two left-moving massless phonons is zero so they do not interact since they necessarily have derivative interactions as befits Goldstones (arising from the spontaneous breaking of bulk translation invariance by the background flux tube). However there are always extra phonons winding around the l -torus, and interacting with these gives rise to the small extra term in eqn(23), as shown in [7] using the Thermodynamic Bethe Ansatz. (It can also be thought of as arising from the zero-point energies of the phonon oscillators, at least to a first approximation.)

So we see that most of the gap between the $E_{gs}^2(l;p)$ for two different p is due to the energy of the massless phonons in the approximation that they are free. To discriminate between the ‘free’ and ‘NG’ models we have to take a microscope to our data, and this we do for $p = 2\pi/l$ (our most accurate $p \neq 0$ calculations) in Fig.39 for $SU(2)$, and in Fig.40 for $SU(6)$. From these figures it is clear that the very small extra piece in the Nambu-Goto energy is indeed necessary (and sufficient) to obtain excellent agreement with our calculated values.

It is interesting to ask to what extent our spectrum constrains the mass μ of the momentum carrying excitation to be zero, as assumed above. To a good approximation a non-zero mass μ will simply shift the value of the quantity $l(E - E_{model})/2\pi$ plotted in Figs.39,40 by $\mu^2 l^2 / 8\pi^2 = (\mu^2/\sigma)(l\sqrt{\sigma})^2 / 8\pi^2$, and this will be very small at small l . Nonetheless the agreement with Nambu-Goto is so good that the constraint turns out to be quite strong: we find $\mu^2/\sigma \ll 1$ for all $l\sqrt{\sigma} \gtrsim 1.5$. Since the bulk mass gap is $m_g/\sqrt{\sigma} \sim 4$ (although some screening masses are smaller by perhaps a factor of ~ 2), this result is telling us that the string excitations are indeed massless, as one expects.

A closed flux tube of length $l\sqrt{\sigma} \sim 2$ is almost as wide as it is long. (Assuming a conventional intrinsic width of $\sim 1/\sqrt{\sigma}$.) So, naively, it looks like a fat blob rather than an ideal string. That its excitations should be given so accurately by the massless phonons characteristic of a thin string is therefore a surprise that is telling us something interesting about the dynamics of flux tubes.

7.4 continuum and $N \rightarrow \infty$

In our complementary study of the glueball spectrum [19] we have also calculated the flux tube spectrum. These calculations are for a large range of N , so as to enable an $N \rightarrow \infty$ extrapolation of the glueball masses, as well as for a range of lattice spacings so as to enable a continuum $a \rightarrow 0$ extrapolation. However, being aimed primarily at the glueball spectrum, they are typically performed at each value of N and $a(\beta)$ for only one or two values of l . These values of l are simply chosen to be large enough for the finite volume corrections to glueball

masses to be negligible and they are not exactly the same, either for fixed N and varying a , or for different N . Since the flux tube spectrum depends quite strongly on l , this means that any comparison based on the results of [19] will, in the present context, have some significant systematic uncertainties. To minimise these, we remove the leading l -dependence by plotting the excited energies in a form that, in the Nambu-Goto approximation, exposes the phonon excitation energy with the dependence on l completely factored out. For the lightest states with $p = 0$ and $n = N_L + N_R$, we plot the quantity

$$\frac{E_n^2(l) - E_0^2(l)}{4\pi\sigma} \stackrel{NG}{=} n, \quad (24)$$

where the equality holds if the calculated values coincide with the Nambu-Goto model. This provides a convenient way to focus on the deviations from Nambu-Goto. While these are l -dependent (see for example Fig.32) this dependence is quite weak once l is modestly large, as it will be here.

In Fig.41 we plot $(E_n^2 - E_0^2)/4\pi\sigma$ for the lightest few $p = 0$ (fundamental) flux tube states in $SU(8)$, as a function of $a^2\sigma$. The values of l are not equal but they lie in a narrow window, $l\sqrt{\sigma} \in (3.78, 3.91)$, and as we can see from Figs.32,33 any variation within this window should be small for these states. What we see in Fig.41 is that as soon as we are away from the coarsest lattice spacing, say $a^2\sigma \lesssim 0.04$, any discretisation errors are not noticeable. This is reassuring: our study of the l -dependence in this paper was carried out for a much smaller lattice spacing, namely $a^2\sigma \simeq 0.0075$.

In Fig.42 we attempt a comparison of the spectra obtained for $N = 2, 3, 4, 6, 8, 12$. The values of l now range over a somewhat wider window, $l\sqrt{\sigma} \in (3.55, 3.85)$. The lattice spacing also varies, $a\sqrt{\sigma} \in (0.069, 0.074)$, but this should be harmless given the discussion of the previous paragraph. In any case we observe that at least for $N \geq 6$ any dependence on N is too small to see. This complements the comparison between $SU(6)$ and $SU(8)$ in Figs.32,33, and reinforces our earlier assertion in [1] that the spectrum of $SU(6)$ is a good approximation to the $SU(\infty)$ spectrum.

8 Conclusions

In this paper we have extended our earlier calculations of the spectrum of closed confining flux tubes that wind around a spatial torus. A major motivation has been to address questions brought into focus by the remarkable recent progress in our theoretical understanding of the dynamics of flux tubes [4, 5, 6, 7, 8].

The analysis in [4, 6] of the universal terms in any effective string action predicts that the first non-universal correction to the ground state energy should be $O(1/l^{\gamma \geq 7})$. While our earlier work [1] was only able to show that $\gamma \geq 5$, in the present paper our calculations of fundamental flux tubes in $SU(8)$ and in $SU(4)$, and of the $k = 2$ flux tube in $SU(4)$, unambiguously support the conclusion that $\gamma \geq 7$. (See Figs.2,3,5,7,9.) This provides further evidence that the theoretical framework of an effective string action is appropriate for describing the stable confining flux tubes of $SU(N)$ gauge theories, even when N is far from being large.

The calculations in [7, 8], using the Thermodynamic Bethe Ansatz to relate the observed energies to world-sheet scattering phase shifts, provide convincing evidence that the first excited state of the $k = 2$ flux tube spectrum, as calculated in [2], is indeed a massive (resonant) mode on the world sheet, as surmised, inconclusively, in [2]. In the present paper we calculate the spectra of $k = 2$ flux tubes in $SU(4)$ and $SU(6)$ and $k = 3$ flux tubes in $SU(6)$, as shown in Figs.12,13,14. Comparing the $k = 2$ massive modes in $SU(4)$ and $SU(6)$ we find that the scaling is much better when it is expressed in units of the bulk mass gap, i.e. the lightest scalar glueball, than when it is expressed in terms of the world-sheet ($k = 2$) tension, as we can see from Figs.15,16. That is to say, the origins of this massive mode lie in the bulk physics, as indeed one would expect if it reflected the binding of two fundamental flux tubes into the $k = 2$ flux tube.

In addition to the above we also investigated the remarkable suppression of screening of flux tubes in representations higher than the fundamental, already pointed out in [2, 18, 3]. Our main improvement is to go from the earlier basis of operators that was not orthogonal, to the orthonormal basis provided by our variational procedure. (So that our operators correspond to our best estimates for the flux tube energy eigenoperators.) This enables us to calculate quantities such as the total overlap between the spaces spanned by two bases in different representations. Since these bases typically contain most of the low-lying eigenoperators, this provides a quantitative measure of the physically interesting screening of flux tubes in one representation to the other. As an example we showed in Fig.18 the overlap in $SU(4)$ between the $k = 2$ symmetric and antisymmetric bases. The overlap decreases very rapidly with increasing flux tube length, and is only significant for operators that are so highly smeared that they wrap strongly around the whole spatial volume. (Why this should be so remains to be understood.) In Figs.19,20 we showed the overlap of the $k = 2A, 2S$ ground states onto the $2S$ and $2A$ bases respectively. Again we see a strong suppression of screening. Our study of the overlap of the adjoint flux tube onto the (singlet) vacuum in $SU(2)$ and $SU(4)$ showed the same features. (See Figs.25–28.)

Amongst other calculations in this paper, we performed a comparison of flux tube spectra for $SU(N)$ groups ranging from $SU(2)$ to $SU(8)$, as displayed in Figs.30–33. We saw that even for $SU(2)$ the spectrum converges with remarkable speed to the Nambu-Goto predictions as l increases. In marked contrast, the spectrum of the adjoint flux tube in $SU(4)$, shown in Fig.36, bears so little relation to the Nambu-Goto spectrum that from this spectrum alone we would not imagine that Nambu-Goto might have something to do with real-world flux tubes. This despite the fact that a well defined ground state for the adjoint flux tube appears to exist in $SU(4)$, as we infer from Figs.24,34. (Perhaps we are seeing in Fig.36 a mix of genuine adjoint states and states composed of a pair of (anti)fundamental flux tubes with equal and opposite momenta.) We also looked more critically at the remarkable apparent agreement between the calculated $p \neq 0$ ground state energies and the Nambu-Goto predictions, which persists to the smallest values of l , even for $SU(2)$, as we see in Fig.37. In fact, as we saw in Fig.38, the same level of visual agreement is obtained with a simple model of free massless phonons on a background flux tube. And indeed at the smallest values of l it is simply the energy due to the momentum that dominates the energy gaps. If however we apply a microscope to the comparisons, as in Figs.39,40, then we see quite clearly that it is only Nambu-Goto that

provides a truly accurate description of the calculated energies.

Some final comments. The fact that the first correction to the Nambu-Goto prediction for the energy spectrum is $\propto 1/(l\sqrt{\sigma})^{\gamma \geq 7}$ [4, 5] means that the spectrum of closed flux tubes is accurately known for all lengths l where the expansion in powers of $1/l^2\sigma$ is convergent. The fact that at smaller l the world sheet theory is approximately integrable [7] means that we have an accurate description for (most) smaller values of l as well. Moreover the corresponding theoretical formalism allows us to identify and incorporate new world sheet phenomena such as massive modes [8]. Such massive modes have been identified in both $D = 3+1$ fundamental flux tubes [17, 8] and in k -strings [2, 8]. Although these massive modes belong to the world-sheet theory they may well influence the glueball spectrum of the bulk $SU(N)$ theory. In a picture where glueballs are based on contractible closed loops of fundamental flux (as at least some of them surely are) the massive modes will produce corresponding excitation gaps in the glueball energy spectrum. This could be encoded in simple flux tube models of glueballs [20, 21]. Finally we note that the strong suppression of gluon screening implied by the observation that the flux carried by long flux tubes remains, to a very good approximation, in a given $SU(N)$ representation, means that an approximation to the theory that neglects screening, e.g. [22], and so is more tractable, may nonetheless form the basis for a good approximation to the dynamics of flux tubes, and perhaps even the bulk theory, in $D = 2 + 1$.

Acknowledgements

We have benefitted from very useful discussions with, in particular, Ofer Aharony, Sergei Dubovsky, Raphael Flauger, Victor Gorbenko and Zohar Komargodski, as well as with other participants at both the recent *Flux Tubes* conference held at the Perimeter Institute (in May 2015), the earlier *Confining Flux Tubes and Strings* conference held at ECT, Trento (in July 2010), and the much earlier *QCD and Strings* workshop at the KITP, UCSB (in 2004). We are grateful to these institutions for hosting these very productive meetings. AA has been partially supported by an internal program of the University of Cyprus under the name of BARYONS. In addition, AA acknowledges the hospitality of the Cyprus Institute where part of this work was carried out. MT acknowledges partial support under STFC grant ST/L000474/1. The numerical computations were carried out on the computing cluster in Oxford Theoretical Physics.

References

- [1] A. Athenodorou, B. Bringoltz and M. Teper, JHEP 1105 (2011) 042 [arXiv:1103.5854].
- [2] A. Athenodorou and M. Teper, JHEP 1306 (2013) 053 [arXiv:1303.5946].
- [3] A. Athenodorou, B. Bringoltz and M. Teper, JHEP 0905 (2009) 019 [arXiv:0812.0334].
A. Athenodorou, B. Bringoltz and M. Teper, Phys.Lett.B656 (2007) 132 [arXiv:0709.0693].

- [4] O. Aharony and Z. Komargodski, JHEP 1305 (2013) 118 [arXiv:1302.6257].
- [5] 2. arXiv:1111.5758 [pdf, ps, other] O. Aharony and M. Dodelson, JHEP 1202 (2012) 008 [arXiv:1111.5758].
O. Aharony, M. Field and N. Klinghoffer, JHEP 1204 (2012) 048 [arXiv:1111.5757].
O. Aharony and N. Klinghoffer, JHEP 1012 (2010) 058 [arXiv:1008.2648].
O. Aharony and E. Karzbrun, JHEP 0906 (2009) 012 [arXiv:0903.1927].
- [6] S. Dubovsky, R. Flauger and V. Gorbenko, JHEP 1209 (2012) 044 [arXiv:1203.1054].
- [7] S. Dubovsky and V. Gorbenko, [arXiv:1511.01908].
3. arXiv:1411.0703 [pdf, other] P. Cooper, S. Dubovsky, V. Gorbenko, A. Mohsen and S. Storage, JHEP 1504 (2015) 127 [arXiv:1411.0703].
S. Dubovsky, R. Flauger and V. Gorbenko, JHEP 1209 (2012) 133 [arXiv:1205.6805].
- [8] S. Dubovsky, R. Flauger and V. Gorbenko, J.Exp.Theor.Phys. 120 (2015) 3, 399 [arXiv:1404.0037].
S. Dubovsky, R. Flauger and V. Gorbenko, Phys.Rev.Lett. 111 (2013) 6, 062006 [1301.2325].
- [9] M. Bill, M. Caselle, D. Fioravanti, F. Gliozzi, M. Meineri, R. Pellegrini and R. Tateo, PoS LATTICE2013 (2014) 372 [arXiv:1401.1414].
- [10] P. Goddard, J. Goldstone, C. Rebbi and C. Thorn, Nucl. Phys. B56 (1973) 109.
J. Arvis, Phys. Lett. B127 (1983) 106.
- [11] L. Mezincescu and P. Townsend, Phys.Rev.Lett.105 (2010) 191601 [arXiv:1008.2334].
- [12] M. Lüscher and Peter Weisz, JHEP 0407 (2004) 014 [hep-th/0406205].
M. Lüscher, Nucl. Phys. B180 (1981) 317.
M. Lüscher, K. Symanzik and P. Weisz, Nucl. Phys. B173 (1980) 365.
- [13] J. M. Drummond, arXiv:hep-th/0411017.
- [14] M. Teper, Phys.Lett. B183 (1987) 345.
M. Teper, Nucl.Phys.Proc.Suppl. 4 (1988) 041.
- [15] B. Lucini and M. Teper, Phys.Rev. D64 (2001) 105019 [arXiv:hep-lat/0107007].
- [16] J. Liddle and M. Teper, arXiv:0803.2128.
K. Holland, M. Pepe, and U.-J. Wiese, JHEP 0802 (2008) 041 [arXiv:0712.1216].
- [17] A. Athenodorou, B. Bringoltz and M. Teper, JHEP 1102 (2011) 030 [arXiv:1007.4720].
- [18] B. Bringoltz and M. Teper, Phys.Lett.B663 (2008) 429 [arXiv:0802.1490].
B. Lucini and M. Teper, Phys.Lett. B501 (2001) 128 [arXiv:hep-lat/0012025].
- [19] A. Athenodorou and M. Teper, in preparation.

- [20] N. Isgur and J. Paton, Phys. Rev. D31 (1985) 2910.
- [21] R. Johnson and M. Teper, Phys. Rev. D66 (2002) 036006 [arXiv:hep-ph/0012287].
T. Moretto and M. Teper, [arXiv:hep-lat/9312035].
- [22] D. Karabali, C. Kim and V. Nair, Phys. Lett. B434 (1998) 103, [arXiv:hep-th/9804132].
D. Karabali, V. Nair and A. Yelnikov, Nucl. Phys. B824 (2010) 387 [arXiv:0906.0783].

A Tables

group	β	$a^2\sigma_{k=1}$	$a^2\sigma_{k=2A}$	$a^2\sigma_{k=3A}$	$l_c\sqrt{\sigma_{k=1}}$
SU(2)	16.0	0.0076416(46)	–	–	0.8953(72)
SU(4)	74.0	0.0074480(55)	0.010098(9)	–	1.0543(37)
SU(6)	171.0	0.0073662(37)	0.01198(3)	0.01357(5)	1.0865(41)
SU(8)	306.25	0.0073745(43)	0.01298(4)	0.01635(10)	1.1000(30)

Table 1: String tensions, σ_k , and the critical length, l_c , below which the theory is no longer confining, for the main calculations in this paper.

$SU(8) ; aE(l, p = 0)$							
l/a	$l_{\perp} \times l_t$	$P = +$				$P = -$	
14	100×200	0.05187(14)	0.3839(62)			0.550(16)	0.740(21)
15	100×200	0.06576(14)	0.3985(86)			0.572(20)	0.766(25)
16	100×200	0.07810(11)	0.3967(28)	0.524(19)	0.644(18)	0.5433(43)	0.675(11)
17	100×200	0.08916(24)	0.4031(20)	0.5433(85)	0.645(12)	0.5560(46)	0.654(11)
18	100×200	0.09950(17)	0.4135(13)	0.5673(40)	0.6581(58)	0.5624(32)	0.619(13)
19	100×200	0.10887(18)	0.4139(29)	0.5803(47)	0.6564(68)	0.5637(48)	0.648(14)
20	70×120	0.11868(27)	0.4214(16)	0.5888(41)	0.6333(78)	0.5741(41)	0.6396(94)
21	70×120	0.12679(55)	0.4220(28)	0.5914(45)	0.6520(75)	0.5674(63)	0.6399(88)
22	70×120	0.13653(47)	0.4237(28)	0.5958(71)	0.6355(75)	0.5811(42)	0.6358(77)
23	70×120	0.14509(46)	0.4245(44)	0.5948(57)	0.6538(54)	0.5855(77)	0.657(11)
24	48×60	0.15350(70)	0.4374(40)	0.605(12)	0.635(12)	0.5862(62)	0.639(10)
25	48×60	0.15966(108)	0.4403(49)	0.6154(57)	0.6518(93)	0.5936(89)	0.657(11),
26	48×60	0.17039(62)	0.4408(48)	0.6190(72)	0.6589(78)	0.5928(49)	0.659(15)
27	48×60	0.17836(71)	0.4477(47)	0.6078(93)	0.6554(62)	0.6107(76)	0.656(12)
28	48×60	0.18730(73)	0.4559(37)	0.604(11)	0.6513(71)	0.5986(99)	0.66195(85)
29	48×60	0.19425(71)	0.4614(21)	0.603(14)	0.650(15)	0.6082(95)	0.684(13)
30	48×60	0.20142(78)	0.4644(37)	0.625(11)	0.629(14)	0.6263(74)	0.688(18)
31	40×48	0.20889(80)	0.4664(45)	0.609(13)	0.6687(62)	0.621(12)	0.70015(87)
32	40×48	0.21944(80)	0.4737(40)	0.6370(79)	0.6610(59)	0.6190(83)	0.64489(84)
64	64×64	0.46461(114)	0.6346(53)	0.7505(59)	0.7580(64)	0.7621(54)	0.766(13)

Table 2: The energies, $E(l, p)$, of the lightest flux tube states with length l , parity $P = P_t = \pm$ and longitudinal momentum $p = 0$. For $SU(8)$ at $\beta = 306.25$.

$SU(6) \ ; \ aE(l, p = 0)$						
l/a	$P = +$				$P = -$	
13	0.03301(24)	0.255(15)				
14	0.05234(29)	0.355(13)				
15	0.06581(18)	0.3981(72)				
16	0.07783(11)	0.3905(54)	0.419(30)	0.601(13)	0.486(13)	0.597(14)
17	0.08890(26)	0.4034(39)	0.513(15)	0.607(14)	0.551(10)	0.632(15)
18	0.09894(25)	0.4084(27)	0.560(13)	0.630(10)	0.542(11)	0.614(11)
19	0.10840(26)	0.4163(37)	0.573(10)	0.635(16)	0.5571(78)	0.649(15)
20	0.11805(25)	0.4220(12)	0.5802(55)	0.609(16)	0.5578(75)	0.640(16)
21	0.12739(42)	0.4212(44)	0.5781(75)	0.618(15)	0.5802(82)	0.644(12)
22	0.13660(68)	0.4327(22)	0.6003(87)	0.632(11)	0.5798(84)	0.646(12)
23	0.14571(58)	0.4296(48)	0.6021(87)	0.6469(70)	0.5999(81)	0.6490(92)
24	0.15308(21)	0.4367(27)	0.5938(65)	0.6304(54)	0.5963(54)	0.6364(68)
25	0.16177(41)	0.4410(24)	0.6066(70)	0.6470(53)	0.5837(90)	0.6569(66)
26	0.17054(41)	0.4491(33)	0.6025(73)	0.6454(80)	0.6048(89)	0.6665(65)
27	0.17806(46)	0.4521(17)	0.5952(95)	0.629(10)	0.6035(42)	0.654(14)
28	0.18721(63)	0.4541(23)	0.6164(61)	0.6455(90)	0.6111(39)	0.6676(61)
29	0.19507(49)	0.4550(40)	0.6112(94)	0.6508(55)	0.6159(53)	0.6639(65)
30	0.20371(56)	0.4675(40)	0.6134(93)	0.648(11)	0.6164(89)	0.679(10)
31	0.21005(46)	0.4622(55)	0.6181(62)	0.6631(68)	0.6321(98)	0.672(14)
32	0.2177(9)	0.4724(42)	0.6021(94)	0.631(12)	0.604(10)	0.674(15)
36	0.2494(11)	0.4921(20)	0.6290(49)	0.6475(57)	0.6384(80)	0.6683(62)
40	0.2820(10)	0.5064(30)	0.6464(57)	0.6655(57)	0.6573(52)	0.6761(52)
44	0.3114(11)	0.5292(34)	0.652(11)	0.6781(73)	0.6885(51)	0.6899(50)
48	0.3424(10)	0.5459(36)	0.678(11)	0.6985(60)	0.6964(61)	0.718(12)
52	0.3731(9)	0.5621(37)	0.7072(91)	0.7196(57)	0.7199(72)	0.725(14)
56	0.4060(11)	0.5825(55)	0.720(11)	0.7376(80)	0.7394(57)	0.731(16)
60	0.4339(10)	0.6089(68)	0.733(11)	0.7505(78)	0.7462(74)	0.7506(72)
64	0.4626(16)	0.6322(38)	0.7576(81)	0.7632(82)	0.7605(53)	0.789(19)

Table 3: The energies, $E(l, p)$, of the lightest fundamental flux tube states with length l , parity $P = P_t = \pm$ and longitudinal momentum $p = 0$. For $SU(6)$ at $\beta = 171.0$.

$SU(4) ; aE(l, p = 0)$							
l/a	$l_{\perp} \times l_t$	$P = +, +$				$P = -, -$	$P = -, +$
13	100×200	0.03291(60)				0.6362(43)	0.228(22)
14	80×160	0.05230(61)	0.214(8)			0.6398(21)	0.281(30)
15	80×160	0.06609(46)	0.256(20)			0.6292(40)	0.336(8)
18	70×120	0.10067(34)	0.324(20)			0.6276(39)	0.448(8)
22	60×80	0.13740(46)	0.4285(21)	0.470(12)	0.6044(42)	0.6247(64)	0.5911(22)
26	52×64	0.17213(44)	0.4504(29)	0.532(7)	0.6199(44)	0.6341(44)	0.6040(38)
30	48×64	0.20607(47)	0.4707(16)	0.575(13)	0.6333(24)	0.6493(23)	0.6253(50)
34	48×64	0.23684(57)	0.4866(17)	0.5980(76)	0.6517(14)	0.6505(47)	0.6405(24)
38	48×64	0.26946(50)	0.5074(9)	0.6381(22)	0.6678(13)	0.6650(47)	0.6583(22)
44	52×64	0.31510(62)	0.5363(10)	0.6551(43)	0.6887(24)	0.6981(31)	0.6800(25)
52	52×64	0.3774(7)	0.5724(22)	0.7037(51)	0.7092(33)	0.7246(49)	0.7184(20)
58	58×64	0.4226(5)	0.6059(17)	0.7328(38)	0.7429(44)	0.7451(44)	0.7485(21)

Table 4: The energies, $E(l, p)$, of the lightest fundamental flux tube states with length l , parity $P = \{P_t, P_{\parallel}\}$ and longitudinal momentum $p = 0$. For $SU(4)$ at $\beta = 74.0$.

$SU(2) ; aE(l, p = 0)$							
l/a	$l_{\perp} \times l_t$	$P = +, +$				$P = -, -$	$P = -, +$
11	100×160	0.01898(20)	0.1053(53)	0.167(16)	0.294(12)	0.8422(13)	0.3075(48)
14	80×140	0.06128(16)	0.2593(29)	0.355(17)	0.377(42)	0.7574(64)	0.4372(38)
18	70×120	0.10504(16)	0.3997(51)	0.5051(35)	0.507(10)	0.7201(13)	0.5728(57)
22	60×80	0.14180(29)	0.5045(11)	0.499(10)	0.6529(45)	0.7013(12)	0.6430(22)
26	52×64	0.17750(24)	0.5028(11)	0.5914(46)	0.7000(40)	0.6942(18)	0.6881(31)
30	48×64	0.21075(37)	0.5045(18)	0.6376(56)	0.7014(62)	0.6812(41)	0.7185(32)
34	48×64	0.24382(43)	0.5155(8)	0.6445(91)	0.7361(28)	0.7000(17)	0.7284(16)
38	48×64	0.27612(60)	0.5287(13)	0.6820(24)	0.7482(56)	0.7027(31)	0.7281(44)
44	44×54	0.3242(9)	0.5537(13)	0.6866(69)	0.7541(73)	0.7210(38)	0.7296(32)
46	46×52	0.34058(60)	0.5589(12)	0.7103(24)	0.7657(34)	0.7328(26)	0.7371(28)
58	58×48	0.43466(74)	0.6237(21)	0.7686(24)	0.7964(38)	0.7793(65)	0.7375(37)
68	68×48	0.5140(12)	0.6848(18)	0.8252(27)	0.8476(44)	0.8270(92)	0.771(24)

Table 5: The energies, $E(l, p)$, of the lightest fundamental flux tube states with length l , parity $P = \{P_t, P_{\parallel}\}$ and longitudinal momentum $p = 0$. For $SU(2)$ at $\beta = 16.0$.

$aE_k(l, p = 0)$							
$SU(4)$			$SU(6)$				
l/a	$k = 2A$		l/a	$k = 2A$		$k = 3A$	
13			16	0.1460(14)	0.2778(168)	0.1742(11)	0.3962(75)
14	0.0727(20)	0.144(12)	20	0.2088(17)	0.3794(121)	0.2433(21)	0.4627(99)
15			24	0.2649(23)	0.4740(80)	0.3020(32)	0.5178(72)
18	0.1463(9)	0.264(11)	28	0.3198(29)	0.5346(84)	0.3569(39)	0.570(16)
22	0.1951(8)	0.4092(78)	32	0.3633(22)	0.5672(63)	0.4198(53)	0.613(12)
26	0.2409(7)	0.4570(85)	36	0.4192(25)	0.6131(77)	0.4762(50)	0.667(13)
30	0.2859(9)	0.5081(38)	40	0.4615(42)	0.6551(106)	0.5259(67)	0.732(15)
34	0.3258(9)	0.5484(13)	44	0.5144(50)	0.7158(133)	0.5806(74)	0.789(13)
38	0.3700(14)	0.5891(20)	48	0.5624(40)	0.7508(142)	0.6405(79)	0.840(11)
44	0.4346(10)	0.6483(17)	52	0.6183(60)	0.8019(113)	0.7015(83)	0.893(17)
52	0.5123(14)	0.7075(26)	64	0.7661(109)	0.9448(61)	0.863(14)	1.003(41)
58	0.5769(13)	0.7646(26)					
60	0.5974(17)	0.7817(20)					

Table 6: The energies of the ground and first excited states of a flux tube of length l and momentum $p = 0$ carrying flux $k = 2A$ and $k = 3A$. For $SU(4)$ at $\beta = 74$ and $SU(6)$ at $\beta = 171$ as shown.

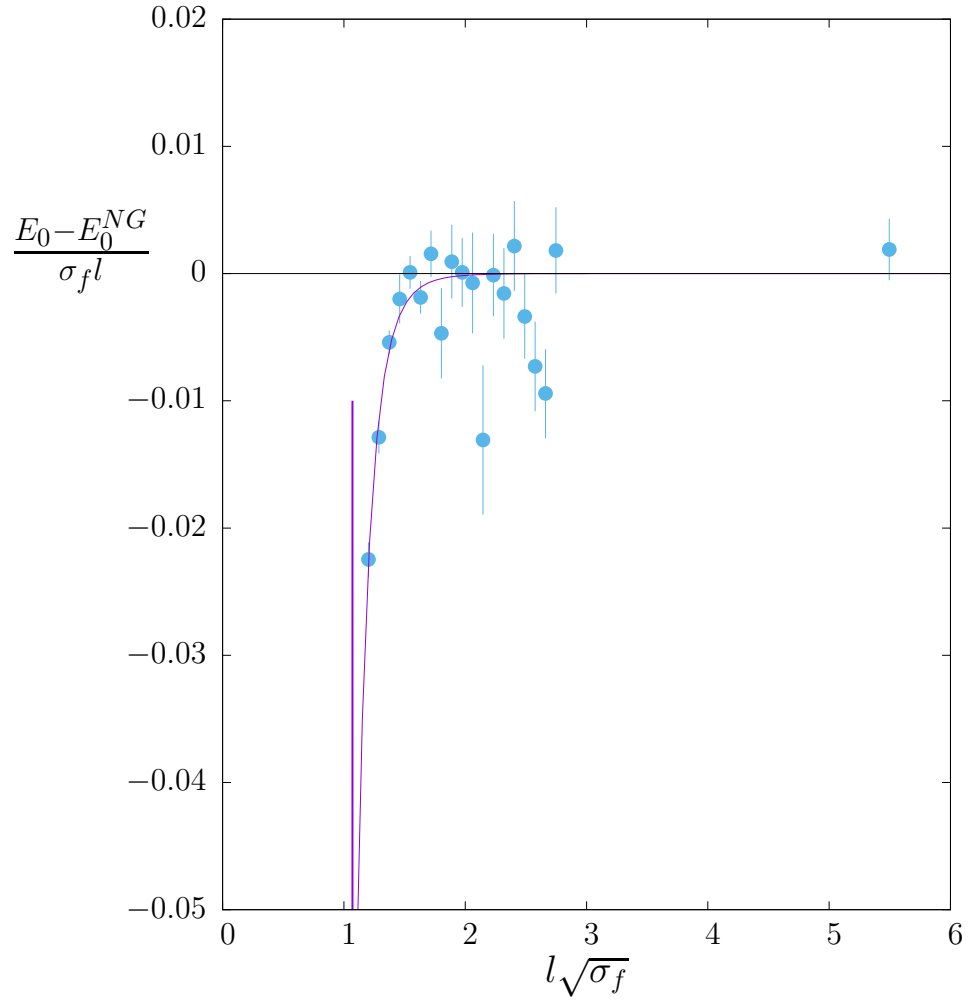


Figure 1: Best fits to SU(8) ground state energy with Nambu-Goto plus a $O(1/l^9)$ correction. Vertical line indicates the deconfining transition.

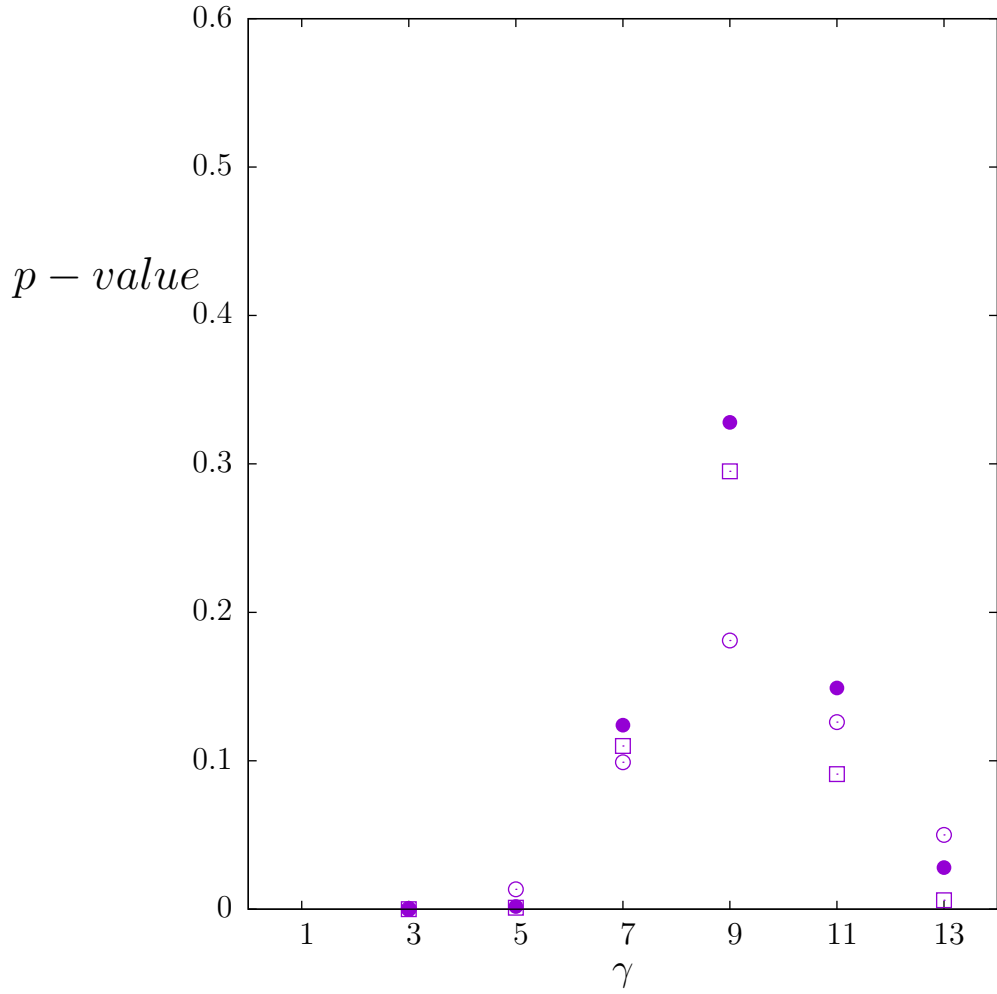


Figure 2: Best fits to SU(8) ground state using Nambu-Goto with a $O(1/l^\gamma)$ correction for various γ : p -value for $l \in [14, 17]$ for three mass fits as explained in text.

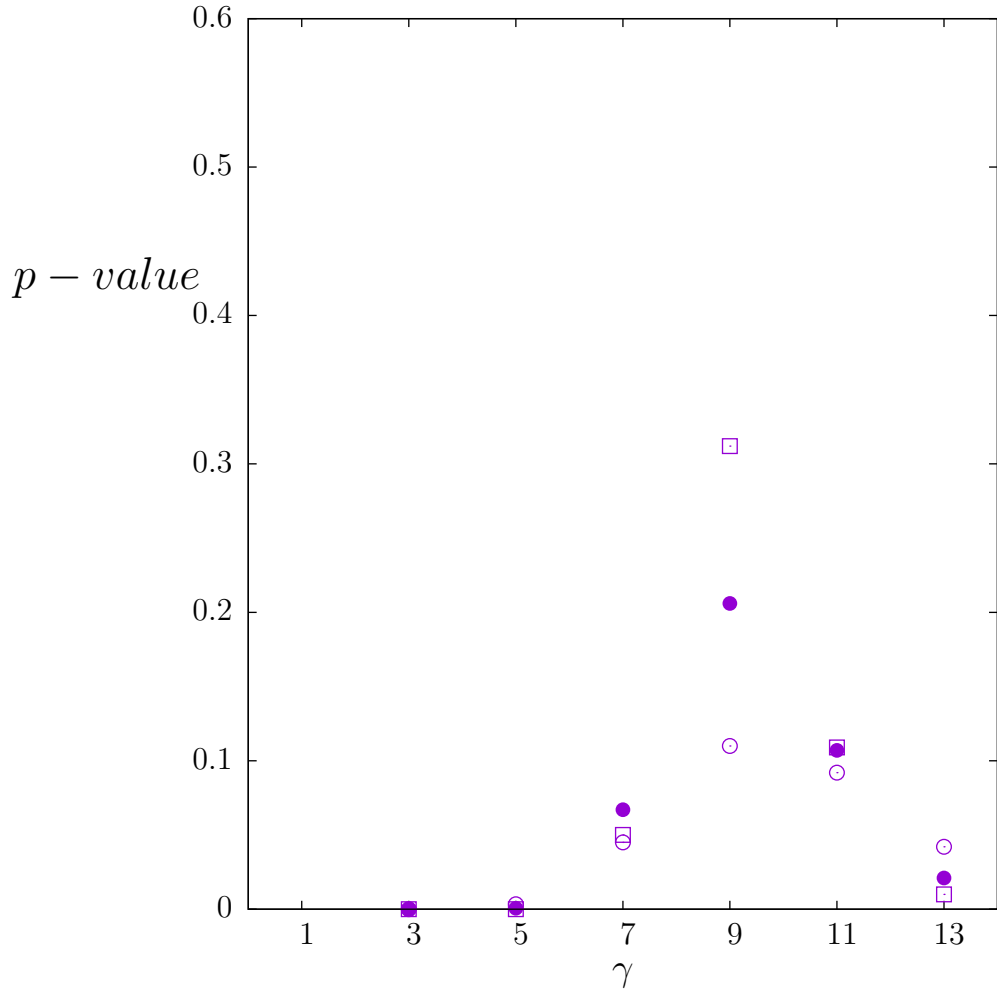


Figure 3: Best fits to SU(8) ground state using Nambu-Goto with a $O(1/l^\gamma)$ correction for various γ : p -value for $l \in [14, 18]$ for three mass fits as explained in text.

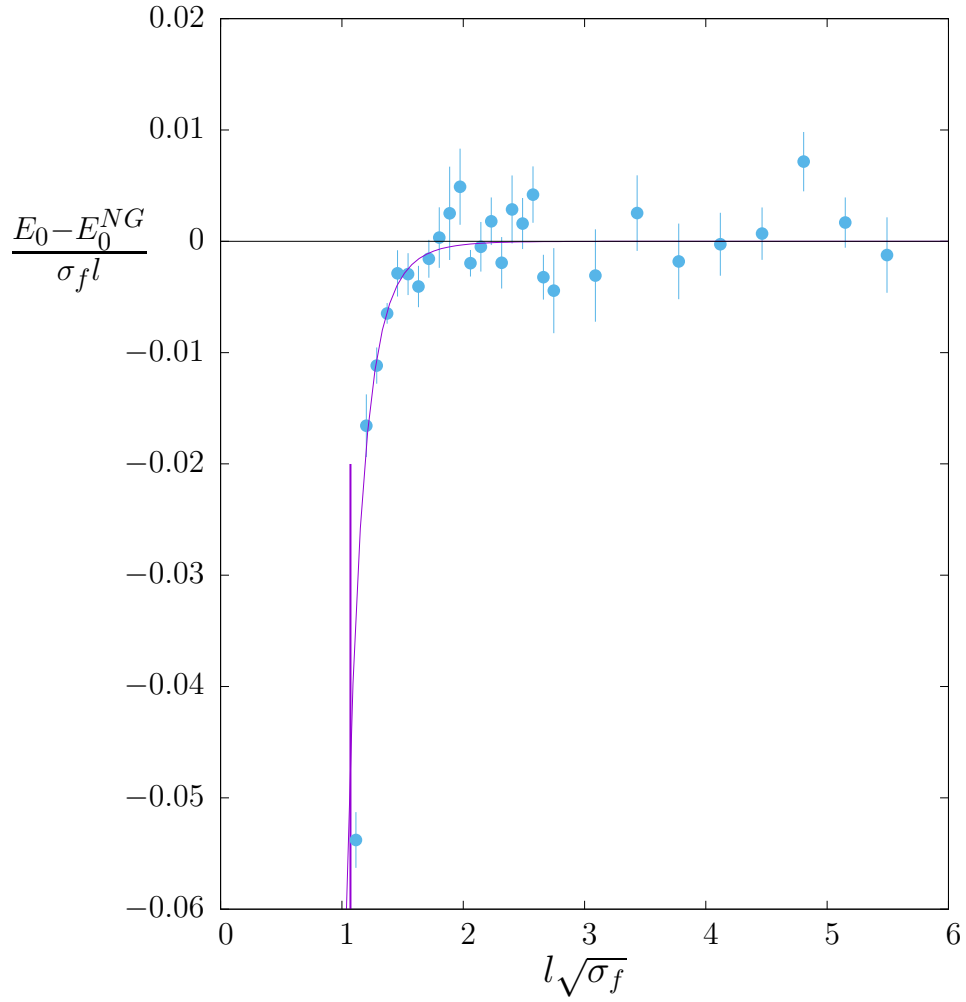


Figure 4: Best fits to SU(6) ground state energy with Nambu-Goto plus a $O(1/l^7)$ correction. Vertical line indicates the deconfining transition.

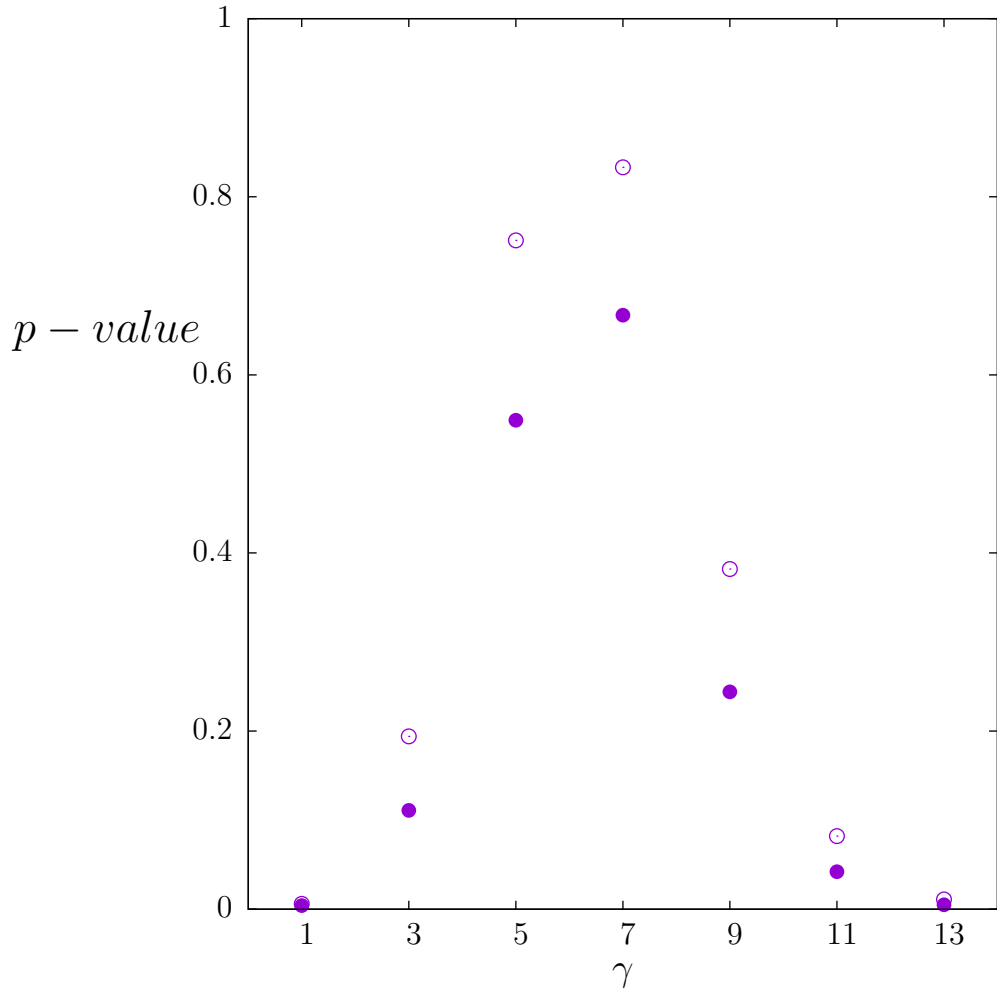


Figure 5: Best fits to SU(6) ground state energy using Nambu-Goto with a $O(1/l^r)$ correction: p -value for $l \in [14, 17]$, ●, and for $l \in [14, 18]$, ○, versus γ .

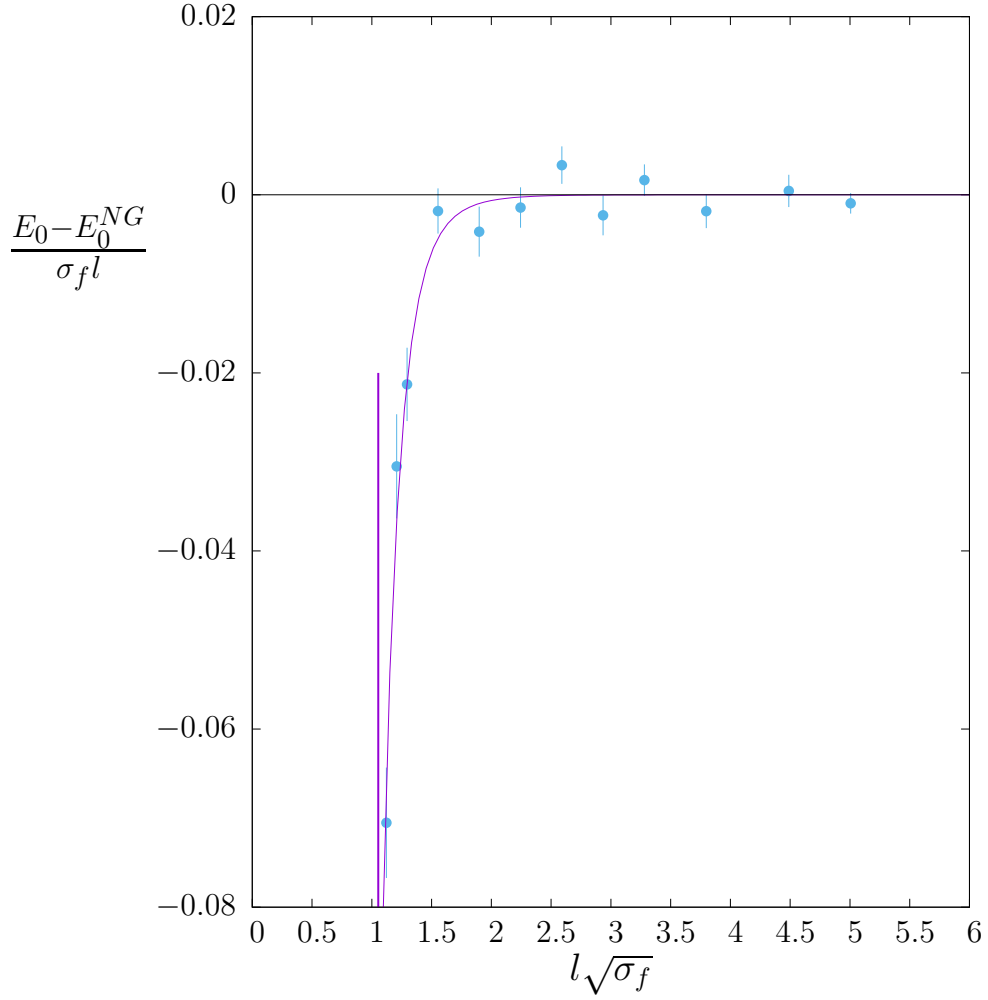


Figure 6: Best fits to SU(4) $k = 1$ ground state energy with Nambu-Goto plus a $O(1/l^7)$ correction. Vertical line indicates the deconfining transition.

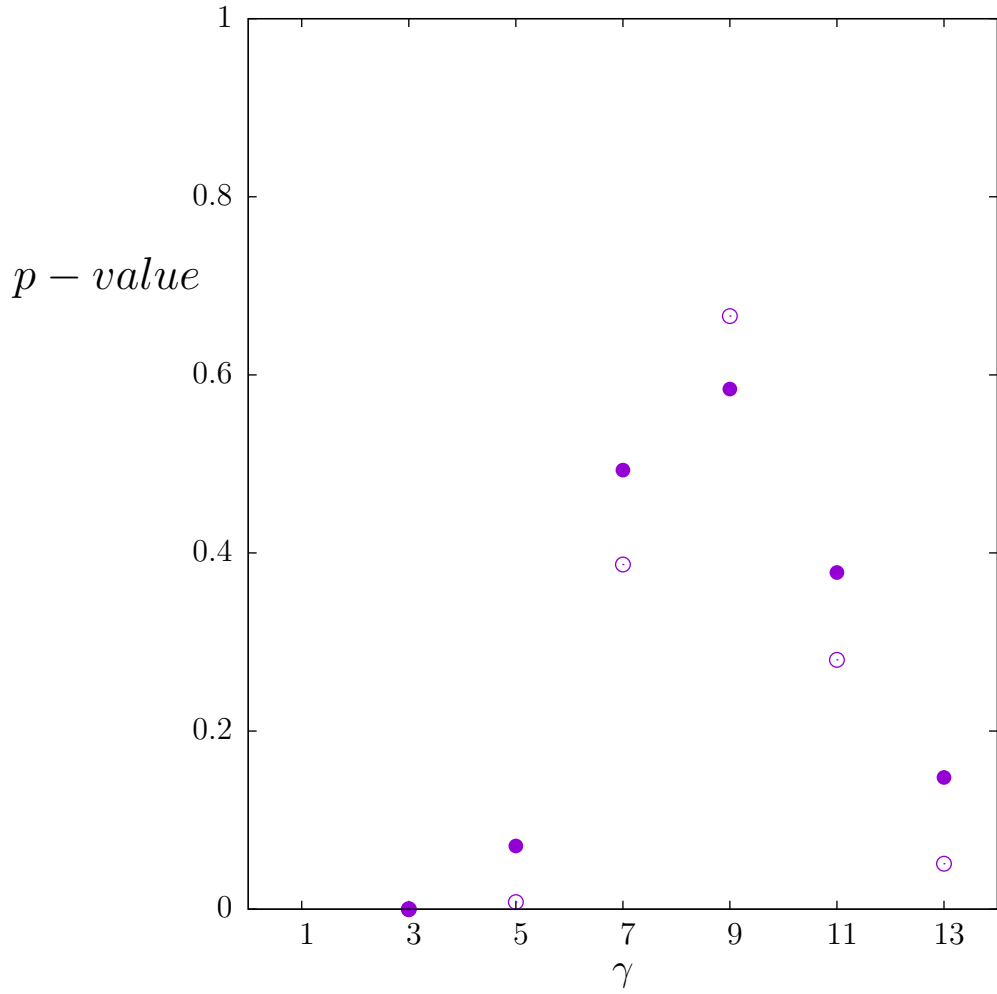


Figure 7: Best fits to SU(4) $k = 1$ ground state energy using Nambu-Goto with a $O(1/l^\gamma)$ correction: p -value for all $l \in [13, 60]$, \bullet , and for $l \in [13, 18]$, \circ , versus γ .

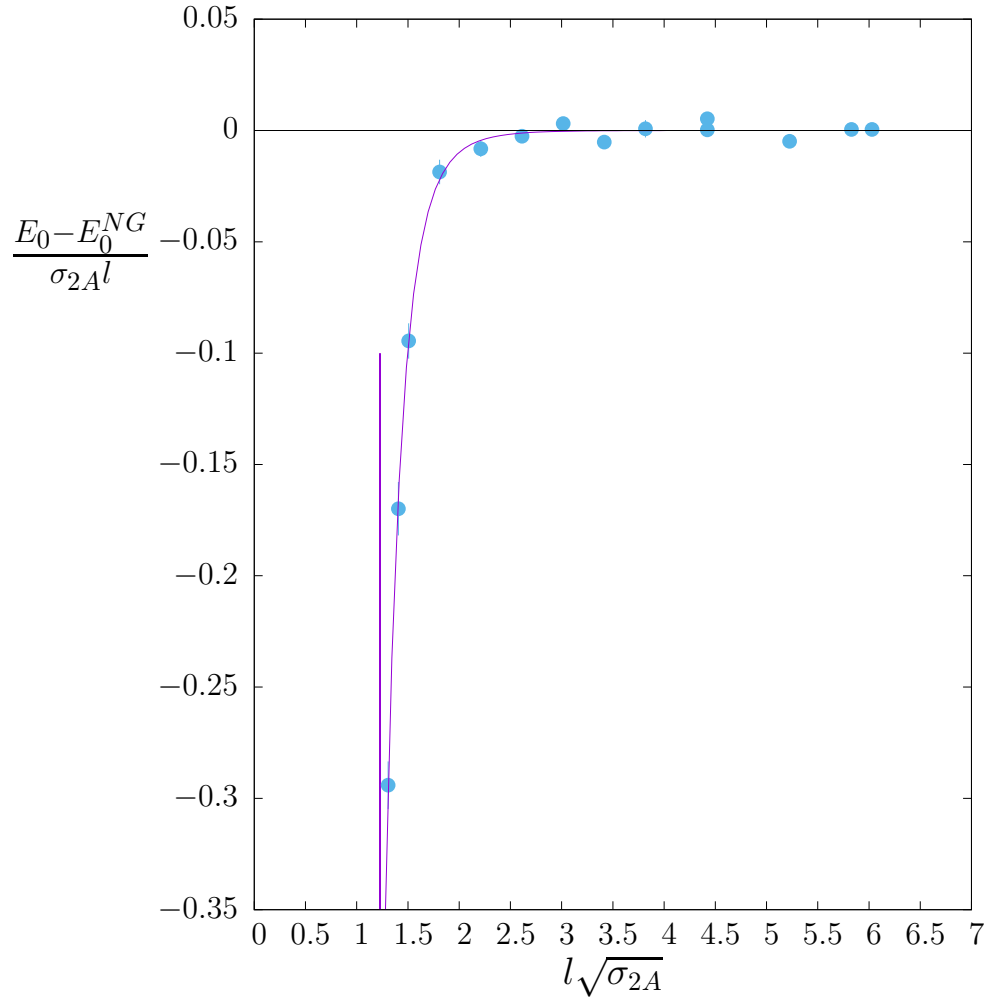


Figure 8: Best fits to SU(4) $k = 2A$ ground state energy with Nambu-Goto plus a $O(1/l^7)$ correction. Vertical line indicates the deconfining transition.

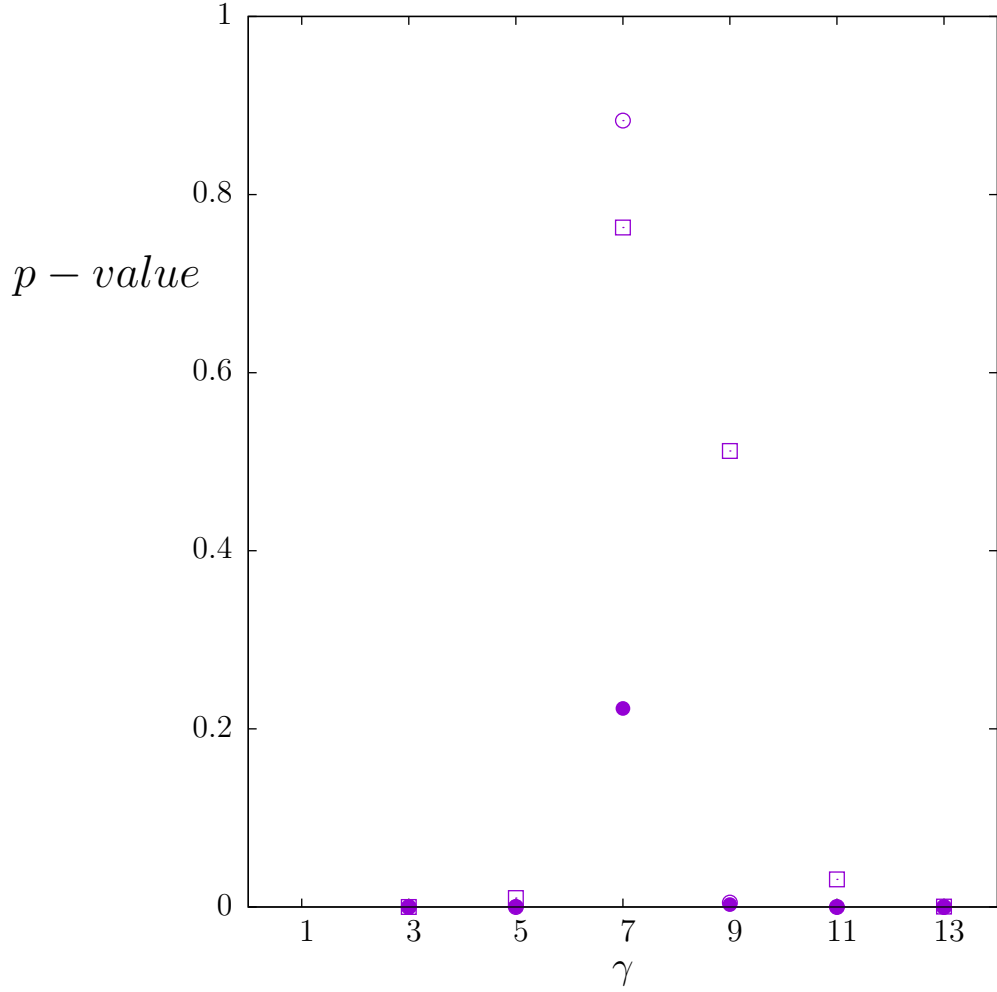


Figure 9: Best fits to $SU(4)$ $k = 2A$ ground state energy using Nambu-Goto with a $O(1/l^\gamma)$ correction: p -value for all $l \in [13, 60]$, \bullet , and for $l \in [13, 18]$, \circ , versus γ . Also fits $l \in [14, 18]$, \square , that exclude the shortest flux tube.

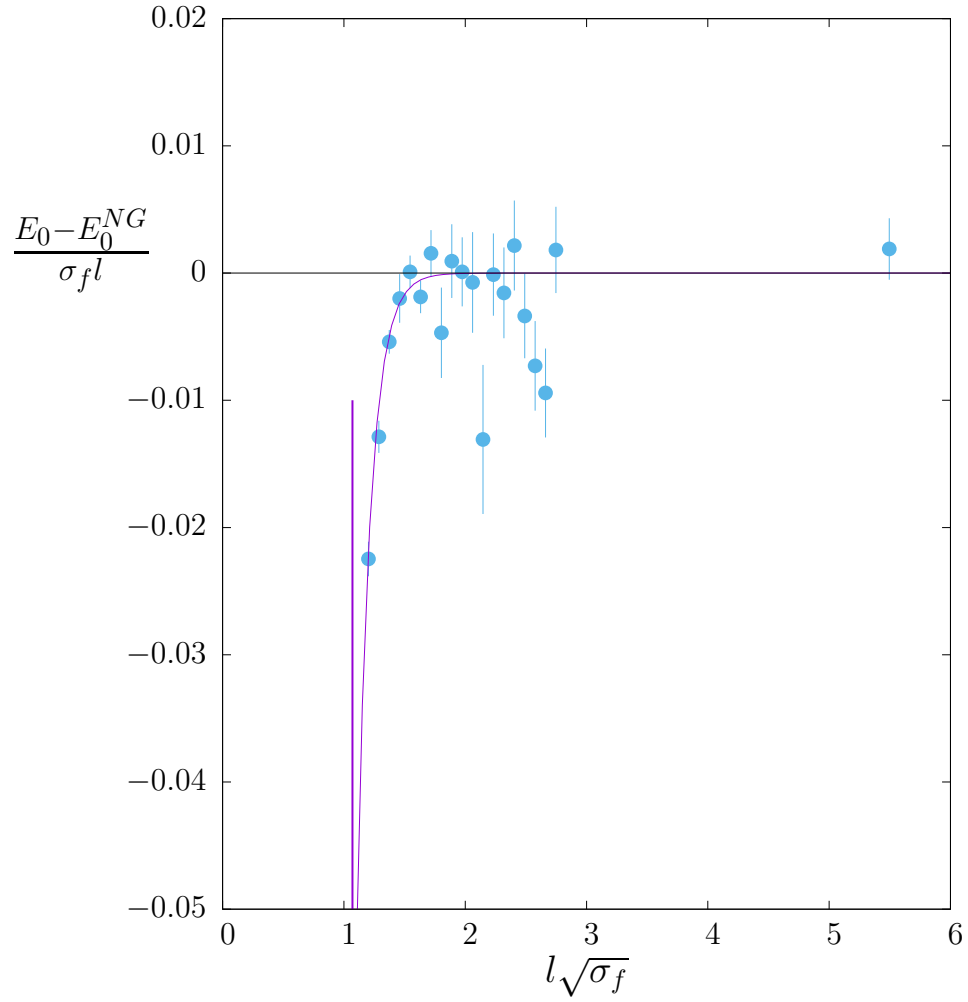


Figure 10: Best fits to SU(8) ground state energy with Nambu-Goto plus a $\propto e^{-\mu l}$ correction. Vertical line indicates the deconfining transition.

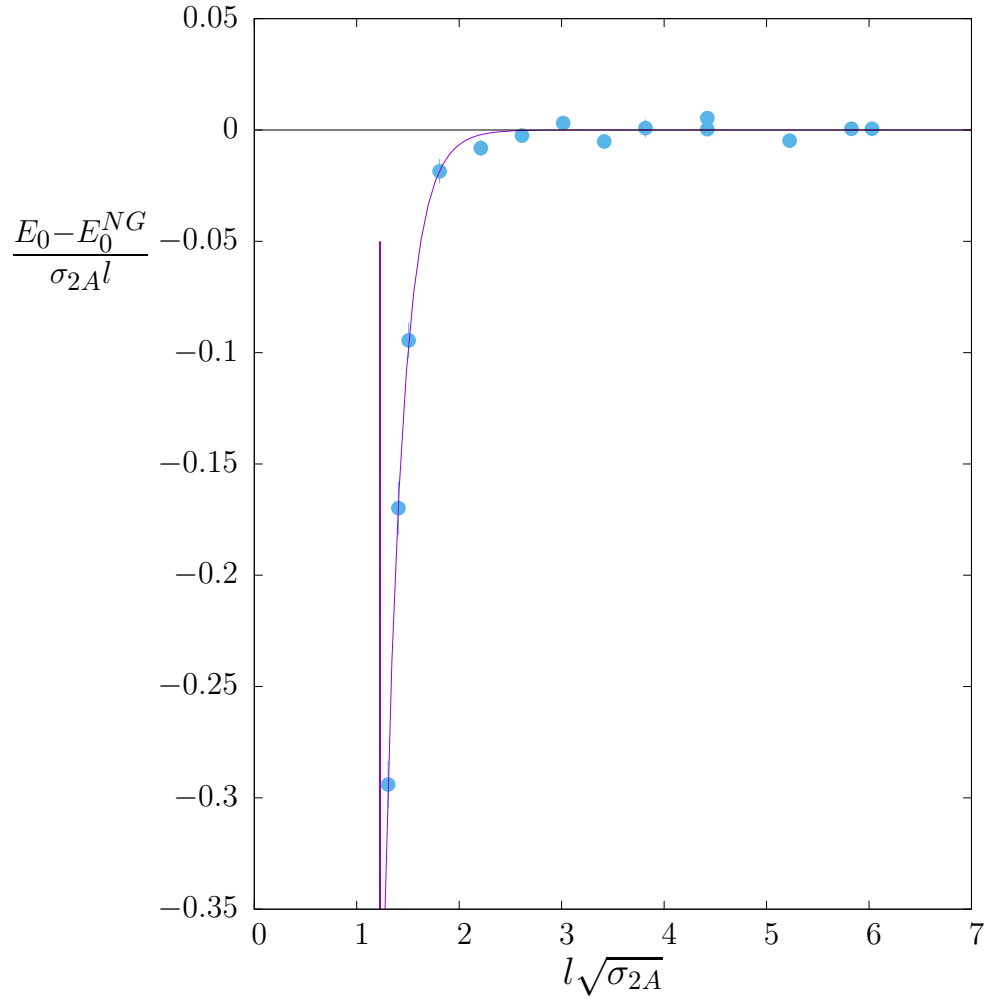


Figure 11: Best fits to SU(4) $k = 2A$ ground state energy with Nambu-Goto plus a $\propto e^{-\mu l}$ correction. Vertical line indicates the deconfining transition.

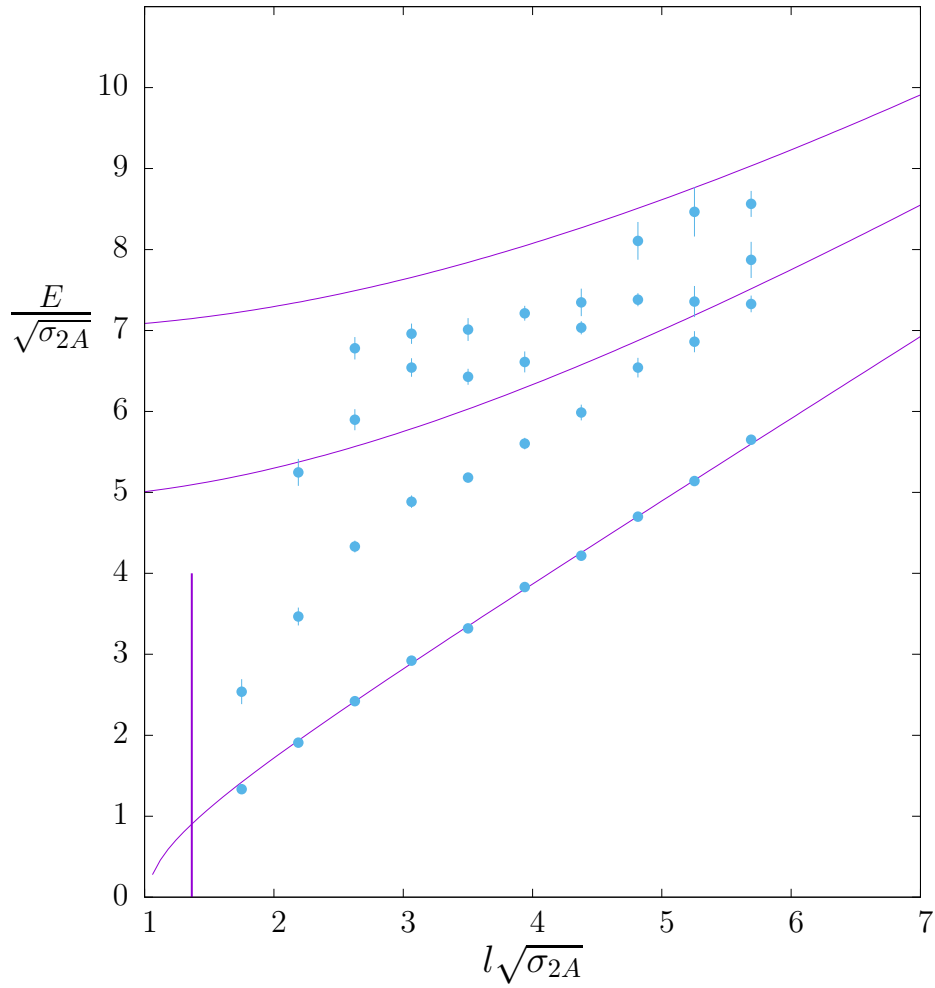


Figure 12: SU(6) at $\beta = 171$. $k = 2A$ spectrum with $p = 0$ and parity $P_t = +$, Vertical line locates deconfining transition.

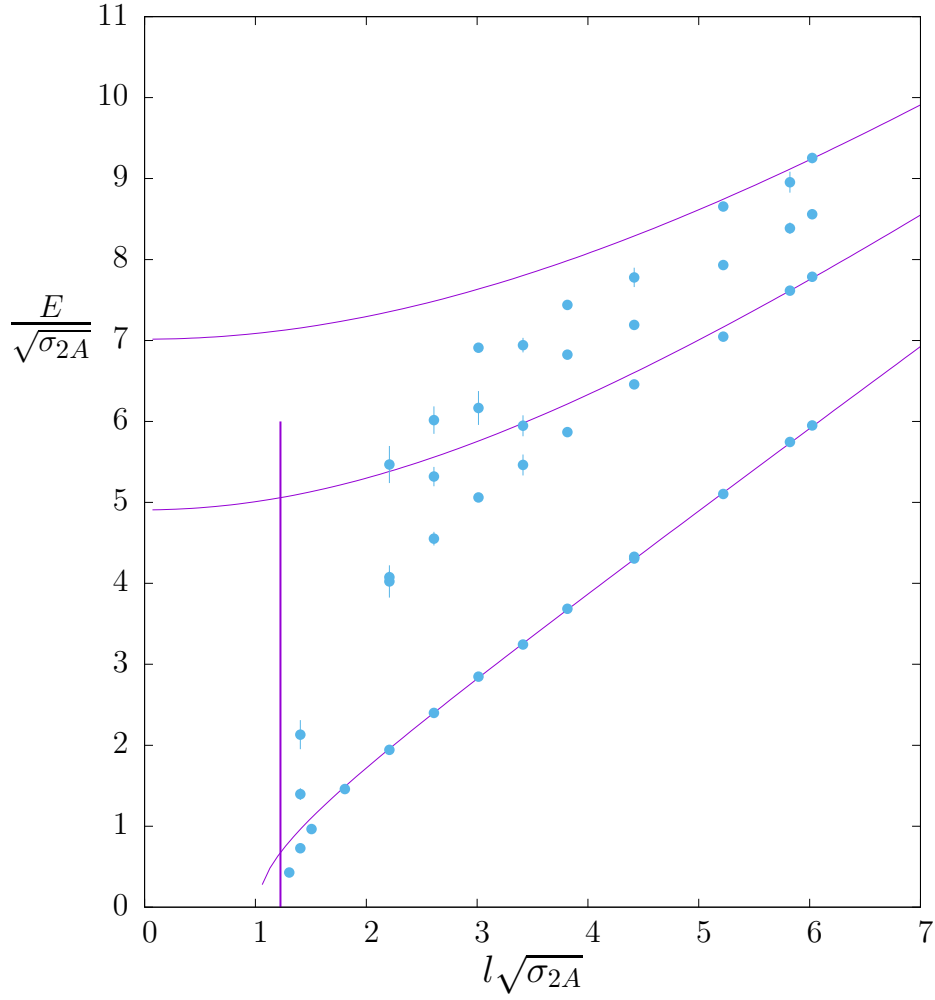


Figure 13: SU(4) at $\beta = 74$. Lightest $k = 2A$ states with $p = 0$ and parities $P_t, P_{\parallel} = +, +$. Vertical line locates deconfining transition.

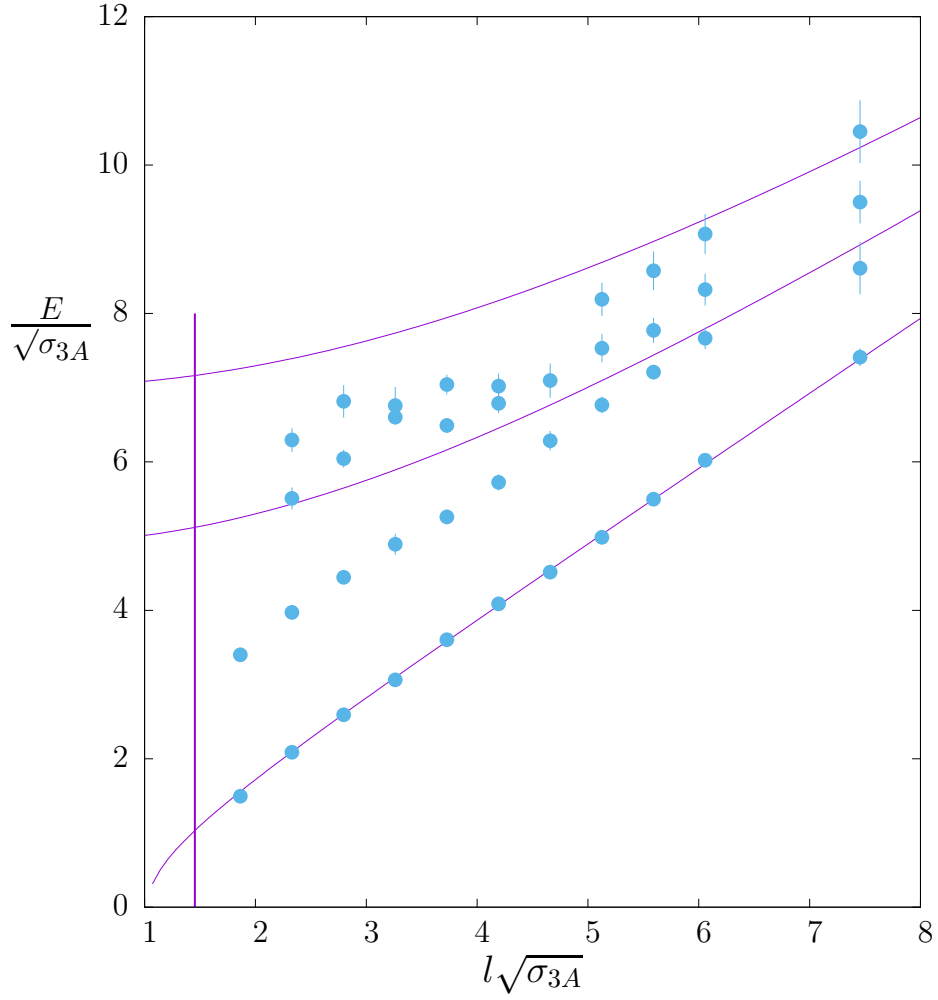


Figure 14: SU(6) at $\beta = 171$. $k = 3A$ spectrum with $p = 0$ and parity $P_t = +$, Vertical line locates deconfining transition.

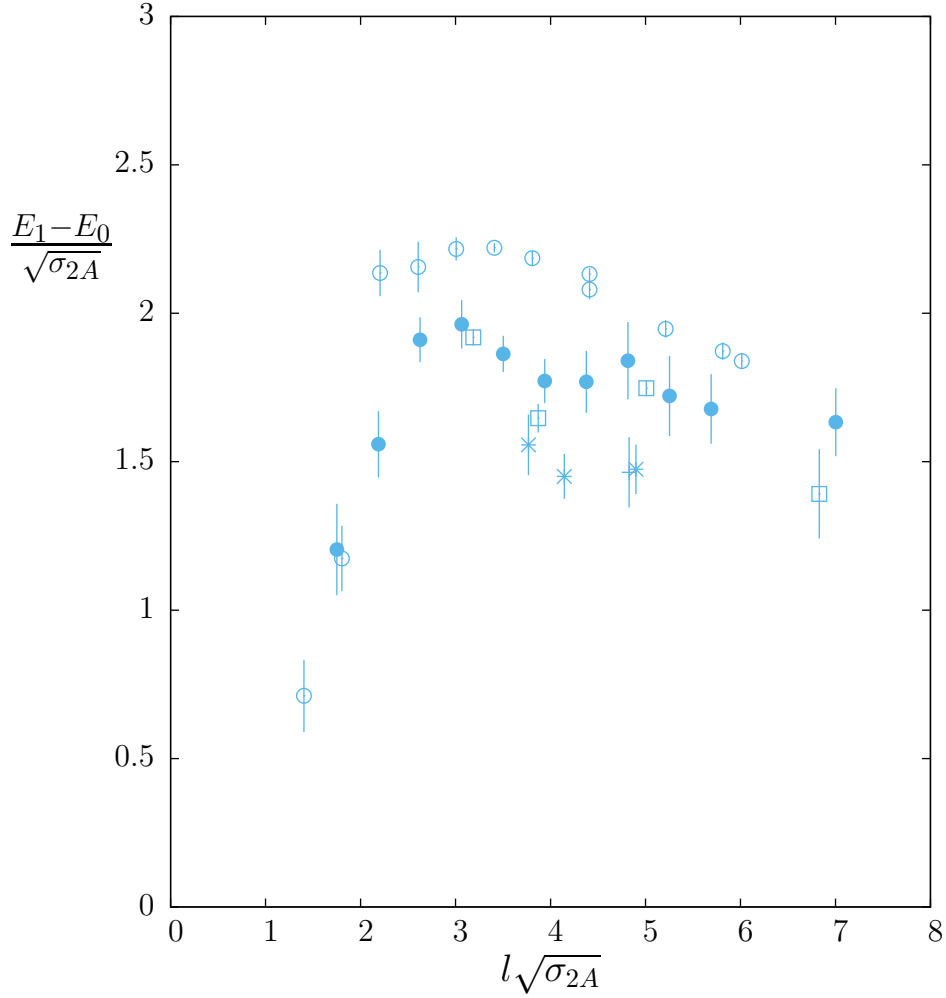


Figure 15: Difference between ground and first excited energies of a $k = 2A$ flux tube of length l , in units of the $k = 2A$ string tension. For $SU(4)$, \circ , $SU(6)$, \bullet , $SU(8)$, \square , $SU(12)$, $+$, and $SU(16)$, \star .

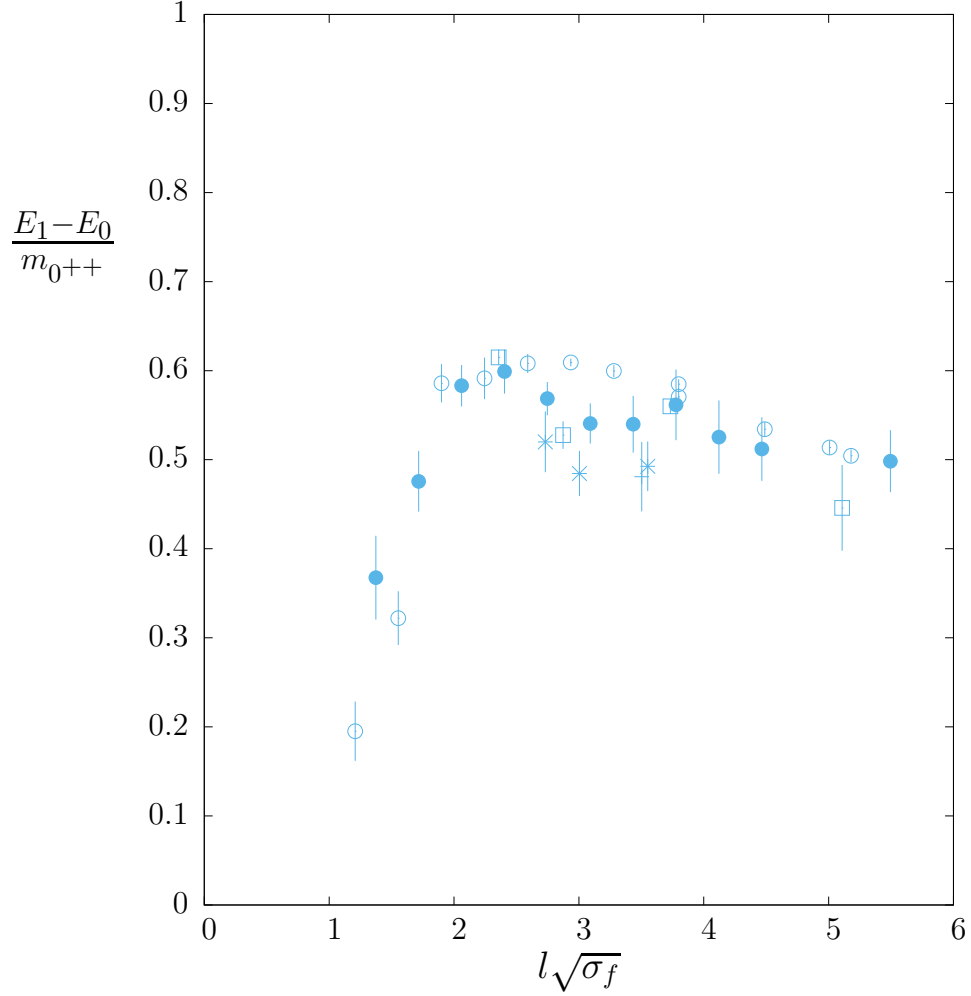


Figure 16: Difference between ground and first excited energies of a $k = 2A$ flux tube of length l , in units of the $l = \infty$ mass gap. For $SU(4)$, \circ , $SU(6)$, \bullet , $SU(8)$, \square , $SU(12)$, $+$, and $SU(16)$, \star .

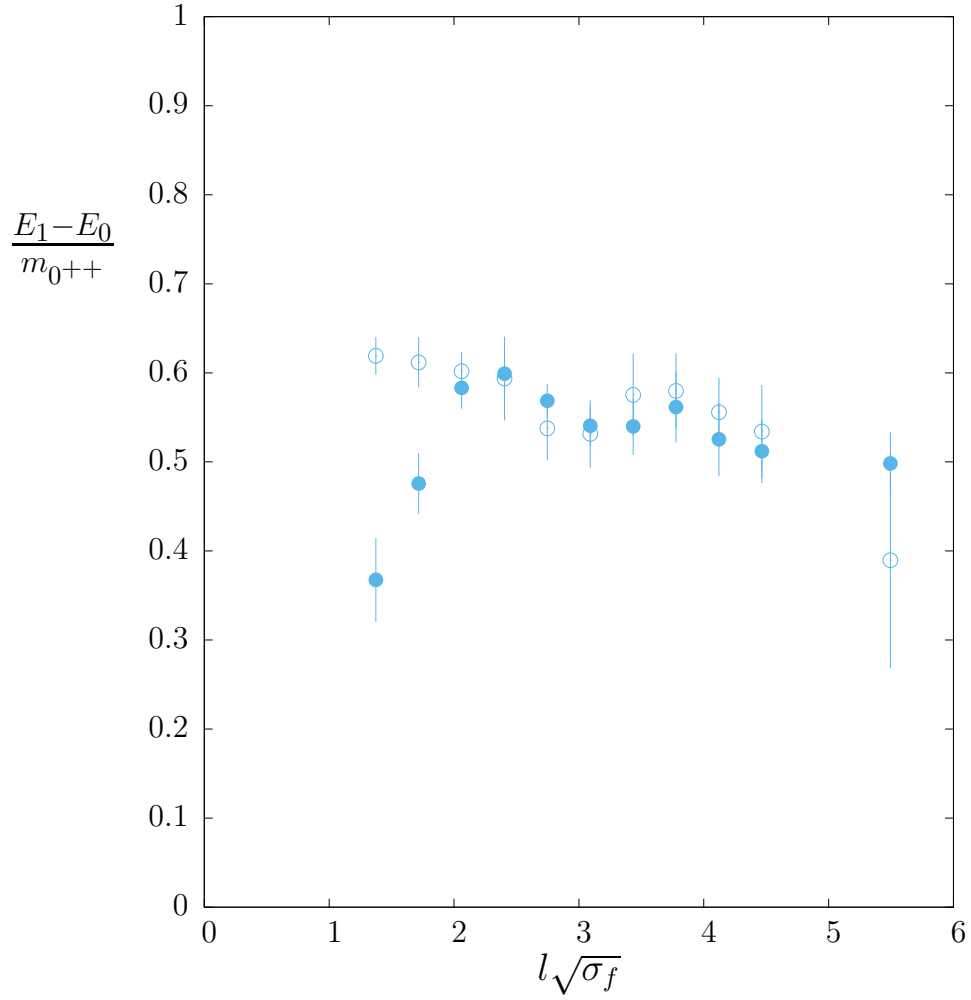


Figure 17: Difference between ground and first excited energies of a $k = 2A$, \bullet , and $k = 3A$, \circ , flux tubes of length l , in units of the $l = \infty$ mass gap. For $SU(6)$ at $\beta = 171$.

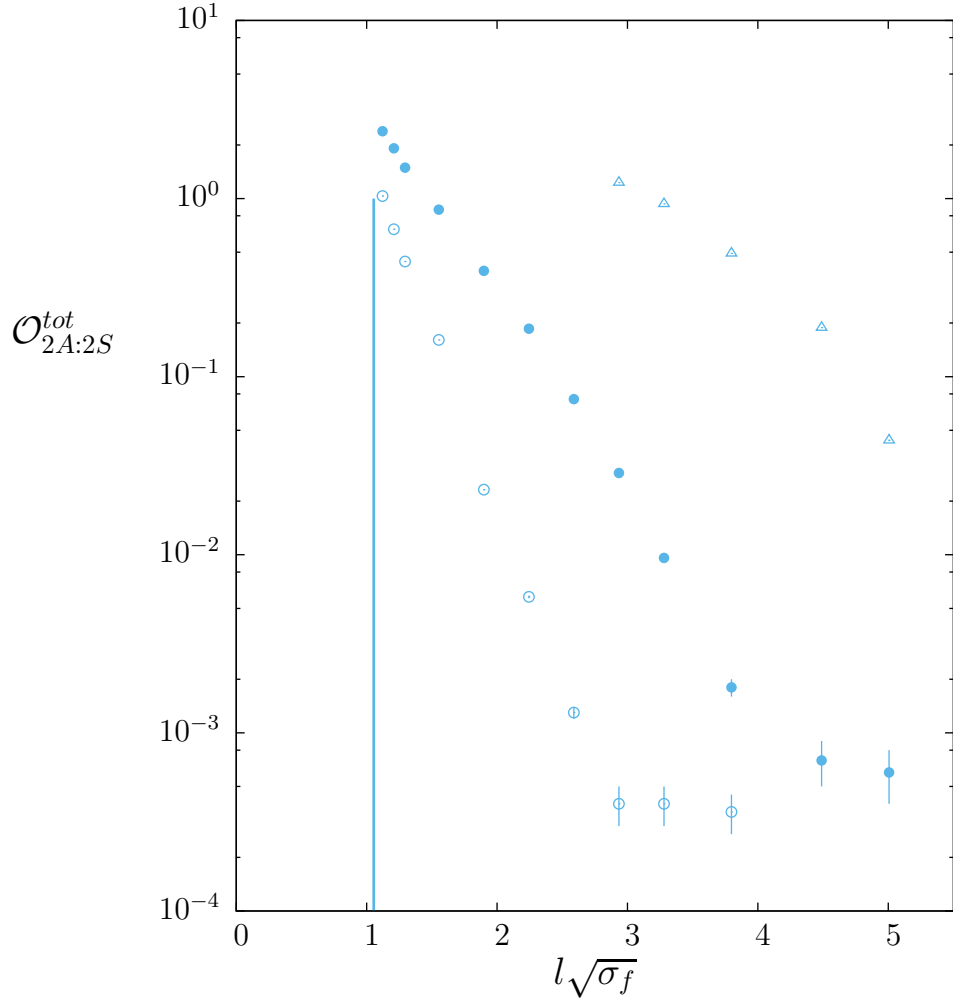


Figure 18: Overlap squared of $k=2A$ basis onto the $k=2S$ basis, using blocking levels 1 to 4, \circ , 1 to 5, \bullet , and 1 to 6, \triangle . Normalisation such that maximum possible overlap is 68, 85, 102 respectively. In $SU(4)$ at $\beta = 74$. Vertical line locates the deconfining transition.

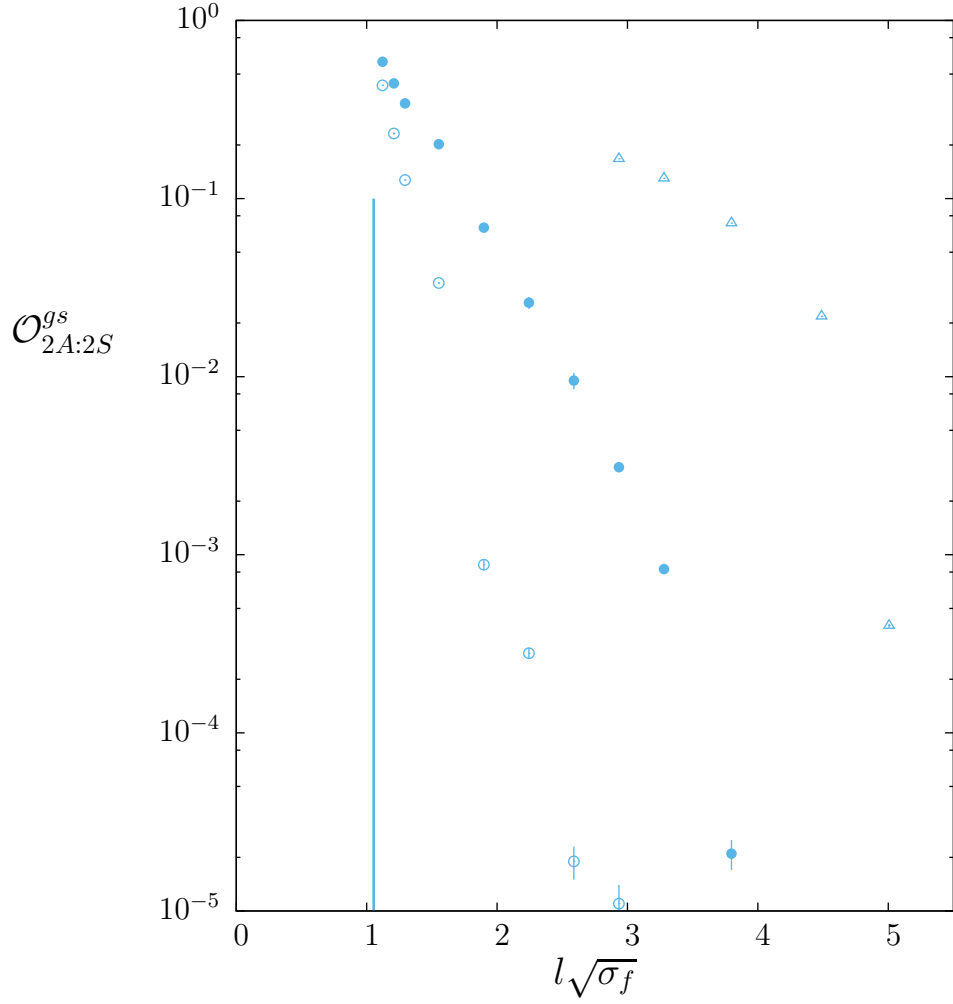


Figure 19: Overlap squared of $k=2A$ (variational) ground state onto the whole $k=2S$ operator basis, using blocking levels 1 to 4, \circ , 1 to 5, \bullet , and 1 to 6, \triangle . In $SU(4)$ at $\beta = 74$. Vertical line locates the deconfining transition.

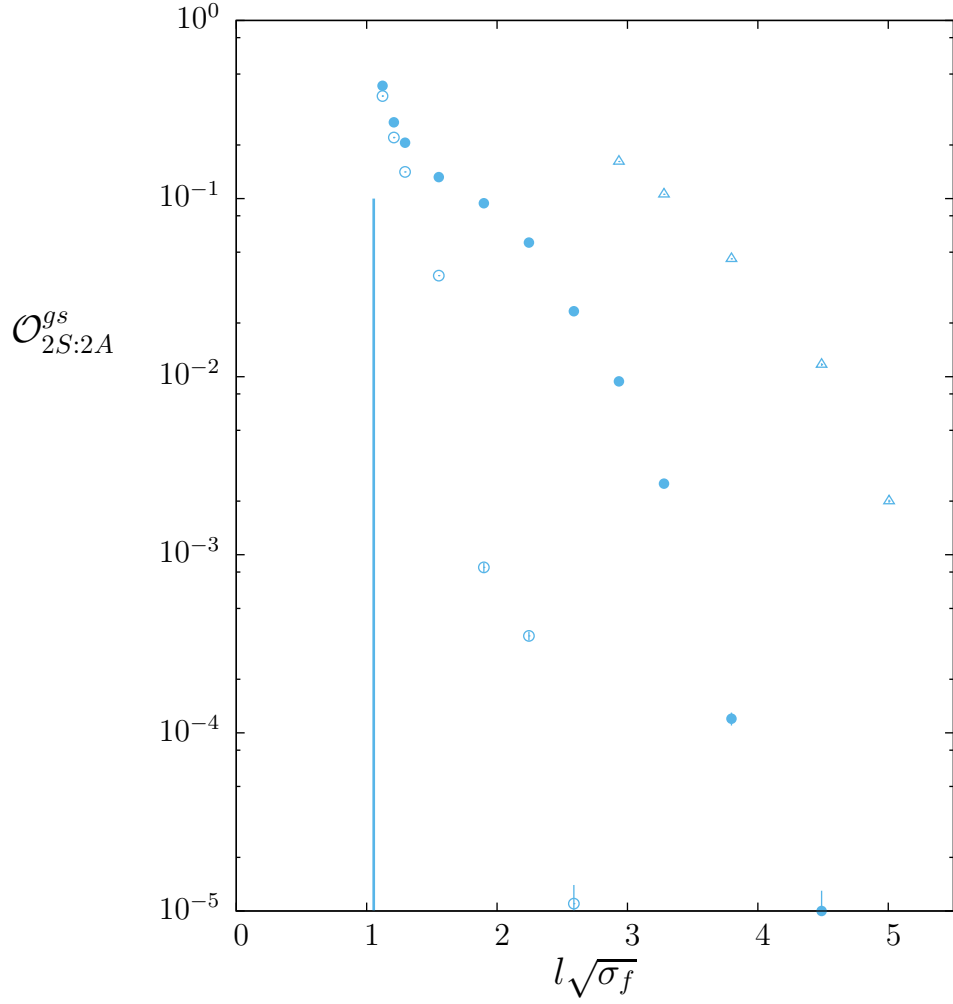


Figure 20: Overlap squared of $k=2S$ (variational) ground state onto the whole $k=2A$ operator basis, using blocking levels 1 to 4, \circ , 1 to 5, \bullet , and 1 to 6, \triangle . In $SU(4)$ at $\beta = 74$. Vertical line locates the deconfining transition.

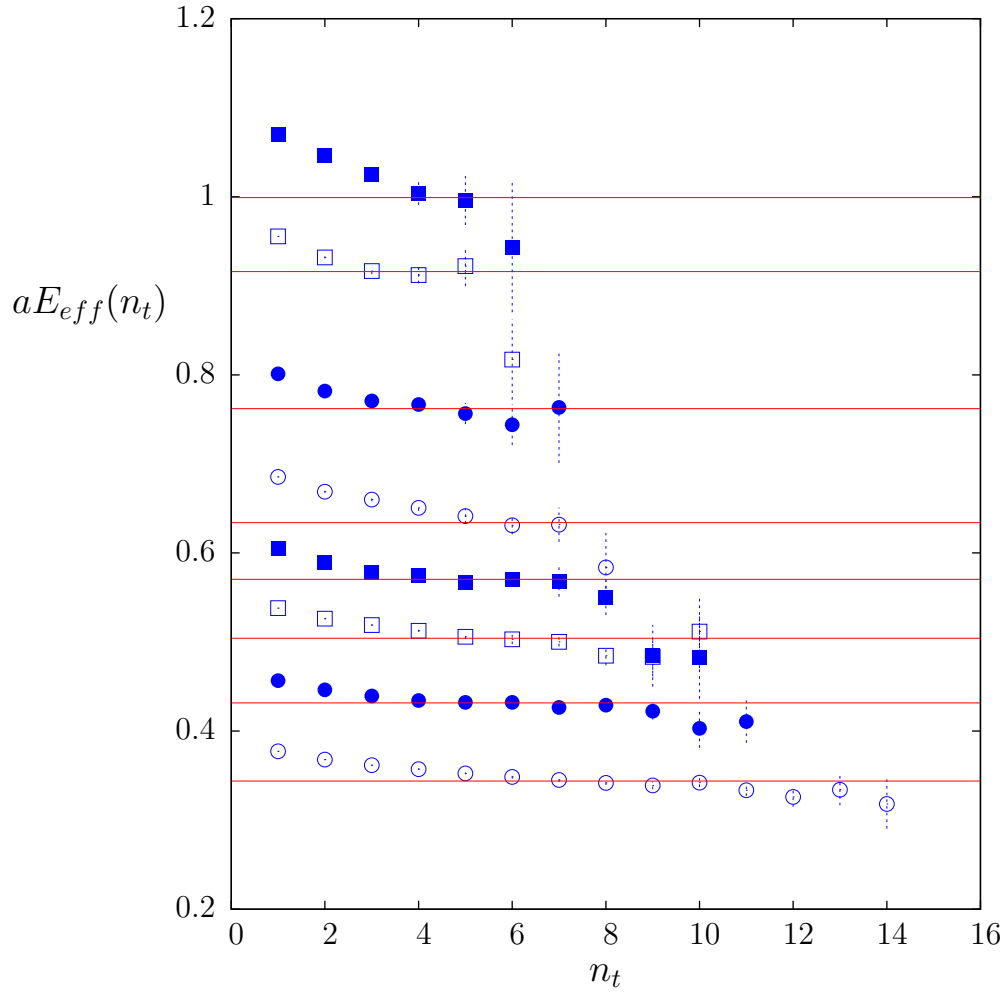


Figure 21: Effective energy of the $k=2S$ (variational) ground state versus $n_t = t/a$, for $l = 22, 26, 30, 34, 38, 44, 52, 58$ (in ascending order), in $SU(4)$ at $\beta = 74$.

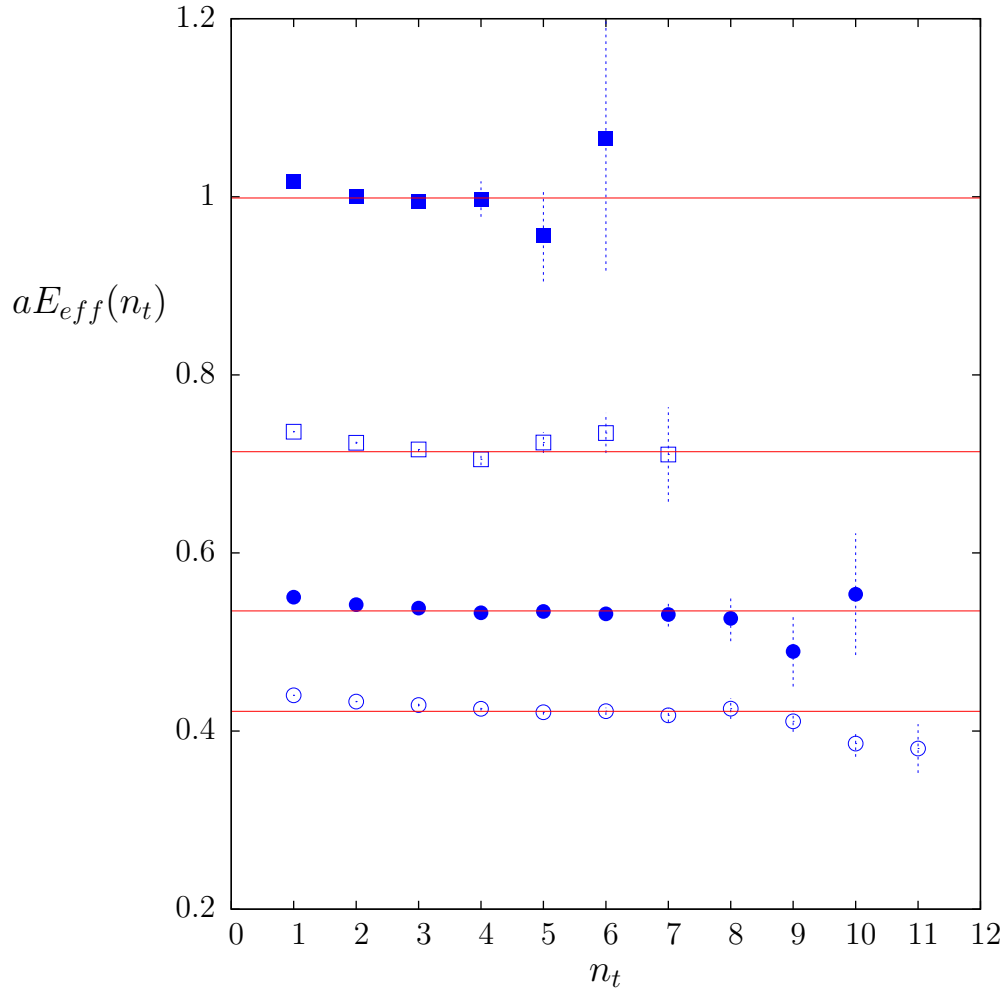


Figure 22: Effective energy of the k=2S (variational) ground state versus $n_t = t/a$, for $l = 28, 34, 44, 60$ (in ascending order), in $SU(8)$ at $\beta = 306.25$.

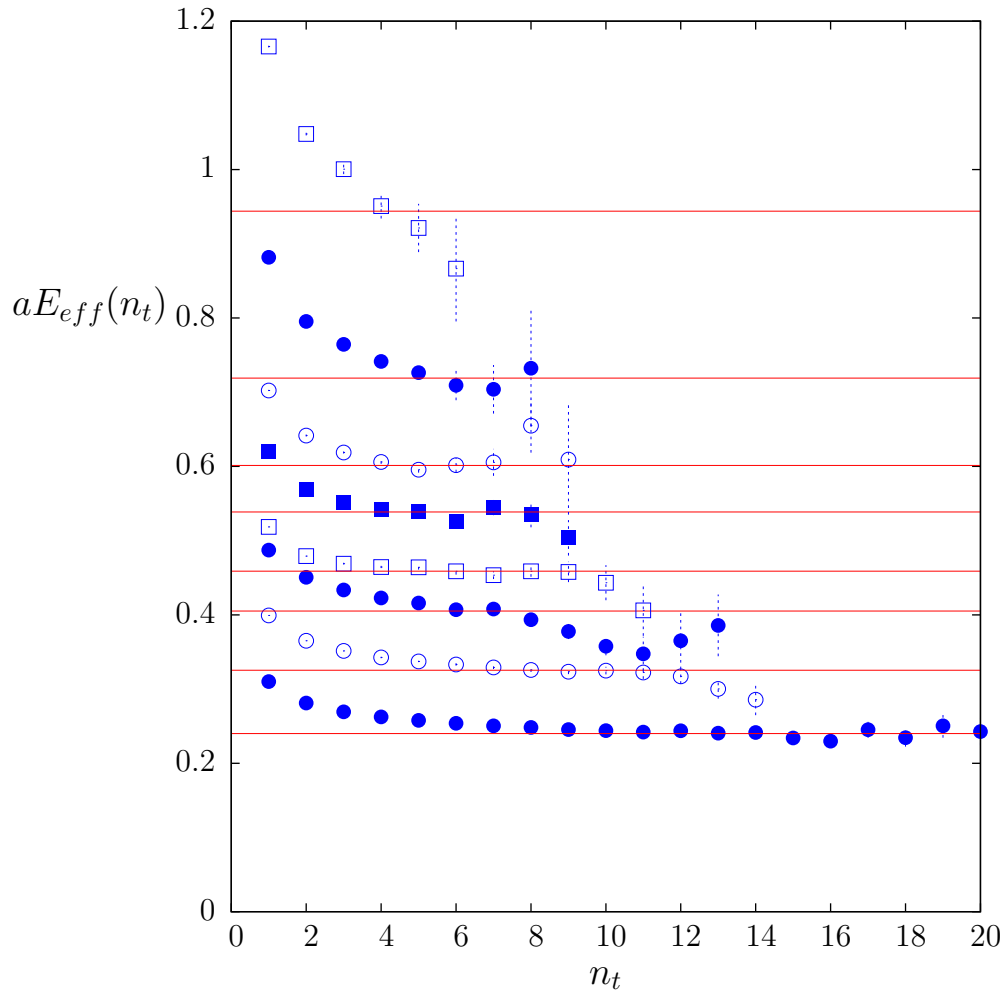


Figure 23: Effective energy of the adjoint $k=0$ ground state versus $n_t = t/a$, for $l = 18, 22, 26, 30, 34, 38, 46, 58$ (in ascending order), in $SU(2)$ at $\beta = 16$.

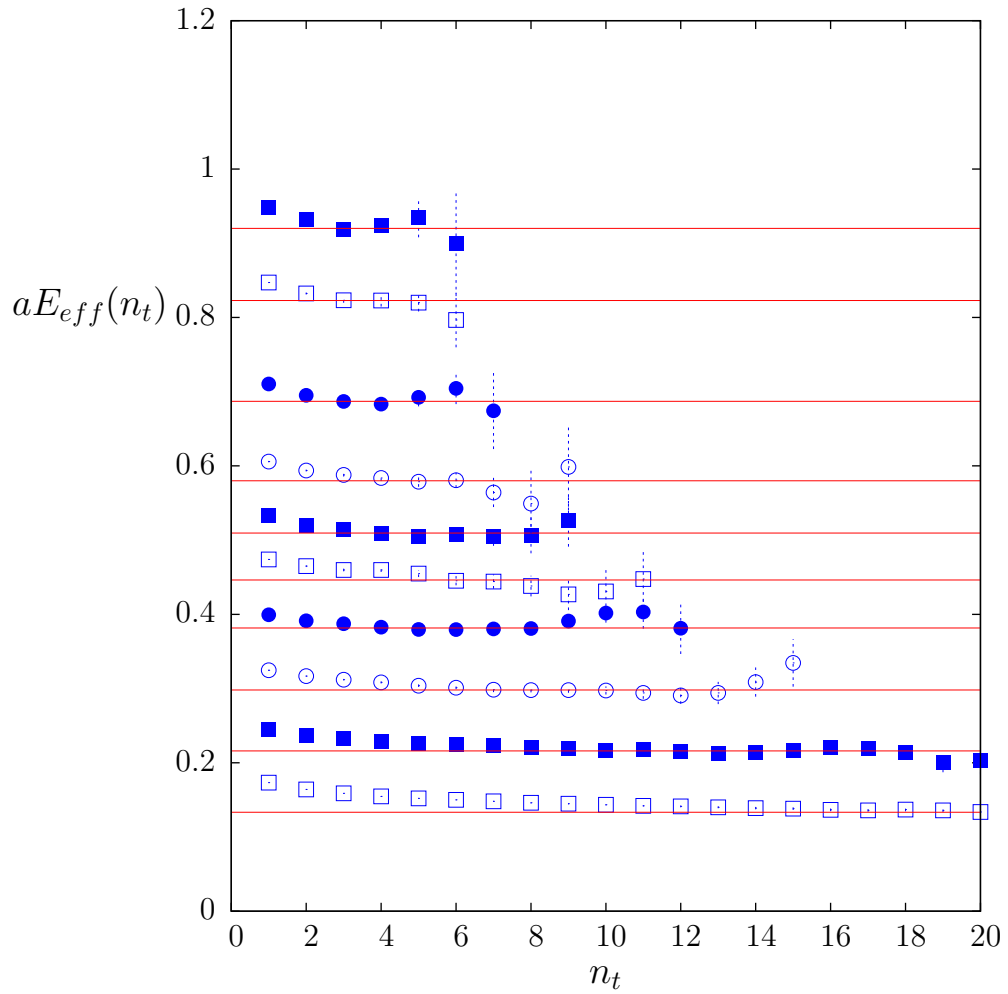


Figure 24: Effective energy of the adjoint $k=0$ ground state versus $n_t = t/a$, for $l = 15, 18, 22, 26, 30, 34, 38, 44, 52, 58$ (in ascending order), in $SU(4)$ at $\beta = 74$.

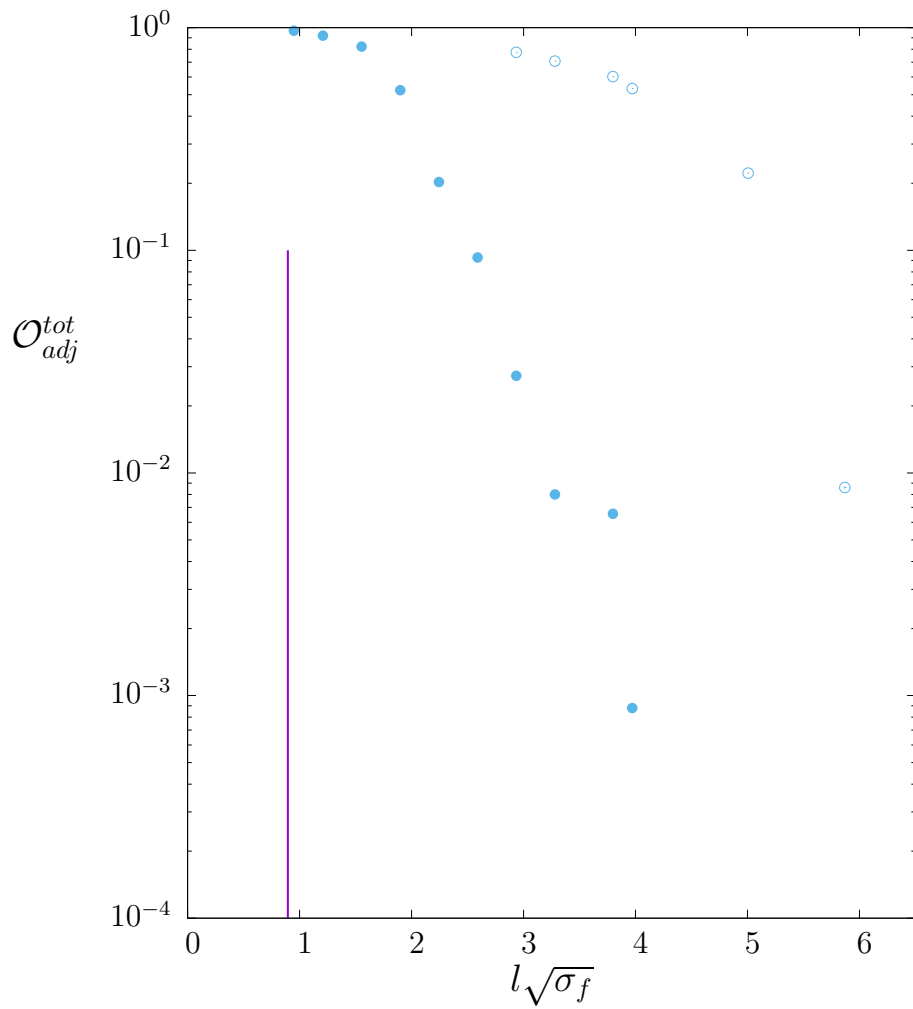


Figure 25: Overlap squared of our adjoint flux loop basis on to vacuum, in SU(2) at $\beta = 16$. Operators up to blocking level 5, \bullet , and up to 6, \circ . Vertical line denotes deconfining transition.

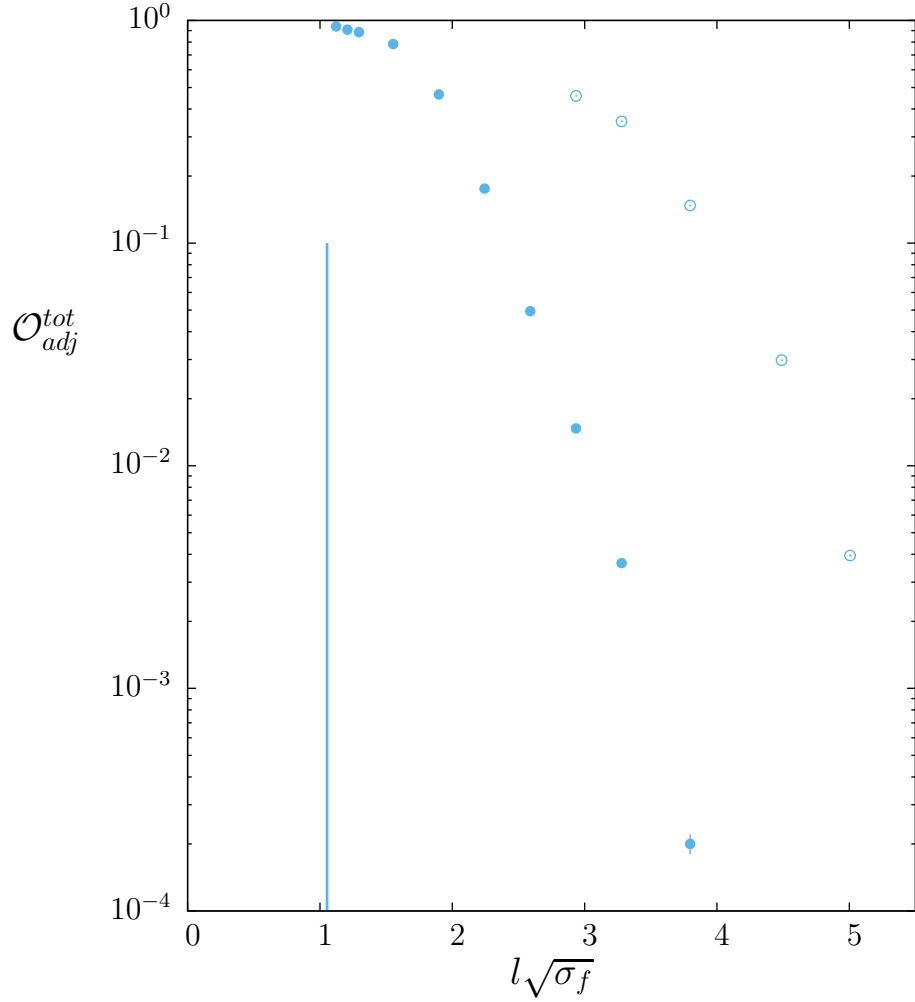


Figure 26: Overlap squared of our adjoint flux loop basis on to the vacuum, where basis includes operators up to blocking level 5, ●, and 6, ○. In SU(4) at $\beta = 74$. Vertical line denotes deconfining transition.

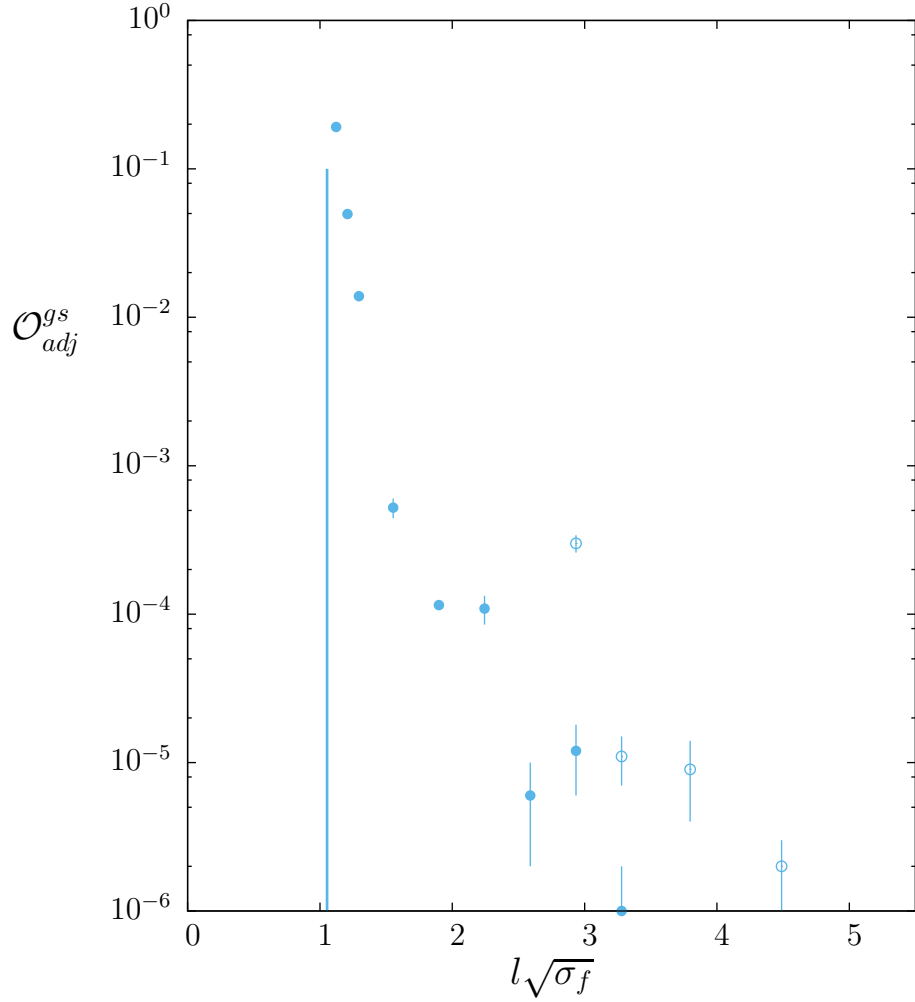


Figure 27: Overlap squared of the best variational ground state adjoint flux loop operator onto to vacuum, where basis includes operators up to blocking level 5, ●, and 6, ○. In SU(4) at $\beta = 74$. Vertical line denotes deconfining transition.

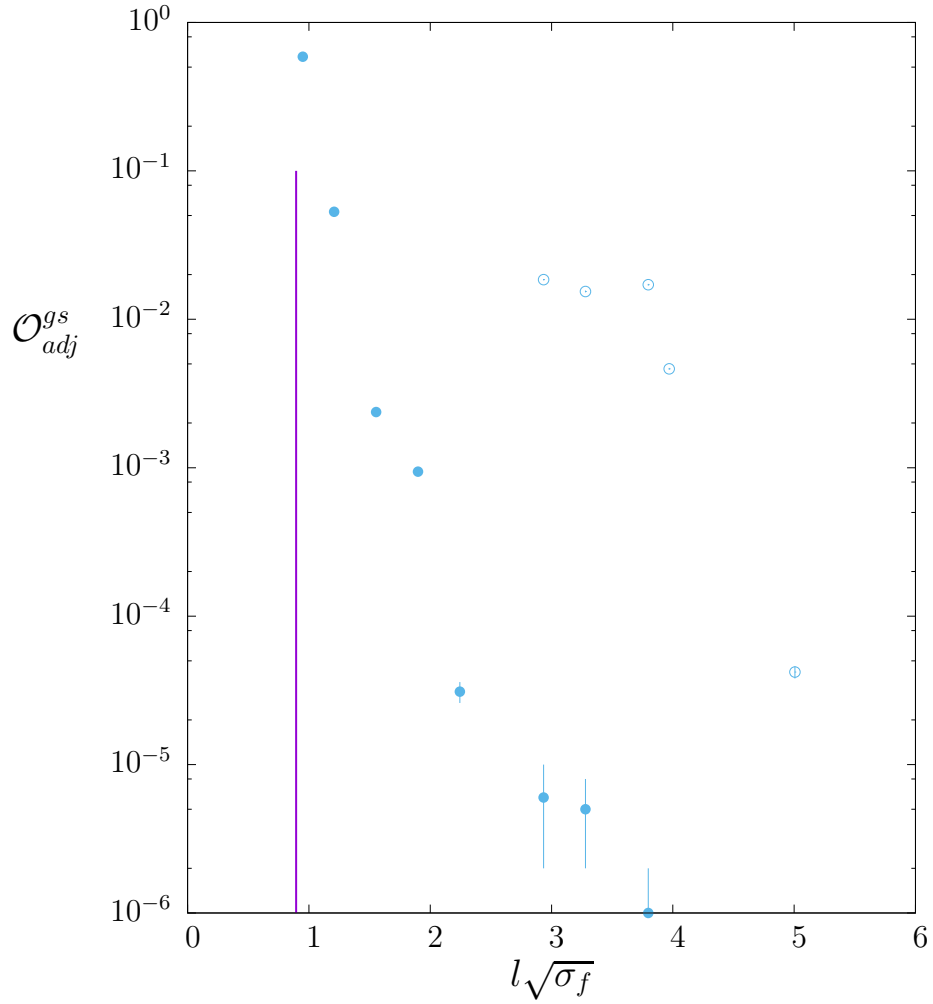


Figure 28: Overlap squared of the best ground state adjoint flux loop operator onto to vacuum, in SU(2) at $\beta = 16$. Operators up to blocking level 5, \bullet , and up to 6, \circ . Vertical line denotes deconfining transition.

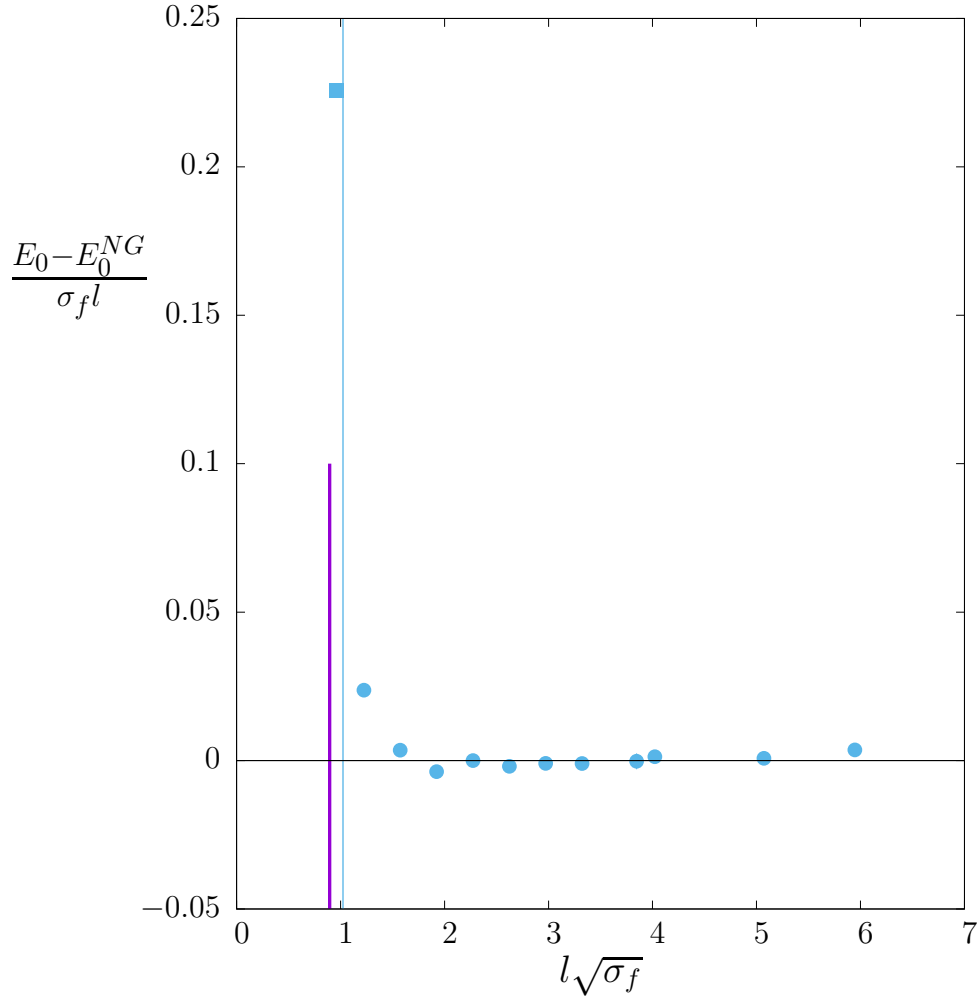


Figure 29: Ground state energy minus Nambu-Goto energy in $SU(2)$ at $\beta = 16$. To left of light vertical line E_0^{NG} is tachyonic and for \blacksquare we have set it to zero. Thick vertical line locates the deconfining transition.

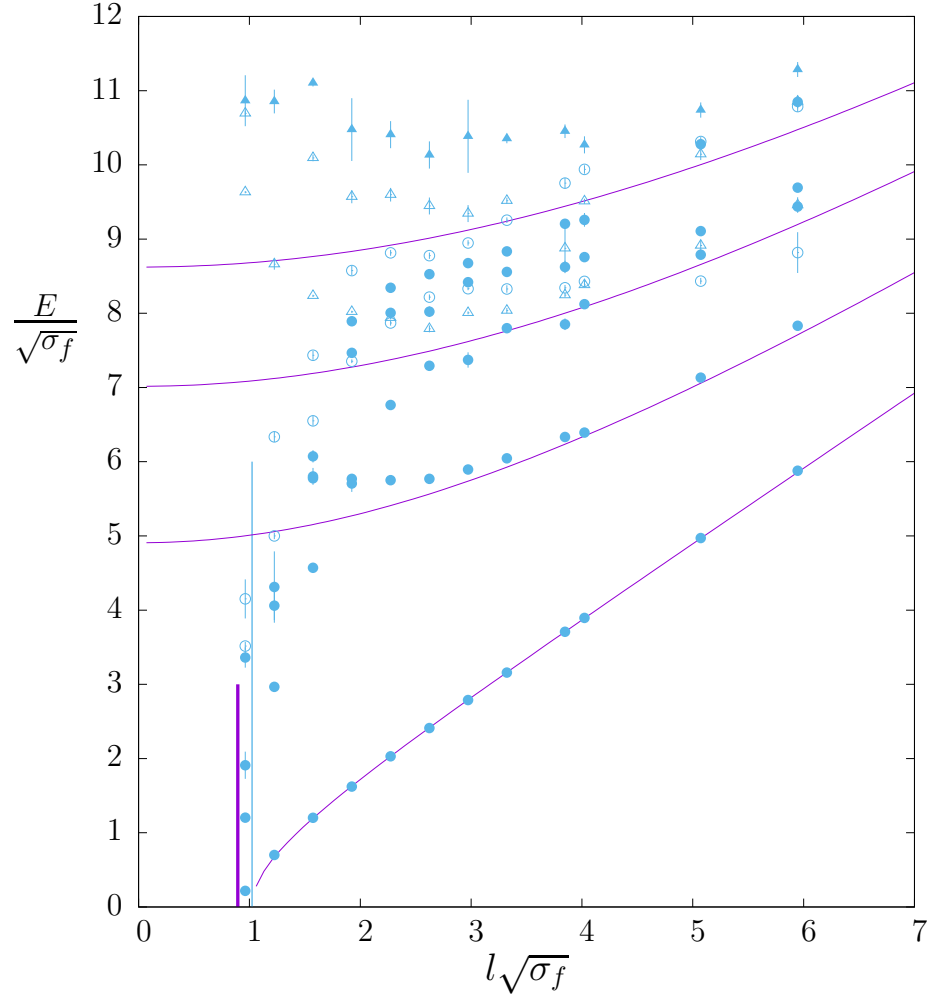


Figure 30: SU(2) at $\beta = 16$. Spectrum with $p = 0$ and parities $P_t, P_{\parallel} = +, +, \bullet, -, +, \circ, +, -, \blacktriangle, -, -, \triangle$. Thick vertical line is deconfining transition; thin vertical is NG tachyonic transition.

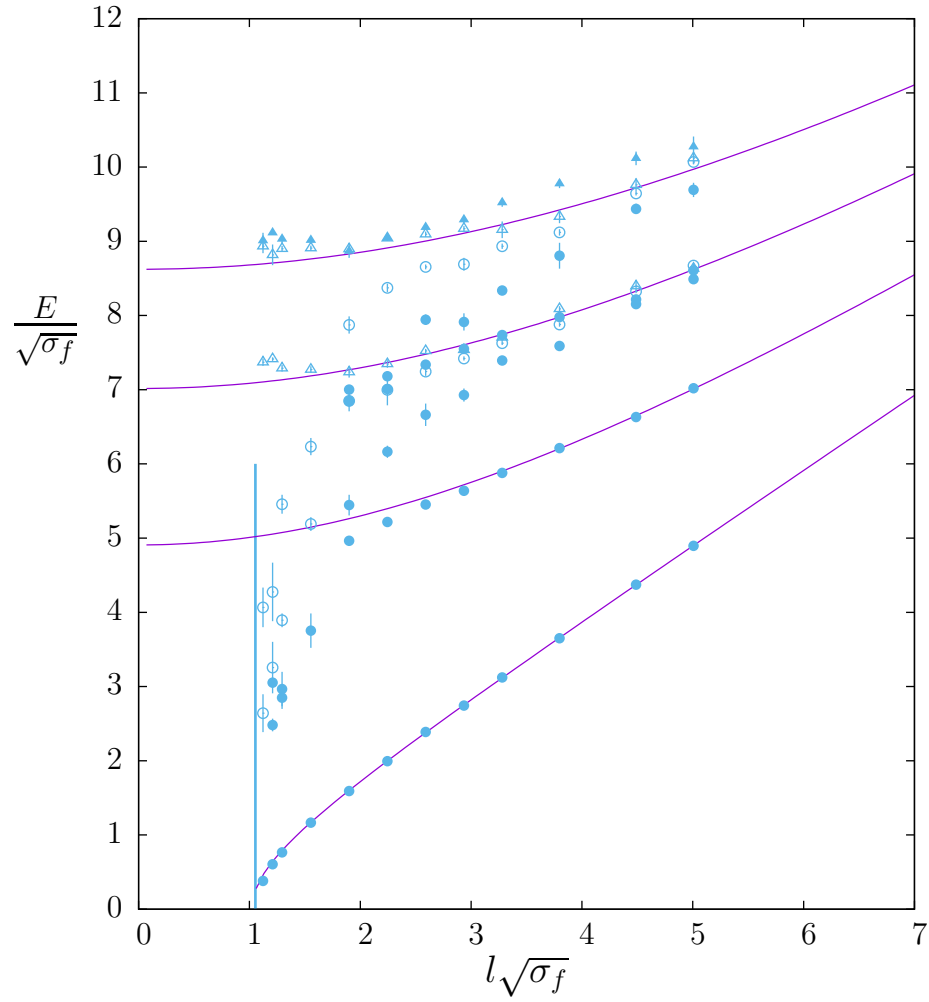


Figure 31: $SU(4)$ at $\beta = 74$. Spectrum with $p = 0$ and parities $P_t, P_{||} = +, +, \bullet, -, +, \circ, +, -, \blacktriangle, -, -, \triangle$. Vertical line is deconfining transition.

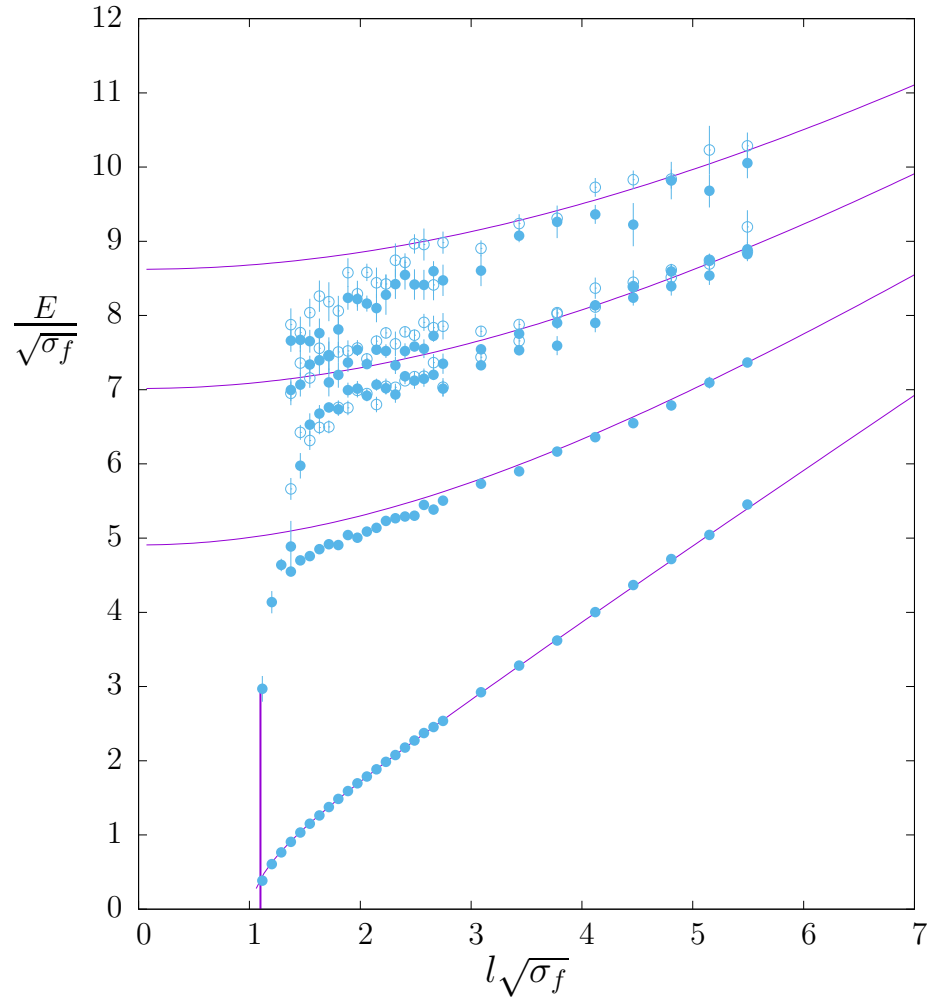


Figure 32: SU(6) at $\beta = 171$. Spectrum with $p = 0$ and parities $P_t = +$, \bullet , and $P_t = -$, \circ . Vertical line is deconfining transition

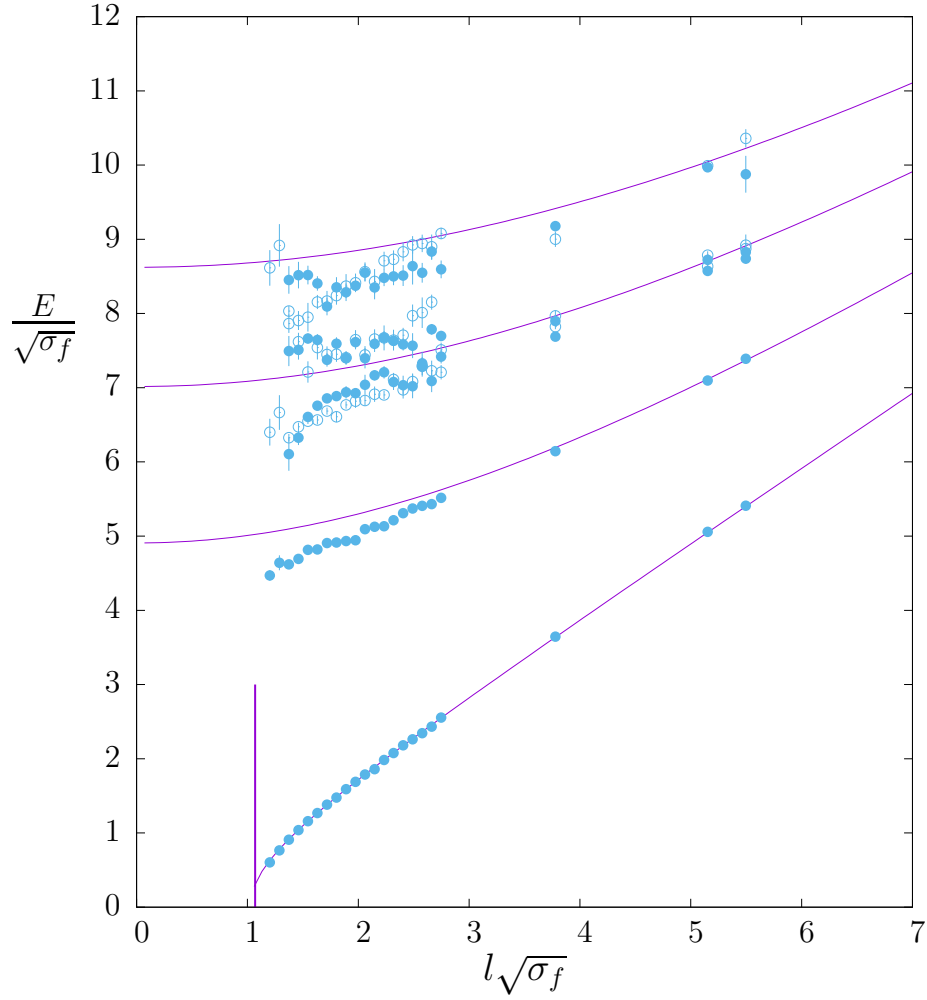


Figure 33: SU(8) at $\beta = 306.25$. Spectrum with $p = 0$ and parities $P_t = +, \bullet$, and $P_t = -, \circ$. Values at $l/a = 44, 60$ are from [19]. Vertical line is deconfining transition

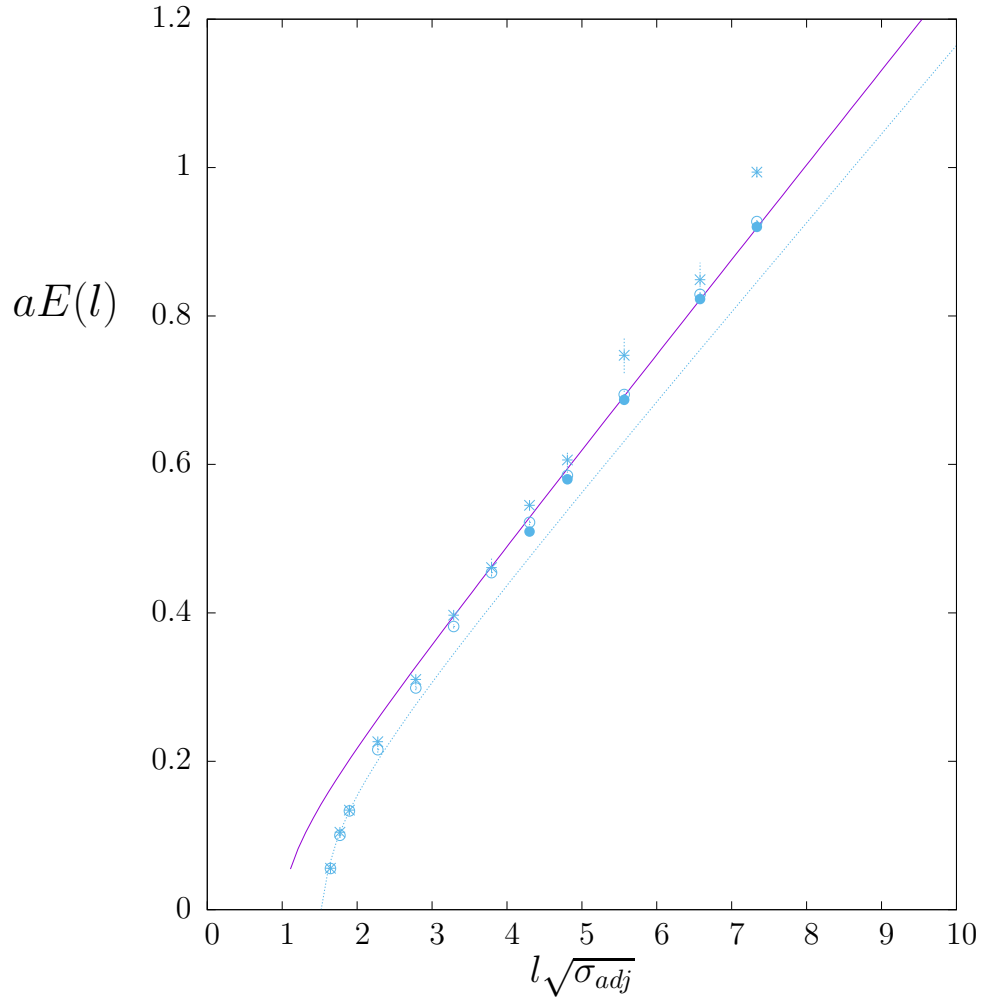


Figure 34: Adjoint flux tube ground state energies for $SU(4)$ at $\beta = 74$ for operator bases with blocking levels ≤ 4 (\times), ≤ 5 (\circ), and ≤ 6 (\bullet). Solid line is Nambu-Goto fit to largest blocking levels; dashed line is twice the energy of a fundamental flux tube.

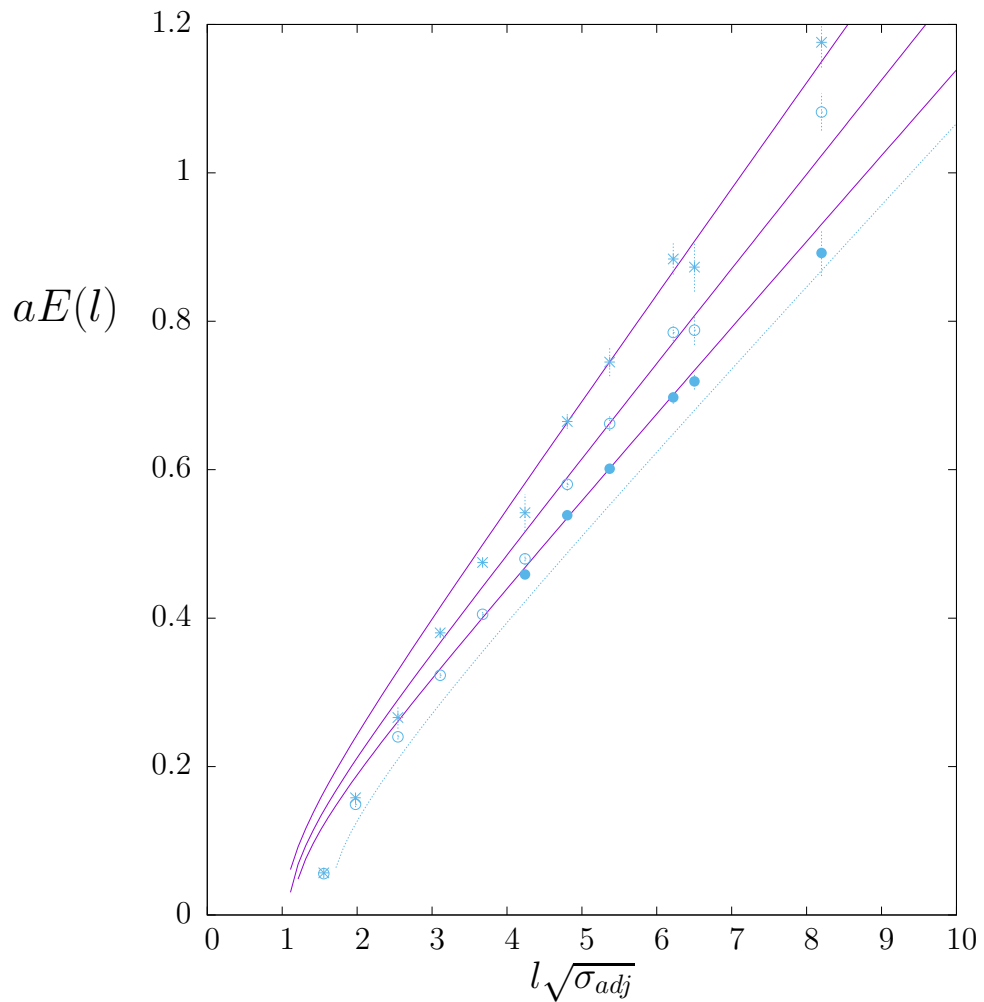


Figure 35: Adjoint flux tube ground state energies for $SU(2)$ at $\beta = 16$ for operator bases with blocking levels ≤ 4 (\times), ≤ 5 (\circ), and ≤ 6 (\bullet). Solid lines are Nambu-Goto fits to largest l ; dashed line is twice the energy of a fundamental flux tube.

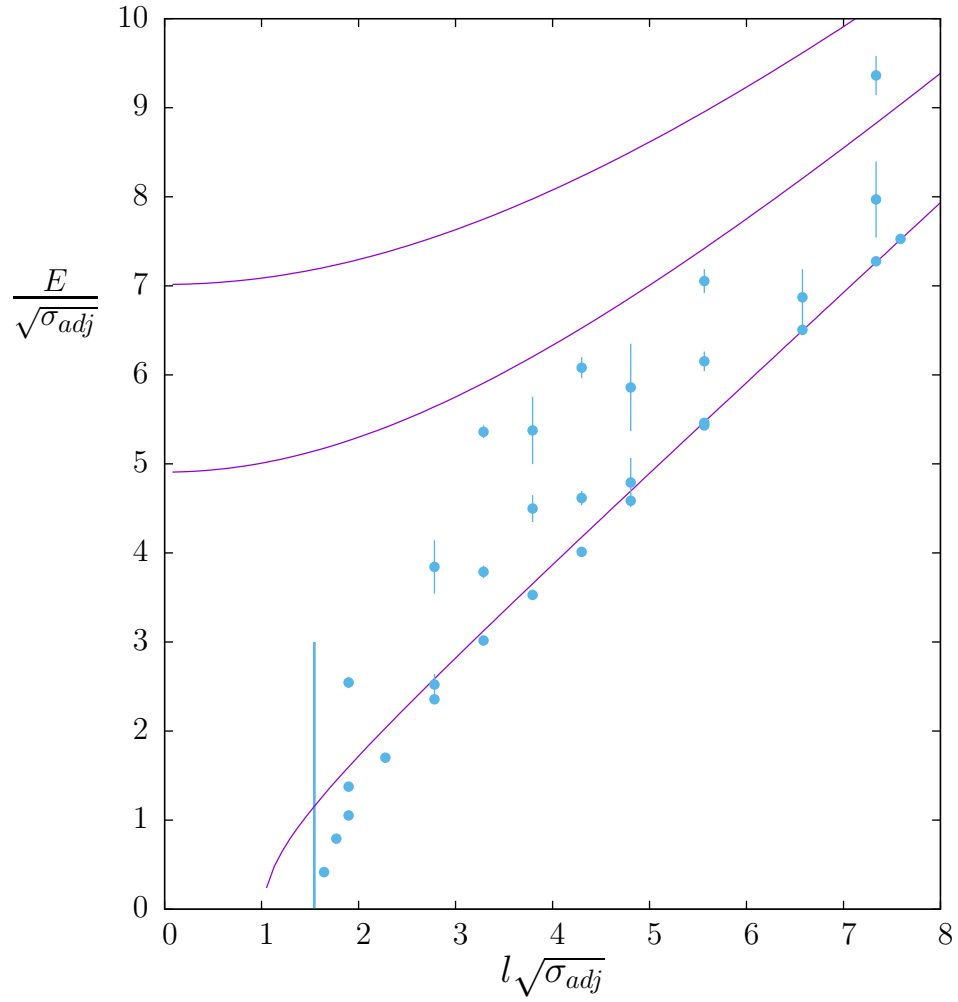


Figure 36: Adjoint flux tube in SU(4) at $\beta = 74$. Spectrum with $p = 0$ and parities $P_t, P_{||} = +, +$. Vertical line locates deconfining transition.

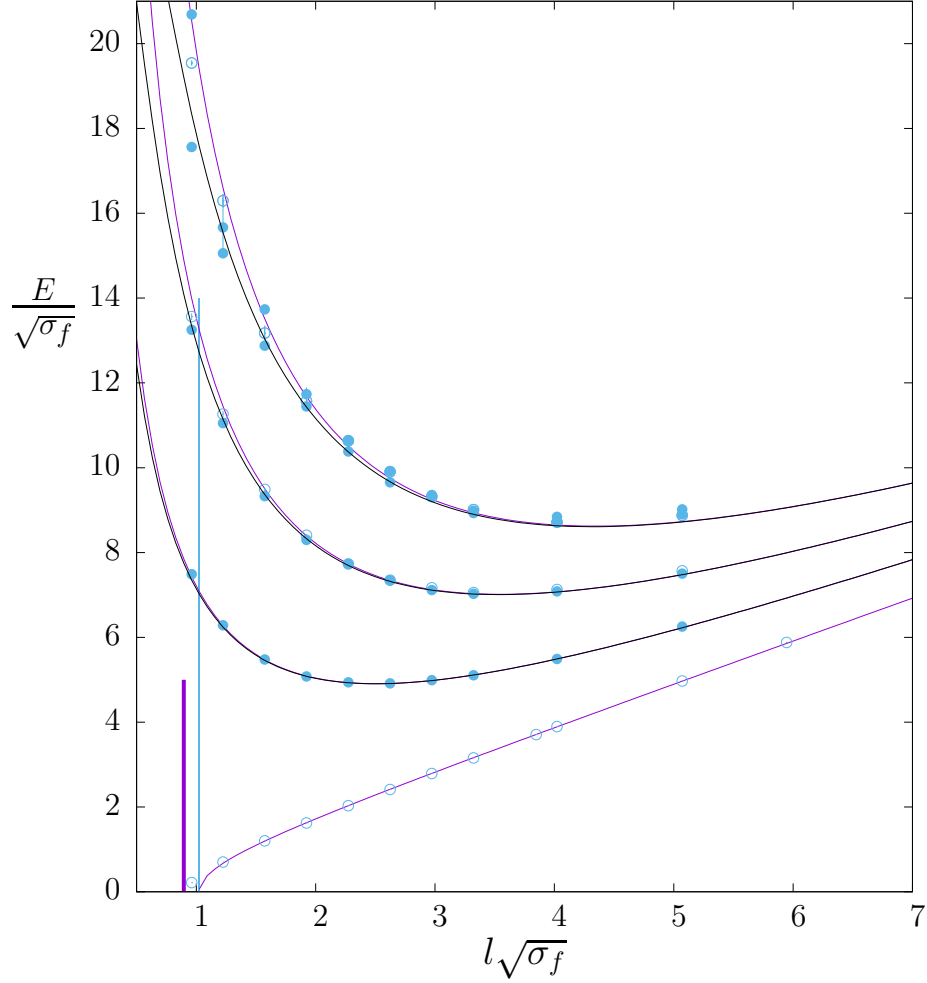


Figure 37: SU(2) at $\beta = 16$. Ground state energies for momenta $p = 0, 2\pi/l, 4\pi/l, 6\pi/l$ and parities $P = +, \bullet$, and $P = -, \circ$. Solid curves are continuum NG; dashed curves are NG with a 'lattice' dispersion relation. Thick vertical line is deconfining transition; thin vertical line is NG tachyonic transition.

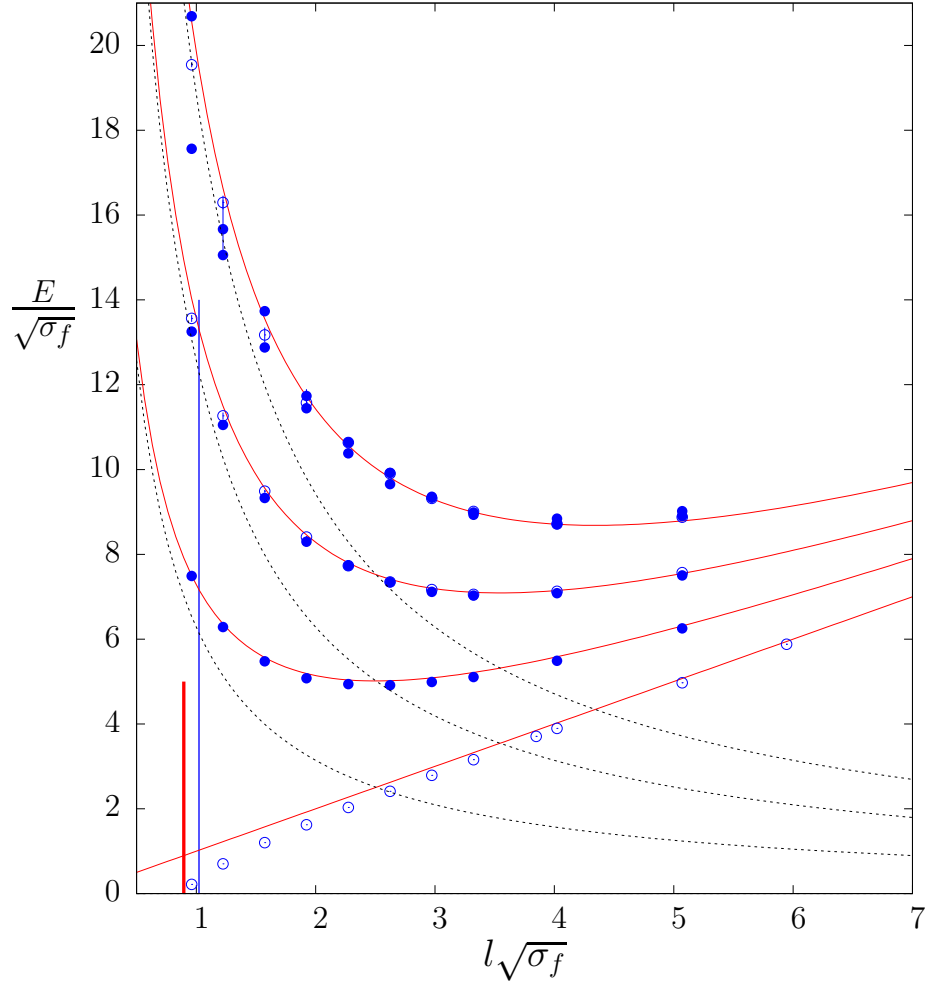


Figure 38: SU(2) at $\beta = 16$. Ground state energies for momenta $p = 0, 2\pi/l, 4\pi/l, 6\pi/l$ and parities $P = +, \bullet$, and $P = -, \circ$. Solid curves are the prediction for free phonons on a background string, $E = l\sigma_f + p$. Dashed curves are the continuum prediction for just a massless free particle, $E = p = 2\pi q/l$. Thick vertical line is deconfining transition; thin vertical line is NG tachyonic transition.

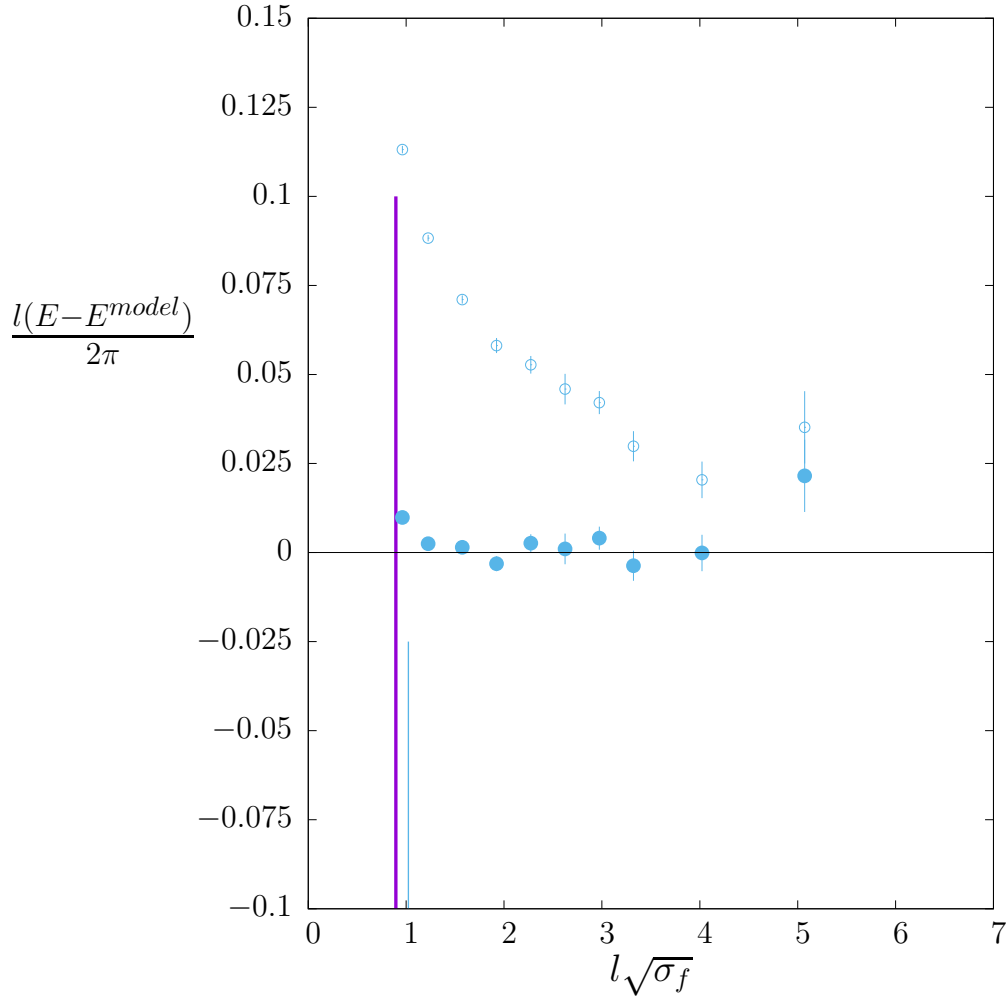


Figure 39: SU(2) at $\beta = 16$. Energy of ground states for momenta $p = 2\pi/l$ and parity $P = -$ with two different model energies subtracted: Nambu-Goto (●) and free massless phonons (○) on a background flux tube. Thick vertical line is deconfining transition; thin vertical line is Nambu-Goto tachyonic transition.

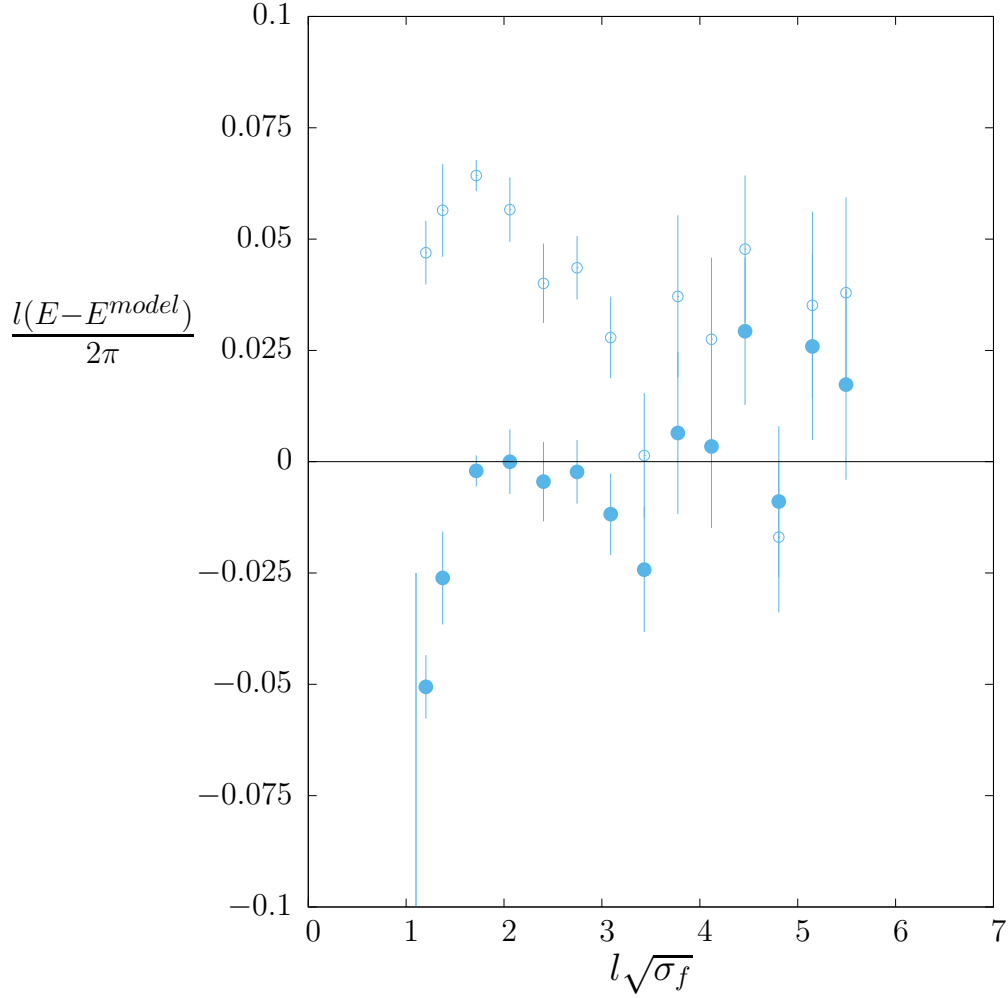


Figure 40: SU(6) at $\beta = 171$. Energy of ground states for momenta $p = 2\pi/l$ and parity $P = -$ with two different model energies subtracted: Nambu-Goto (\bullet) and free massless phonons (\circ) on a background flux tube. Vertical line is deconfining transition.

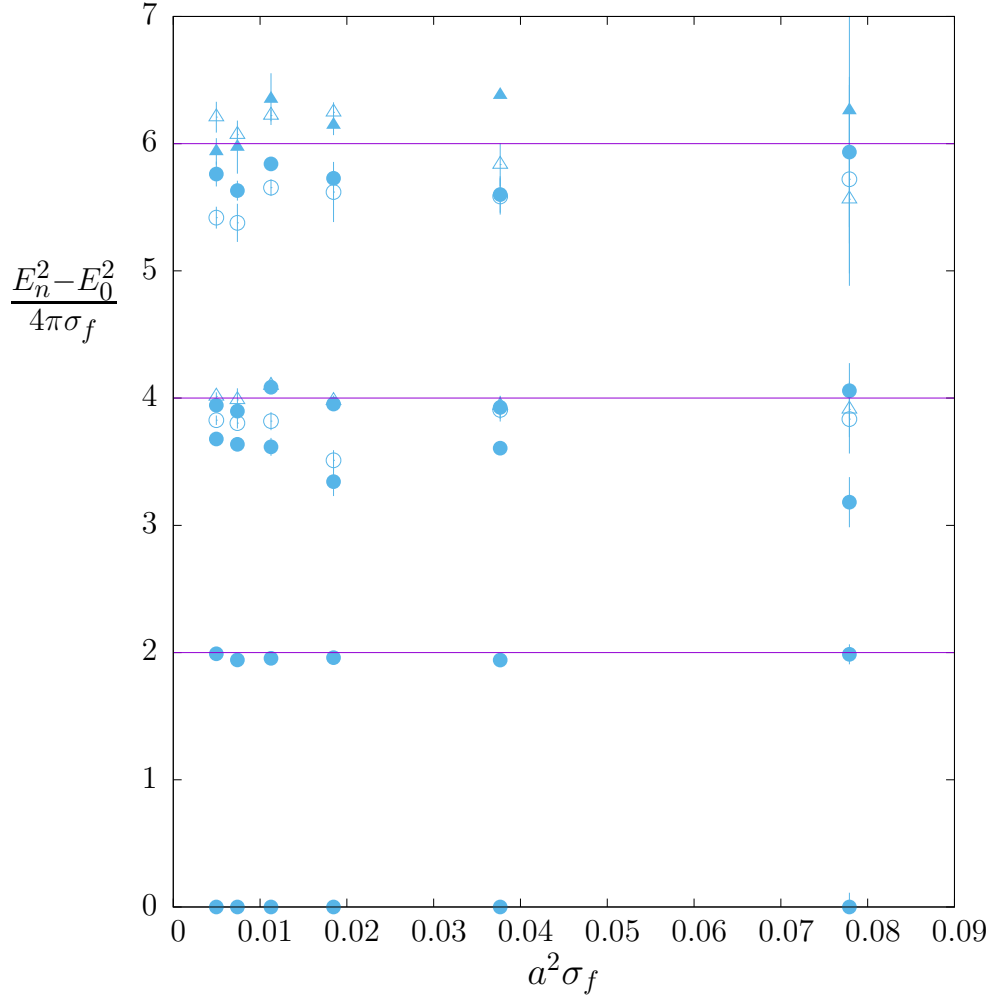


Figure 41: Approach to continuum limit in SU(8). Flus tube lengths lie in narrow range $l\sqrt{\sigma_f} \in (3.78, 3.91)$. Spectrum with $p = 0$ and parities $P_t, P_{\parallel} = +, +, \bullet, -, +, \circ, +, -, \blacktriangle, -, -, \triangle$.

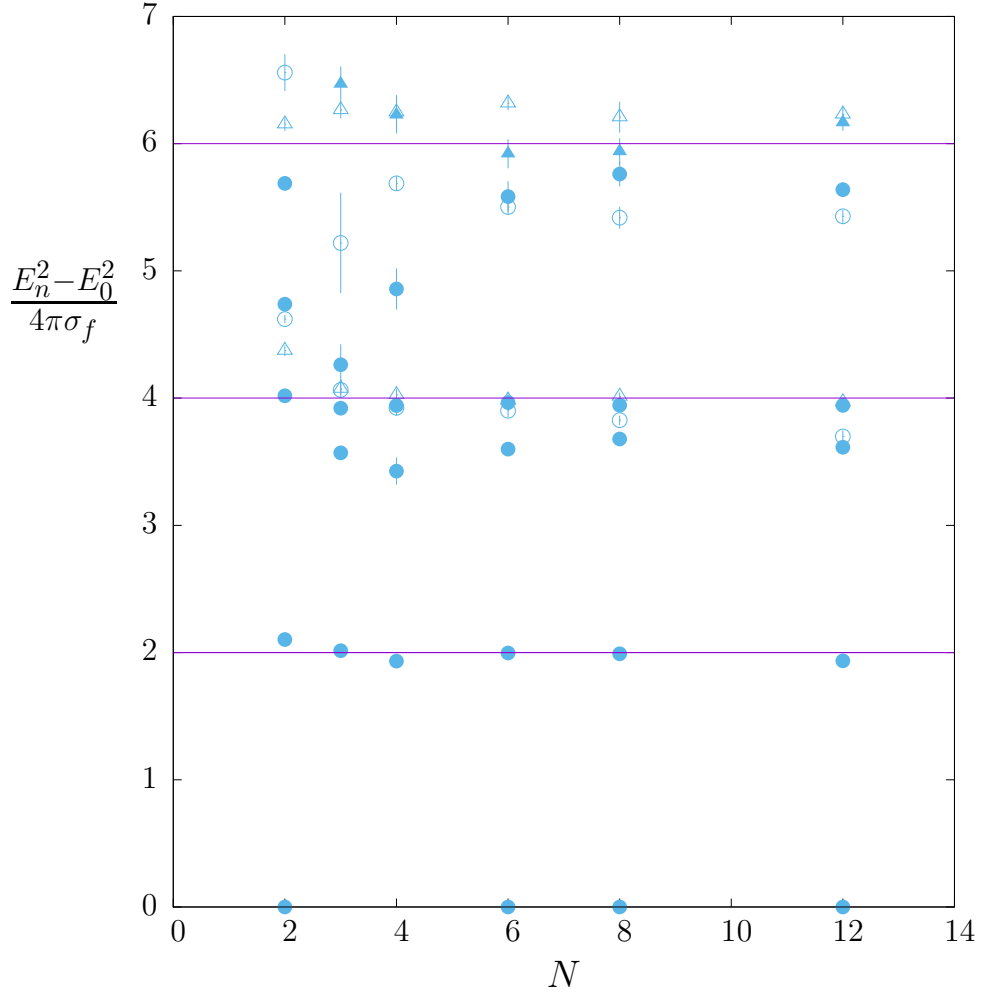


Figure 42: Variation of $p = 0$ flux tube spectrum with N . Lengths and lattice spacings lie in narrow ranges $l\sqrt{\sigma_f} \in (3.55, 3.85)$ and $a\sqrt{\sigma_f} \in (0.069, 0.074)$. Parities $P_t, P_{\parallel} = +, +, \bullet, -, +, \circ, +, -, \blacktriangle, -, -, \triangle$.